Chapter 6

Evaluation of Global and Regional Climate Models in simulating spatial and temporal patterns of seasonal rainfall variability in the Australian region

Jozef Syktus and Greg McKeon

Climate Impacts and Natural Resource Systems, Queensland Department of Natural Resources and Mines, 80 Meiers Rd, Indooroopilly 4068, Australia

6.1 Introduction

Numerical climate models, both global and limited domain, provide an alternative 'mechanistic-based' approach to forecasting rainfall and other climate variables compared to statistical systems derived from analyses of historical data. For many years numerical weather prediction models have been used routinely to make short-term weather predictions with a high degree of skill and, in recent years, it has also been demonstrated that these models have some predictive ability at seasonal time scales (Kumar *et al.* 1996, Zwiers 1996, Barnston *et al*. 1999, Mason *et al.* 1999, Barnston *et al.* 2000). The American Meteorological Society recently released a policy statement on Seasonal to Interannual Climate Prediction (AMS 2001) which stated:

> The skill of seasonal climate prediction has improved substantially over the past two decades, largely in response to increased understanding of the El Niño/Southern Oscillation (ENSO) phenomenon. Routine, scientifically based, skilful, seasonal forecasts are now possible for some parts of the world, for some seasons. These seasonal climate predictions are able to project the mean conditions and some of the statistical characteristics of the climate a season or two in advance. The seasonal predictions are primarily of use to organizations that have a decision-making process that can intelligently use probabilistic input and that are engaged in activities that are sensitive to seasonal climate variations and involve significant economic stakes.

Trial operational seasonal climate forecasts have been produced since 1997 at the International Research Institution (IRI), Columbia University, and since late 1998 at CINRS using a suite of Global Climate Models, GCMs (Mason *et al.* 1999, Syktus *et al.* 2001).

The successful application of seasonal climate forecasts requires that meaningful information is available at both the regional and local scale. However, GCMs used in current seasonal climate forecasting systems lack the spatial resolution to derive realistic values of climate variables at the scale required by many users. This shortcoming is particularly apparent for precipitation, where sub-grid processes such as synoptic weather systems, thunder storms and tropical cyclones can cause large variation in rainfall intensity and amount. Increases in horizontal resolution (30 – 80 km) of GCMs are currently limited by available computing resources. An alternative approach is to nest (RCMs) within the coarser grid resolution of a GCM. RCMs are: 1) able to account for important local factors such as orographic forcing; 2) are physically based; and 3) are able to produce a consistent response to forcings. The main limitations of the nesting

approach are that the higher resolution information is only available for the region over which the nesting is applied and there is no physical feedback from the RCM on the GCM.

This chapter will examine the ability of a GCM and a doubly nested GCM/RCM (280 km, 75 km, 15 km resolution) system forced by observed monthly sea surface temperatures SSTs to simulate the long term rainfall pattern (means and variability) of Australia for the period 1965-2000. Ensembles of output at both the GCM and RCM scale were generated by perturbation of the initial (1965) state of the atmosphere. This comparison of rainfall climatology is an essential first step in the evaluation of GCM/RCM systems to provide accurate rainfall forecasts. The next chapter will build on this analysis by examining the ability of the GCM/RCM system to forecast selected monthly rainfall compared with an existing statistical forecasting system. However, the results presented in this and the following chapter need to be interpreted carefully as they represent the upper level of skill assuming that the key driver of climate (i.e. SSTs) is able to be simulated with 100% accuracy.

6.2 Experimental design

The research reported in this paper examined the use of a GCM and a double nested GCM/RCM system in simulating the multi-decadal climate of the Australian region for the 1965-2000 period. The models used and their applied resolutions are shown in Table 6.1.

The NCEP-MRF9 (Kumar *et al.* 1996) AGCM at T40/L18 resolution (Table 6.1) was used to produce an ensemble of ten integrations forced with monthly historical SSTs for the period 1965-2001. Each member of the ensemble was produced by slightly perturbating the 1965 initial conditions. The history files produced by the NCEP GCM were saved at 6-hourly intervals as lateral boundary conditions to subsequently drive the CSIRO Division of Atmospheric Research Limited Area Model (DARLAM), which was designed for regional modelling studies (McGregor *et al.* 1993). The first nesting (75 km) of the RCM was applied across the Australian region and the second (15 km) across the Queensland region only. The details and current parameterisation of DARLAM are given by McGregor (1997), and some of the systematic errors are described by Katzfey (2000).

In addition a new version of the CSIRO T63 GCM (Watterson 2000) forced with historical SSTs and sea ice was used to simulate historical Australian climate since 1871 as part of 'The Climate of the 20th Century' project. This model was run with horizontal grid spacing of approximately 190 km and 18 vertical levels. An ensemble of five integrations were completed for each of the periods 1871-2001 and 1949-2001.

The T63 has improved representation of atmospheric/oceanic processes and land parameterisation and belongs to a group of new generation climate models. The NCEP model used in this study represents state-of-the-art climate modelling from a decade or so ago.

All GCM simulations were forced by observed SSTs which allowed the atmospheric component of the models to be evaluated. However, it does not allow the impact of other climate forcings such as volcanic aerosols and solar variability to be tested. Implicit in

statistical forecast systems is that the effects of climate forcings have been integrated in the SST and atmosphere's response. Hence, it is important to realise that the use of just SST forcing by itself in GCM/RCM simulations could limit the likely explanation of observed rainfall because temporal variation in other forcings are not represented.

The ensembles of model output for these simulations (Table 6.1) were averaged and the mean of each used in subsequent analyses. The observed data for the simulation period (1965-2000) included several El Niño and La Niña events, and both positive and negative phases of the IPO index (Power *et al*. 1999). In Queensland the period included extreme droughts (1965, 1969, 1982, 1991 to 1994), extreme summer wet seasons (1973/74, 1990/91), and two degradation episodes (1960s in South-west Queensland and 1980s in north- eastern Queensland (Carter *et al*. 2000).

Table 6.1. GCMs and RCMs used in simulation experiments.

Model and experiment details	Reference	Model grid spacing (km)
NCEP-MRF9 AGCM T40/L18 – 10 runs: 1965 to 2001	Kumar *et al.* (1996)	280
CSIRO DARLAM RCM 75 km/L18 – 15 runs: 1965 to 2001	McGregor (1997)	75
CSIRO DARLAM RCM 15 km/L18 – 11 runs: 1965 to 2001	McGregor (1997)	15
CSIRO T63/L18 AGCM – 1871 to 2001, 1949 to 2001 (5 runs each)	Watterson (2000)	190

6.3 Large scale circulation features

The ENSO phenomenon is a planetary scale oscillation involving large-scale interactions between the oceans and the atmosphere in the tropical-subtropical Pacific Ocean region. The most direct manifestation of ENSO is the oscillating pressure differences between the Indonesian-Australian region and the southeast Pacific. The traditional measure of this oscillation is the SOI, which is the normalised Tahiti-minus-Darwin pressure difference. The importance of ENSO in the global climate system is illustrated by the fact that it explains the largest amount of climate variability after the seasonal cycle and the monsoon system (Allan 2000). The SOI is also commonly used to forecast rainfall in eastern Australia (McBride and Nicholls 1983, Stone *et al.* 1996). Thus, the ability of GCMs to simulate the pressure differences as measured by the SOI is an important component in assessing their ability to accurately simulate seasonal rainfall. SOI values derived from both the NCEP and CSIRO GCMs were found to be in close agreement with observed SOI values (Figure 6.1), indicating that the simulated atmosphere responded to SSTs in a similar way to that which actually occurred. Correlations for predicted and observed SOI values were high at a monthly timescale (r^2=0.58), and very high for the 5-month running mean (r^2=0.81) for the period 1965-2000. The simulation of SOI values also provides a simple way of converting GCM output into rainfall forecasts using the same approaches as the statistical systems (Stone *et al.* 2001).

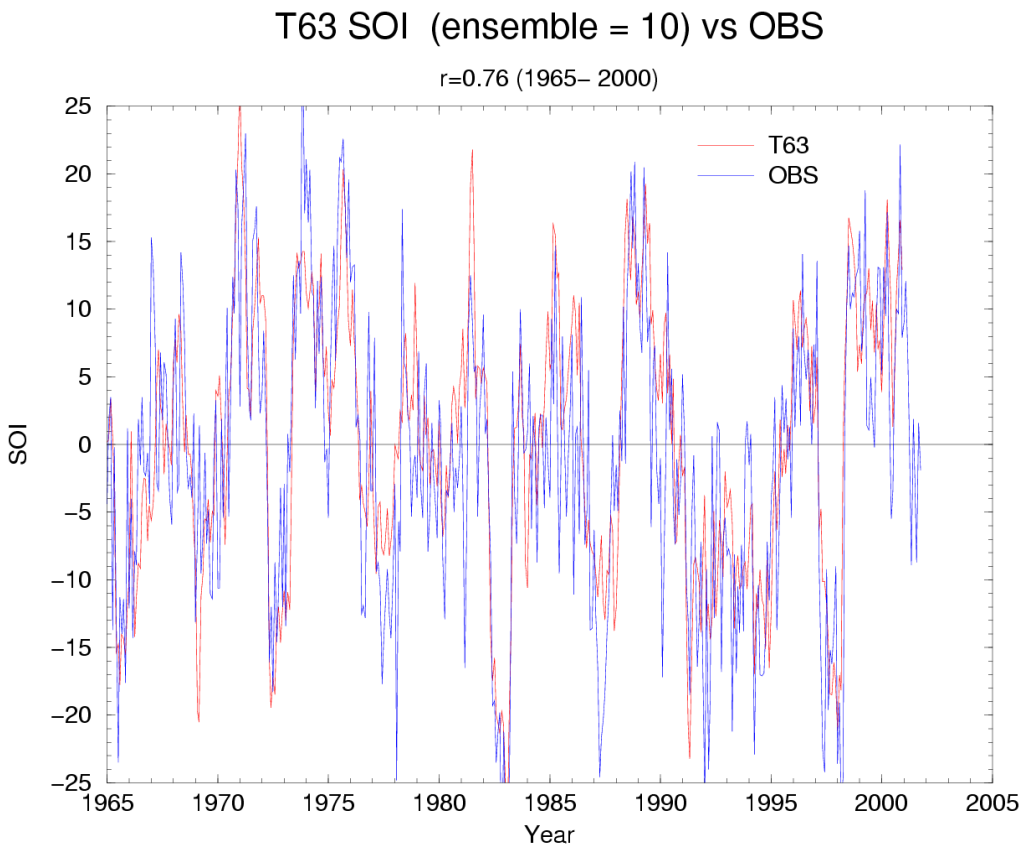

Figure 6.1. Comparison of simulated and observed monthly SOI values from 1965 to 2000. Observed values were calculated from the difference in anomaly of mean sea level pressure between Tahiti and Darwin. Both observed and model data use the same 1965-2000 base period.

6.4 Representation of topography and mesoscale features

The representation of topography is an important input to climate models as it has a strong impact on the simulated climate fields, in particular spatial rainfall distribution. Figure 6.2 shows that the increasing resolution of models T40, T63, RCM75, RCM15 provide much better resolution of topographic input details over the Australian region and, in particular, features such as the Great Dividing Range in eastern Australia (especially high regions of New England in NSW and Mareeba in northern Queensland). The 15 km RCM for Queensland also includes coastal ranges near Gladstone and Mackay which were not represented in the coarser models. As described later, the nesting of RCMs model within a GCM is becoming a valuable downscaling technique for simulating more detailed climatic features over a limited area.

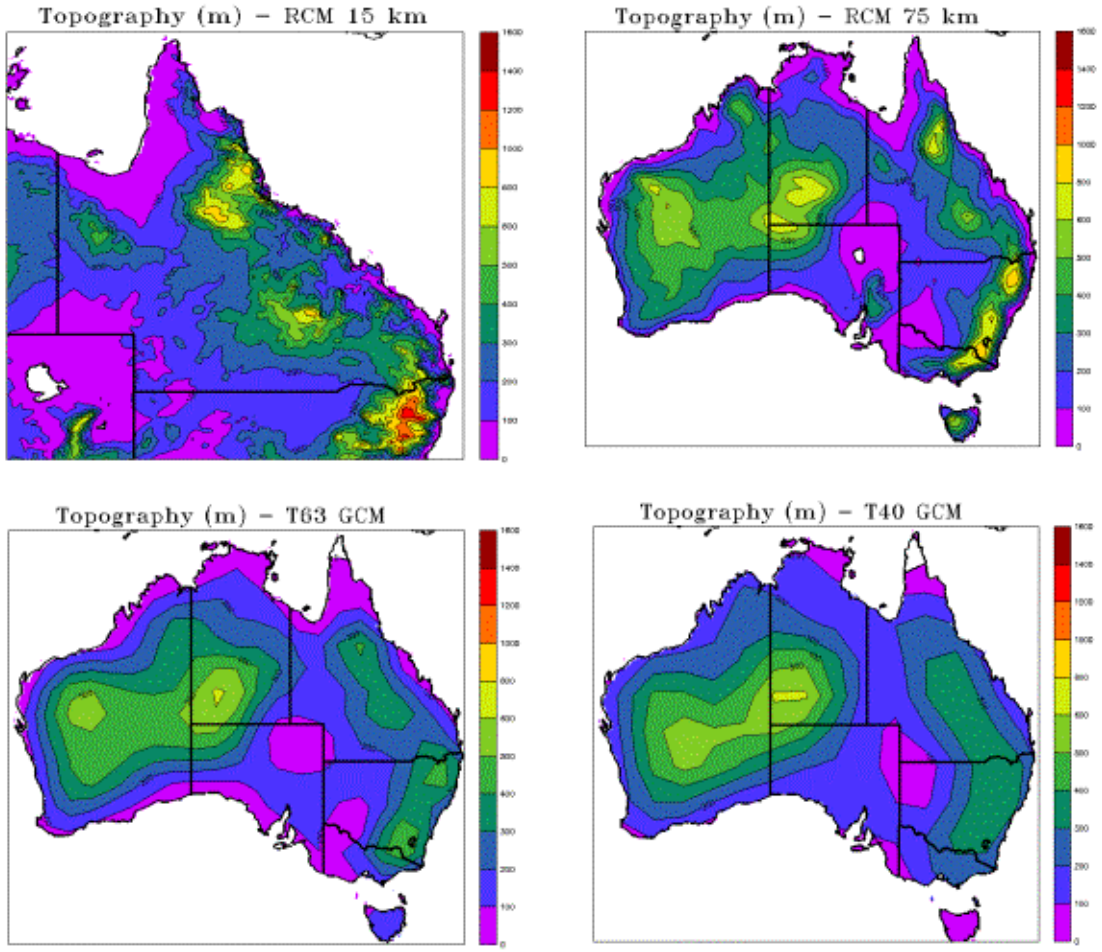

Figure 6.2. Topographical data layers used in the different models (Table 6.1). Examples of high resolution topography can be seen in the State of Environment Report (EPA 1999, page 16). The 15 km RCM topography in Queensland captures coastal ranges near Gladstone and Mackay which are not represented at the coarser resolutions.

6.4.1 Tropical cyclones

Tropical cyclones can be a major source of rainfall in Queensland, especially in La Niña years. The application of RCM at higher spatial resolution provided an opportunity to evaluate the occurrence of tropical cyclones. Inspection of selected mean sea level pressure and precipitation fields at 6 hourly intervals showed features similar to tropical cyclones in the Coral Sea (Figures 6.3a, b and 6.4). The T63 also showed similar fine resolution features, for example, a tropical cyclone in northern western WA becoming a rain depression over arid inland WA (Figure 6.5a, b).

In La Niña years tropical cyclones have tended to track towards Queensland's coast and then deteriorated into rain depressions. In contrast, cyclones paths in El Niño years have been generally south or east (Hastings 1990). Analysis of data from the 75 km RCM for tracks of the 'tropical cyclone-like vortices' (TCLVs, see Walsh and Ryan 2000) show that TCLVs in the model followed paths that were similar to those observed. For example, Figures 6.6 and 6.7 show the simulated paths of TCLVs for 1973/74 (strong La Niña) and 1982/83 (strong El Niño) showing the expected contrasting pattern. Similar

fine resolution features occur in other regions (e.g. northern America) indicating that the models, especially RCMs, are capable of representing important rainfall-producing meteorological phenomena.

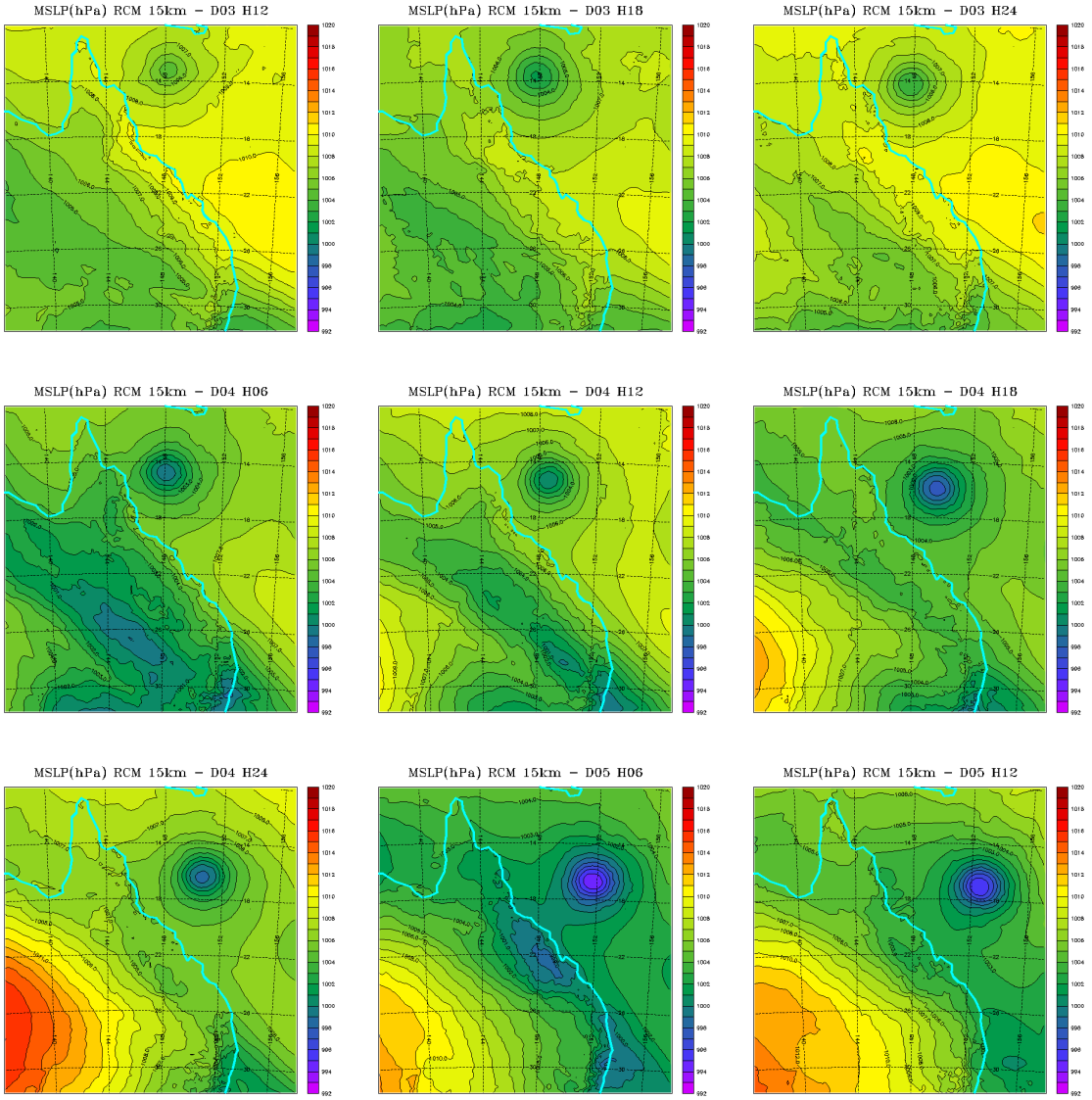

Figure 6.3a. A sequence of simulated mean sea level pressure maps at 6 hourly time intervals from the 15 km RCM. The figure shows a 'tropical cyclone like' feature with an intense low pressure system forming in the Coral Sea with associated rainfall anomalies.

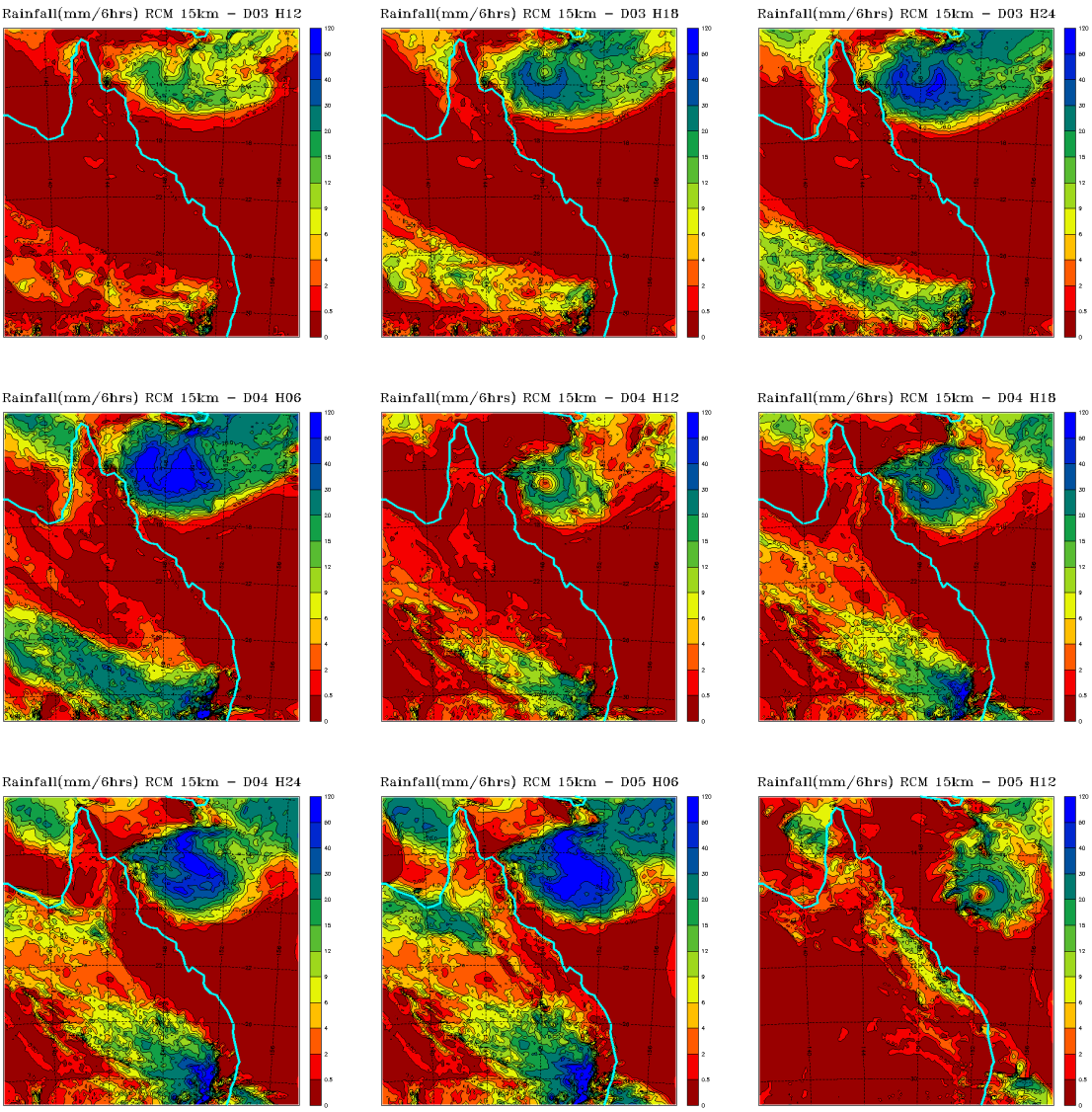

Figure 6.3b. A sequence of simulated rainfall maps at 6 hourly time intervals from the 15 km RCM. The figure shows a 'tropical cyclone like' feature with an intense low pressure system forming in the Coral Sea with associated rainfall anomalies.

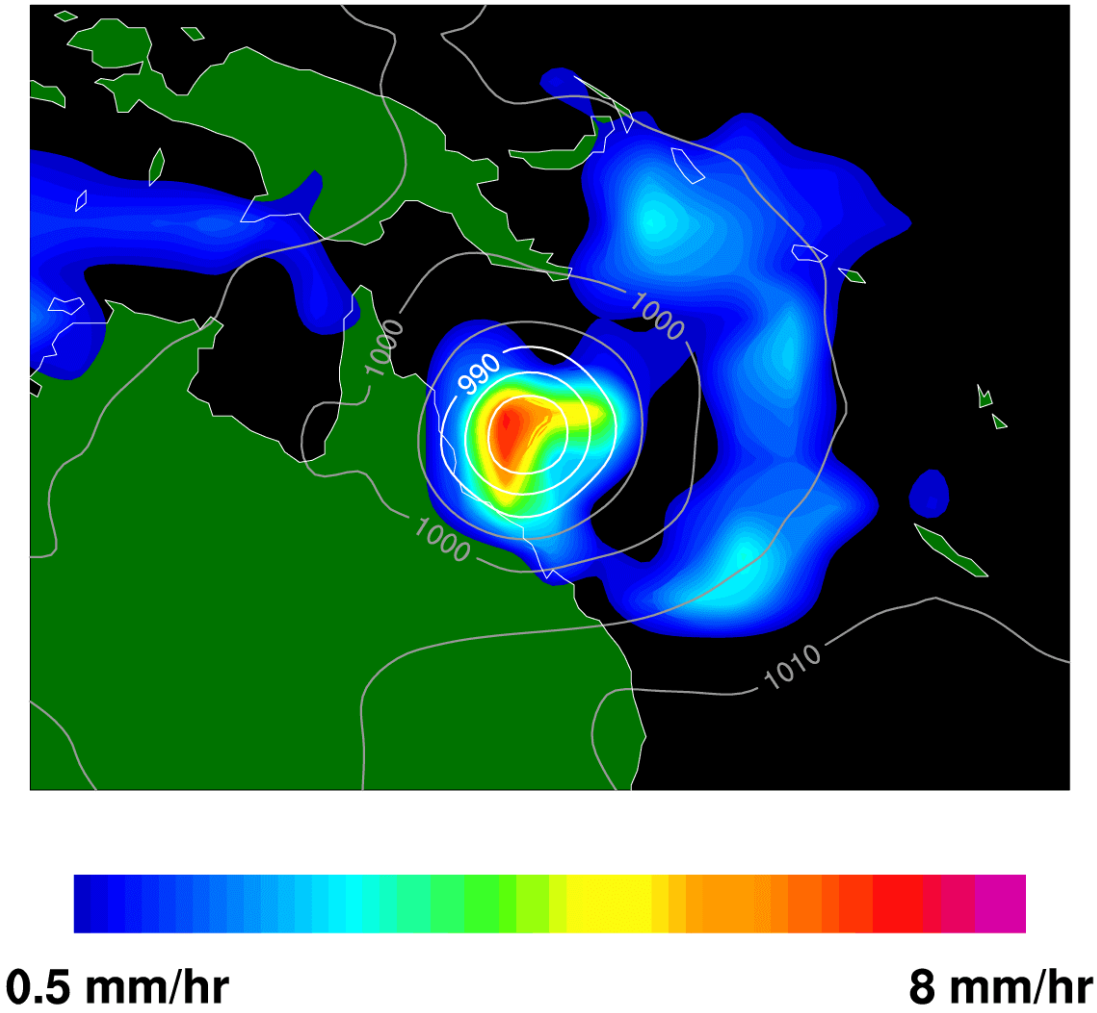

Figure 6.4. An example of observed mean sea level pressure and rainfall associated with a tropical cyclone.

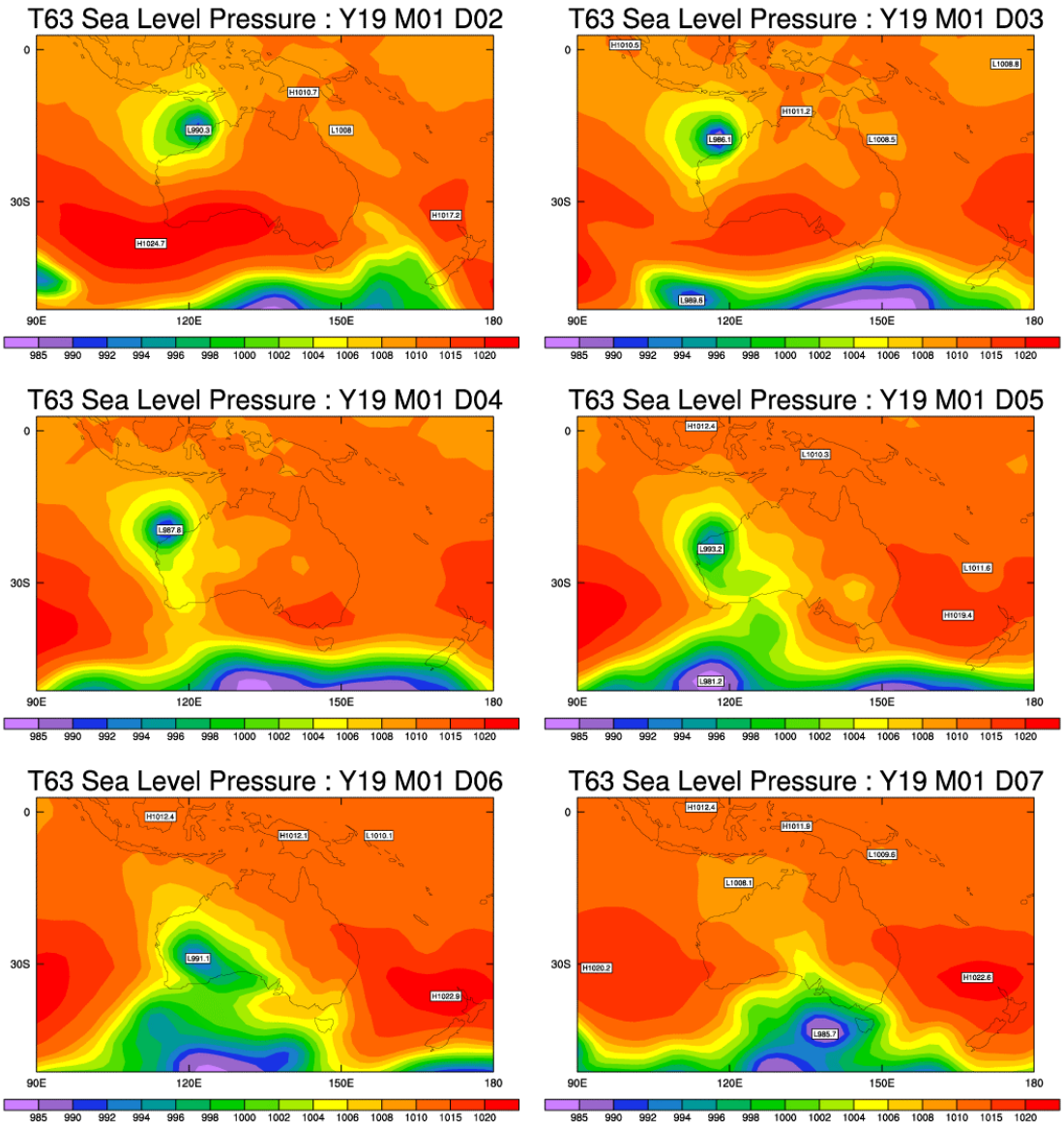

Figure 6.5a. A sequence of simulated pressure fields from the CSIRO T63 model showing a tropical cyclone in north-western Australia crossing the coast and travelling across the arid inland in a south-east direction.

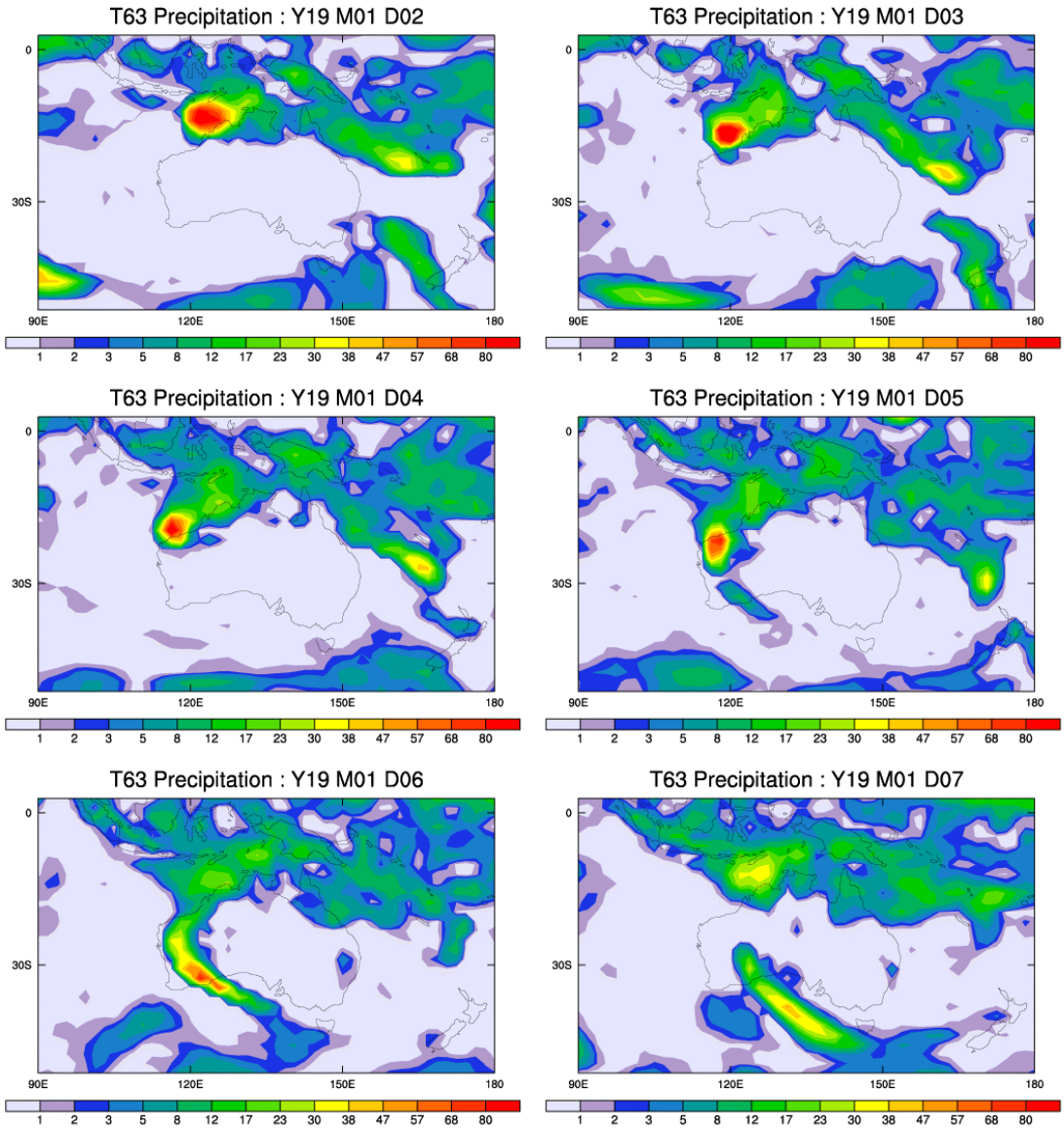

Figure 6.5b. A sequence of simulated rainfall fields from the CSIRO T63 model showing a tropical cyclone in north-western Australia crossing the coast and travelling across the arid inland in a south-east direction. Tropical cyclones are a rare but important source of rainfall in this arid environment.

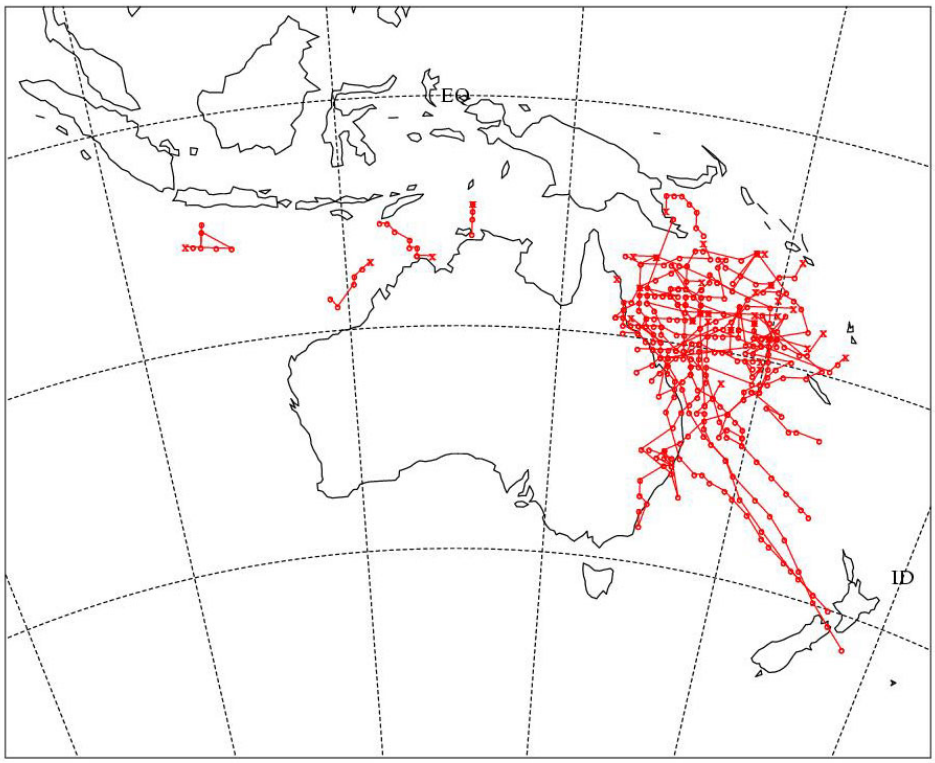

Figure 6.6. Tropical cyclone tracks simulated by the 75 km RCM for the summer of 1973/74.

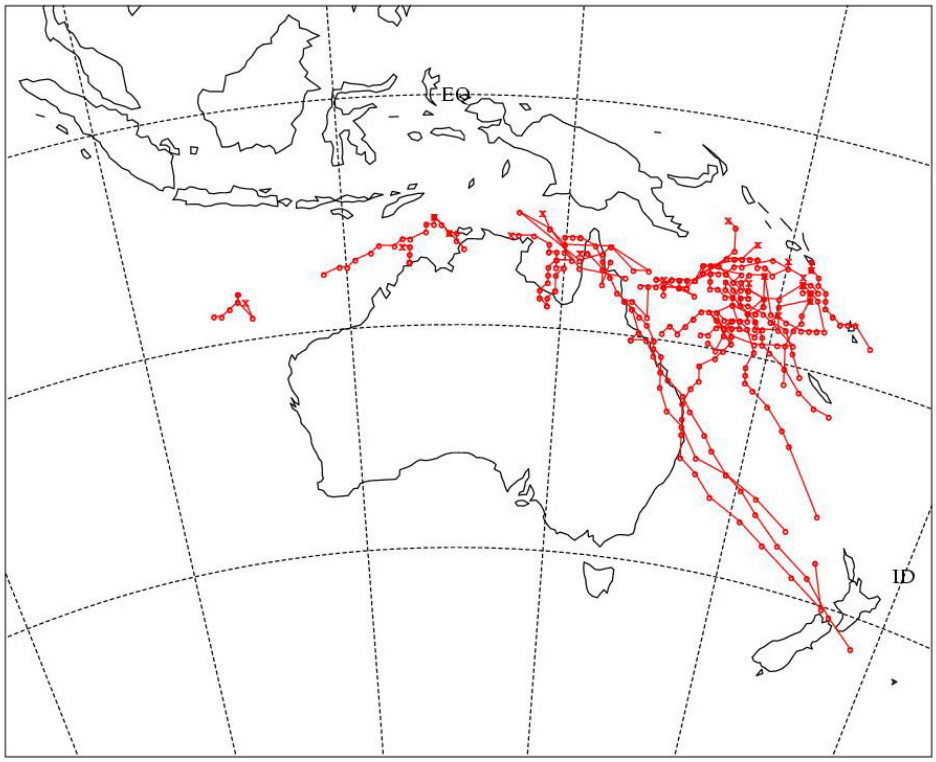

Figure 6.7. Tropical cyclone tracks simulated by the 75 km RCM for the summer of 1982/83.

6.5 Spatial distribution of simulated rainfall climatology

The ability of GCMs and RCMs to simulate the spatial pattern of long term average seasonal rainfall is a critical component of any evaluation process. GCMs, commonly configured with effective grid spacing of 200-300 km, have demonstrated skill in simulating spatial rainfall patterns at global or even continental scales, but are unable to simulate local fine scale patterns which are required by hydrological and agricultural modelling applications. Figure 6.8 illustrates how the spatial pattern of Queensland seasonal rainfall is simulated by three climate models operating at spatial resolutions of 280, 76 and 15 km. The increase in effective spatial resolution is some 350 $\left(\frac{280}{15}\right)$ times between the host GCM and the double nested RCM.

In this evaluation the NCEP GCM was able to simulate the relative east/west pattern in average rainfall across Australia, although it was generally too wet (Figure 6.9). It was unable to resolve the sharp gradient and orographic effects along the eastern part of Australia. The CSIRO T63 GCM performed better than the NCEP T40 with the dry inland in central Australia and the wet coastal strip in north-eastern Australia being well represented (Figure 6.9)

Nesting of the RCM at 75 km resolution within the NCEP GCM considerably improved the spatial pattern of rainfall with many of the sharp gradients in rainfall well represented (e.g. SW WA, top end of NT, northern coastal Queensland, and the difference between east and west Tasmania), but still did not resolve adequately the orographic effect of the Great Dividing Range along the eastern coast of Australia (Figure 6.9). However, at 15 km resolution the spatial pattern of the simulated rainfall were significantly more realistic. For example, 'rain shadow' effects were evident as a result of the coastal ranges near Gladstone and Mackay (Figure 6.11).

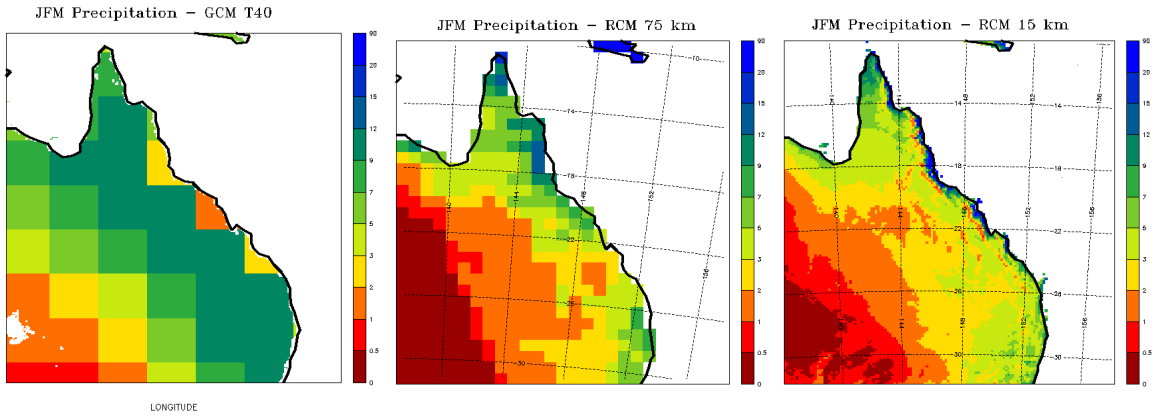

Figure 6.8. Example of seasonal (January - March) precipitation in Queensland simulated by the NCEP GCM and double nested RCM showing how increasing topographical resolution produces more detailed meteorological features such as 'rain-shadows' resulting from coastal ranges near Gladstone and Mackay.

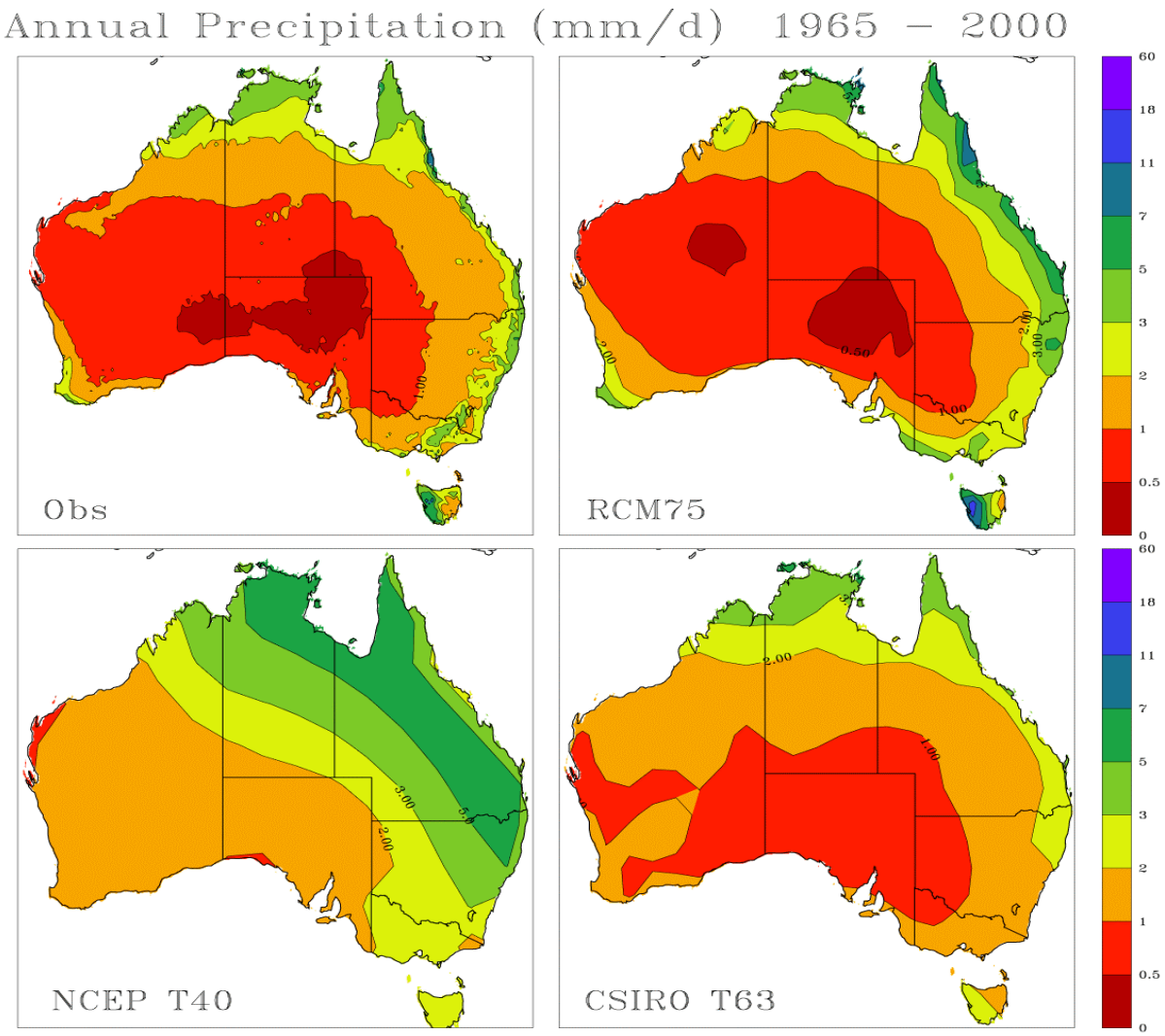

Figure 6.9. Observed and simulated annual rainfall for Australia (mm/day) averaged for 1965-2000.

Given the better performance of the CSIRO T63 relative to the NCEP GCM, the future nesting of RCMs within the CSIRO T63 could be expected to also produce better RCM results.

Inspection of seasonal rainfall patterns shows similar results: the CSIRO T63 performance was superior to the NCEP GCM; and the 75 km RCM nested within the NCEP GCM provided considerable improvement compared to the GCM (T40) (Figure 6.10a, b, c, d). In winter (JJA), spatial patterns from the 75 km RCM were very similar to observed patterns, although slightly wetter at the edges of the continent (south WA, Victoria, coastal Queensland).

For spring, summer and autumn RCM75 and T63 were consistently superior to NCEP T40 in terms of spatial distribution of rainfall with relatively strong rainfall gradients in eastern and northern Australia.

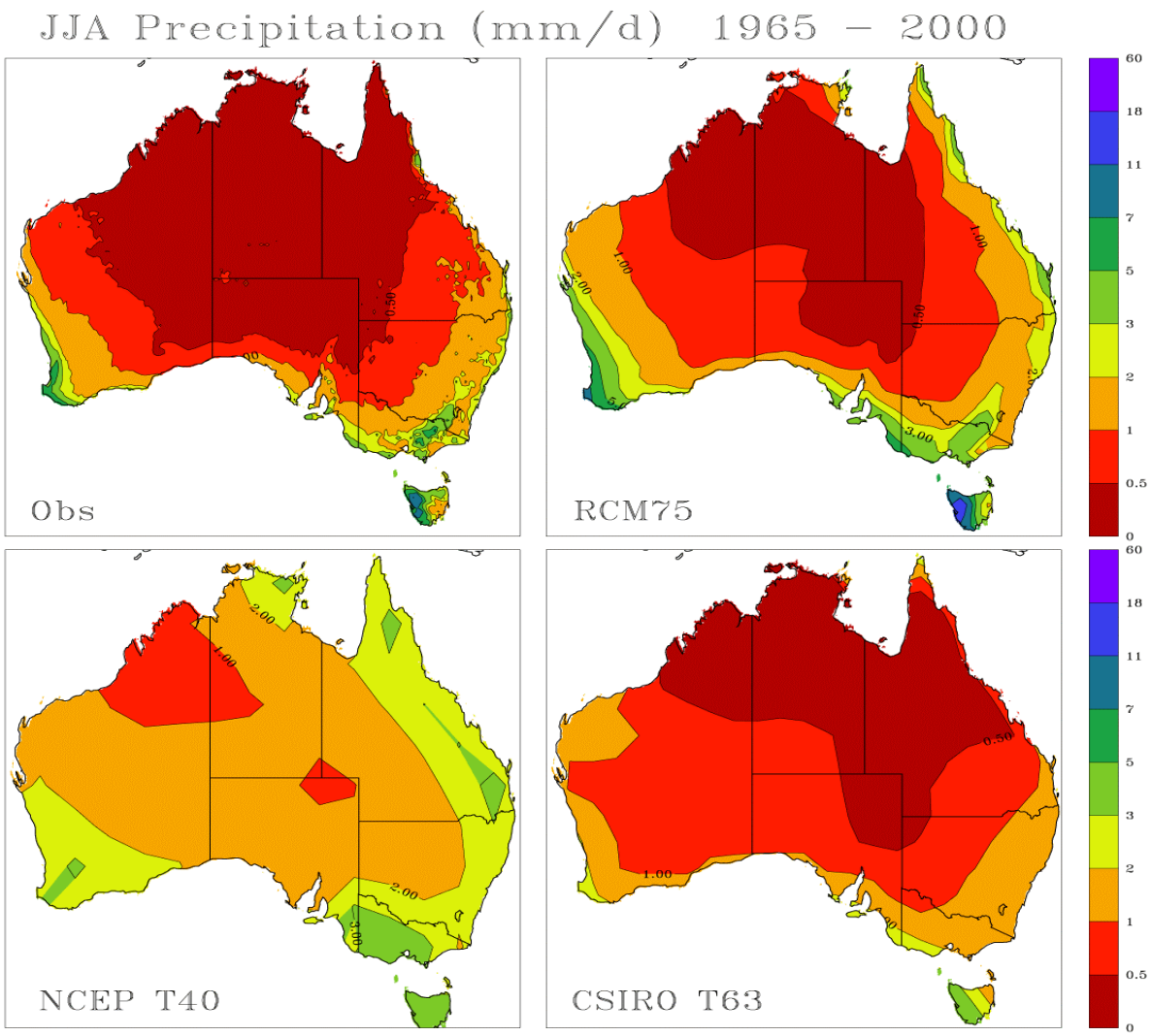

Figure 6.10a. Observed and simulated winter (JJA, June-August) rainfall for Australia (mm/day) averaged for 1965-2000.

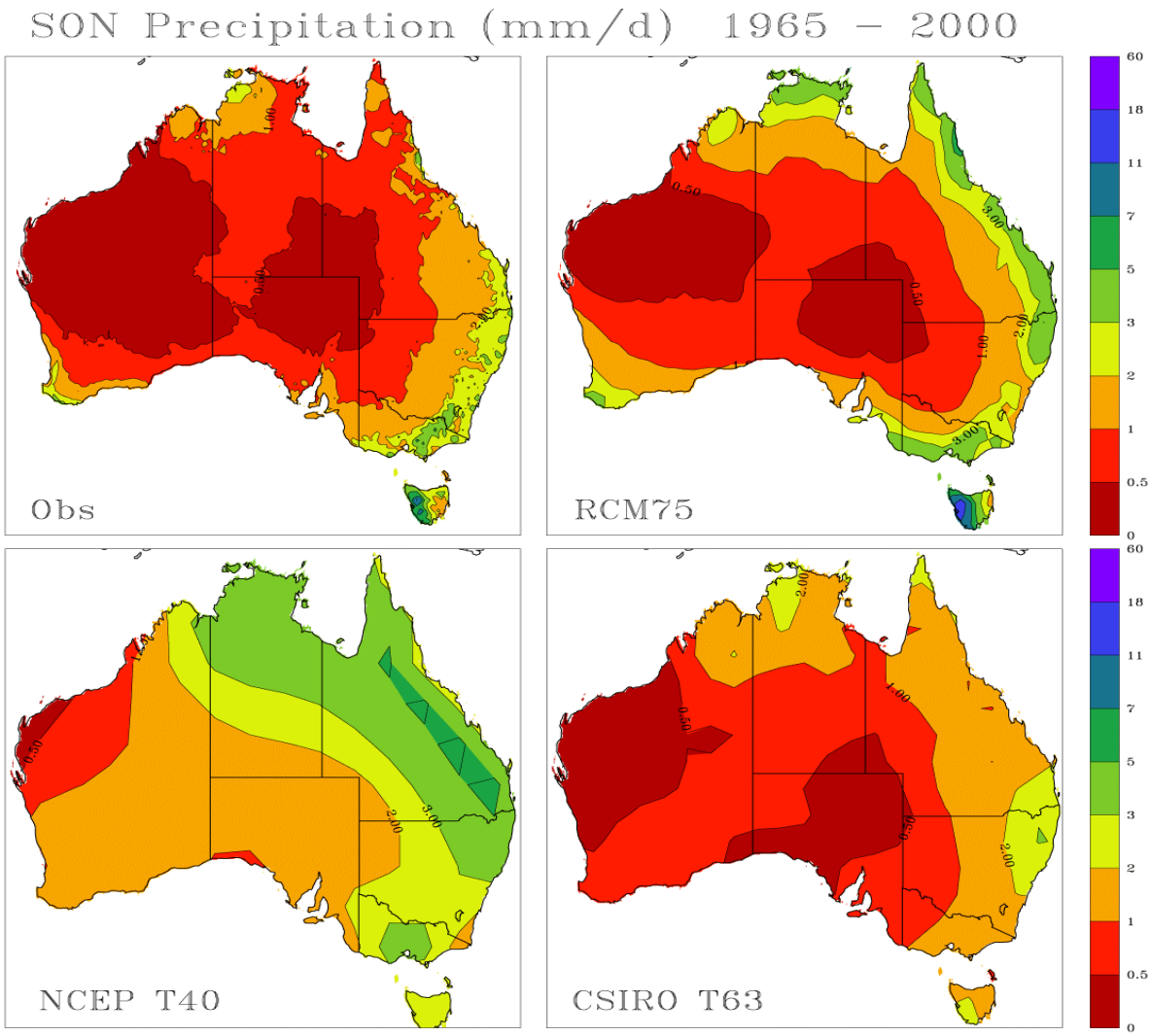

Figure 6.10b. Observed and simulated spring (SON, September-November) rainfall for Australia (mm/day) averaged for 1965-2000.

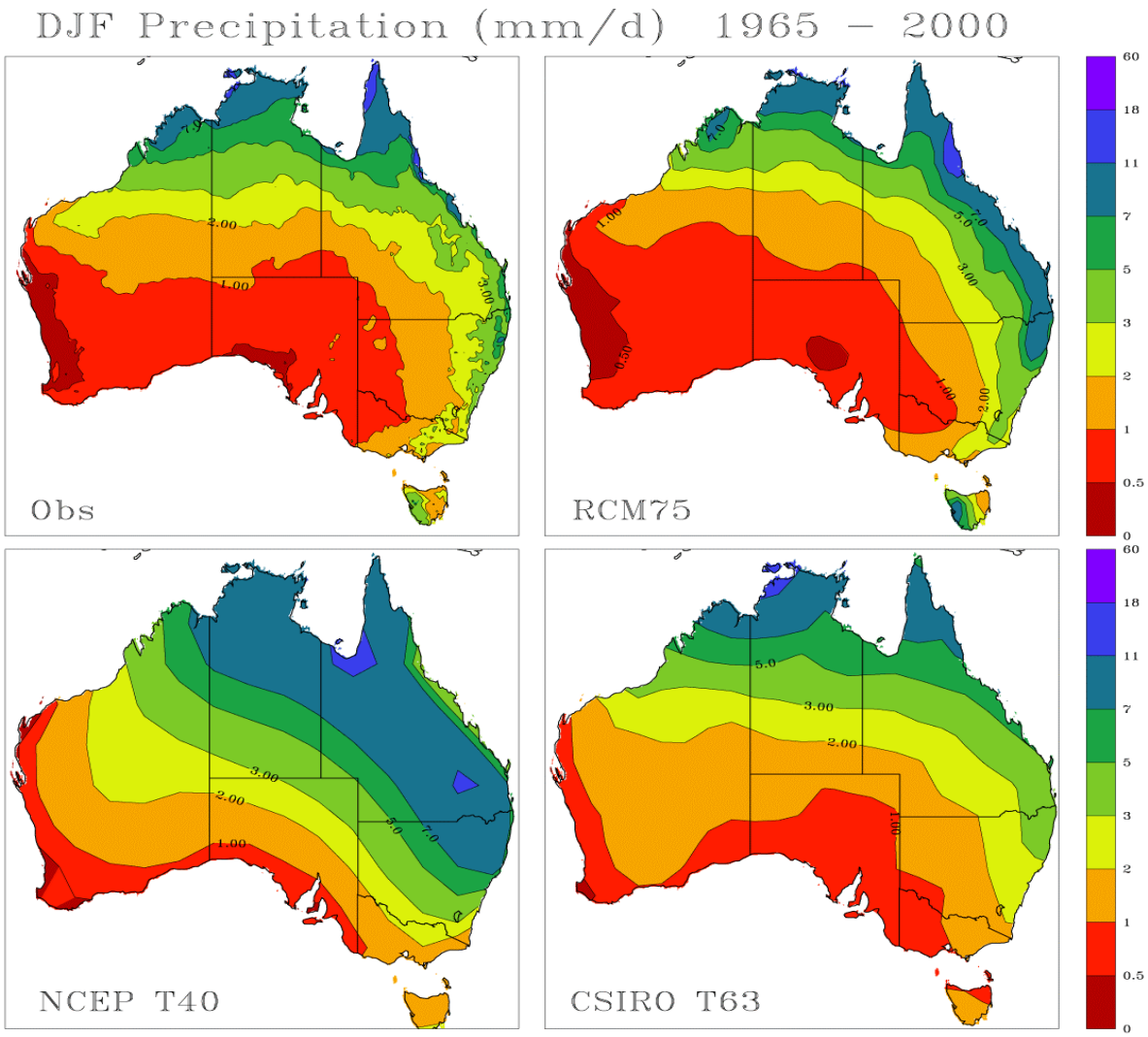

Figure 6.10c. Observed and simulated summer (DJF, December-February) rainfall for Australia (mm/day) averaged for 1965-2000.

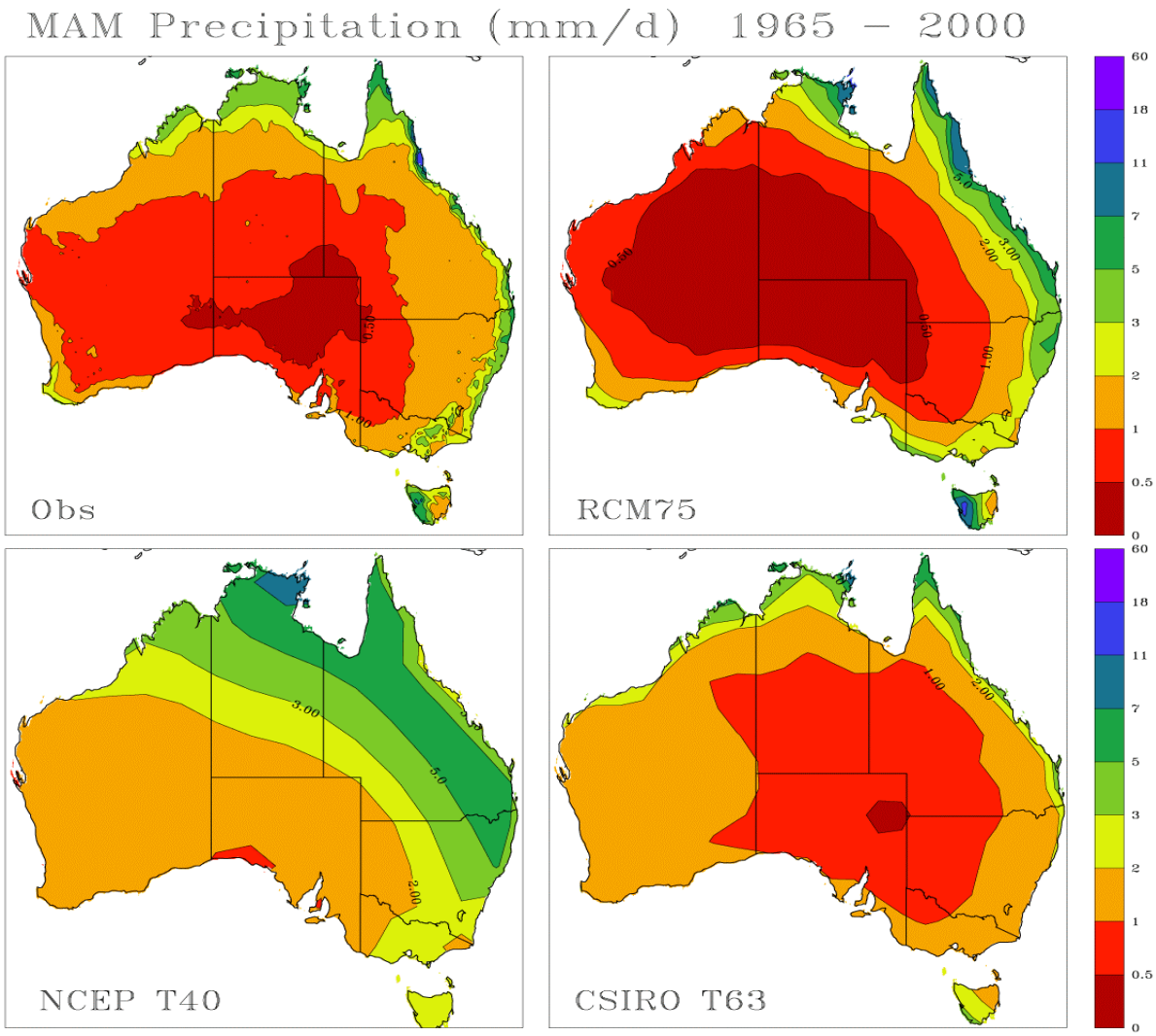

Figure 6.10d. Observed and simulated autumn (MAM, March-May) rainfall for Australia (mm/day) averaged for 1965-2000.

The 15 km RCM simulated sharp coastal gradients and 'rain shadows' in observed summer (DJF) although it was slightly 'wetter' across the transect from coast to inland. The simulated isohyet pattern for summer rainfall was in close agreement, i.e. parallel to coast. For winter (JJA) rainfall the 15 km RCM provided substantial improvement in terms of both average rainfall values and the spatial pattern.

Of particular note was the ability of the 15 km RCM to correctly represent the contrasting isohyet patterns of summer (DJF) and winter (JJA), namely: summer isohyets were parallel to the coast whilst winter (JJA) isohyets ran north/south. For spring (SON), the 15 km RCM performed better compared to the NCEP GCM and the 75 km RCM but was still wetter than observed. In autumn (MAM) there was close agreement in spatial pattern of isohyets and amount of rainfall for the 15 km RCM (Figures 6.11 and 6.12a, b, c, d).

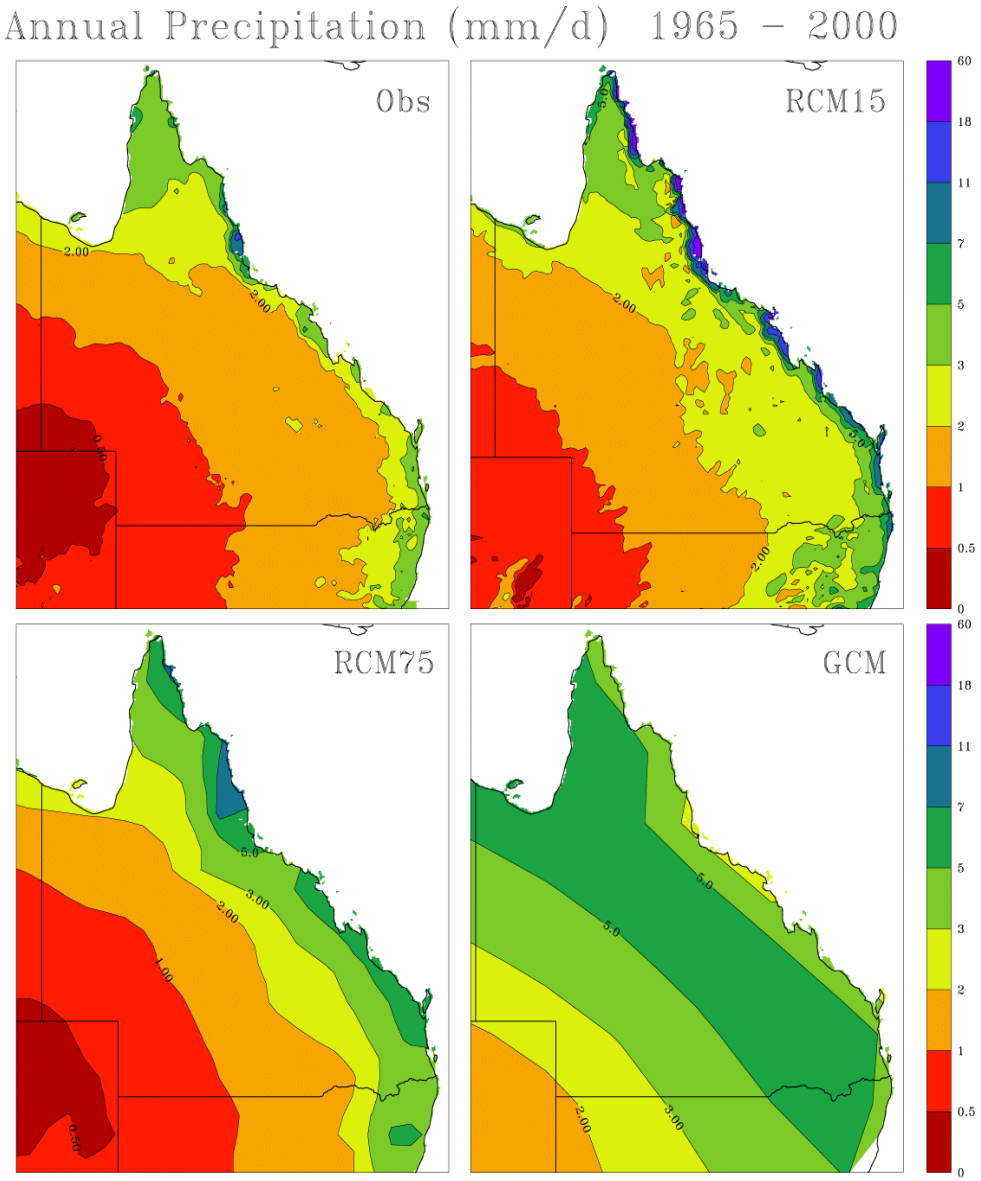

Figure 6.11. Observed and simulated annual precipitation for Queensland (mm/day) averaged for years 1965 to 2000. Simulated precipitation is from models with varying resolution: T40 (280 km), RCM75 (75 km) and RCM15 (15 km).

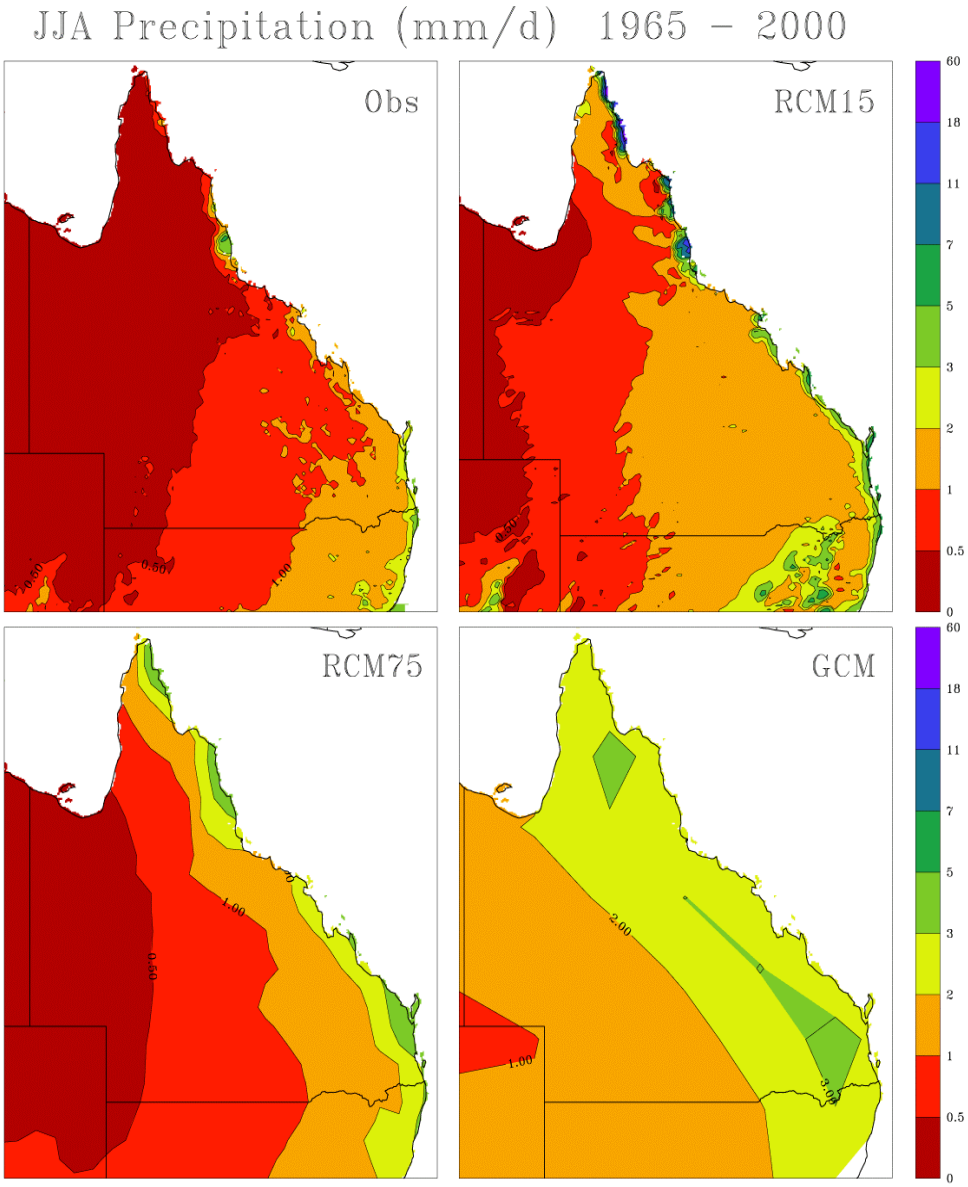

Figure 6.12a. Observed and simulated winter (JJA) rainfall for Queensland (mm/day) averaged for 1965-2000. Simulated rainfall was from models with varying resolution. T40 (280 km), RCM75 (75 km) and RCM15 (15 km).

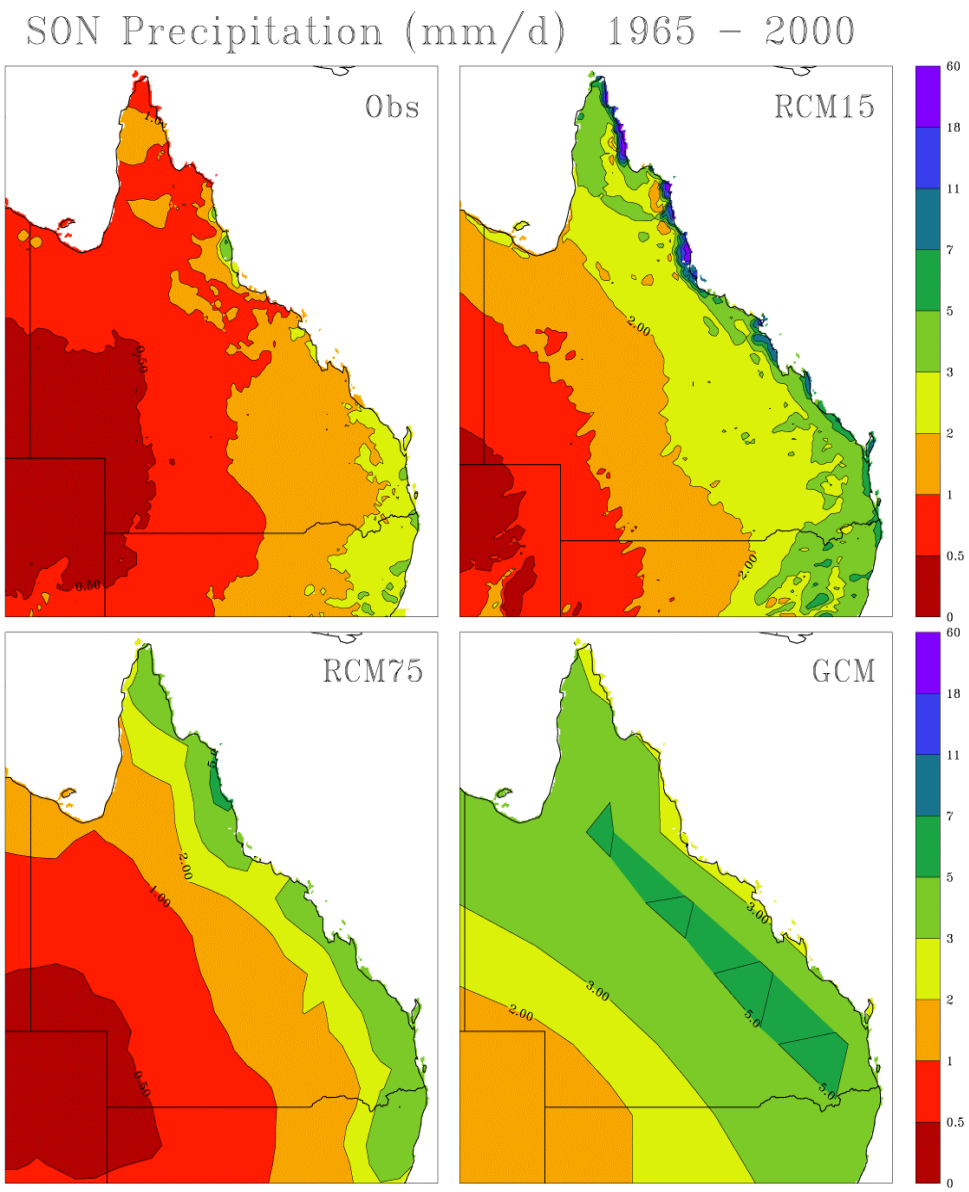

Figure 6.12b. Observed and simulated spring (SON) rainfall for Queensland (mm/day) averaged for 1965-2000. Simulated rainfall was from models with varying resolution. T40 (280 km), RCM75 (75 km) and RCM15 (15 km).

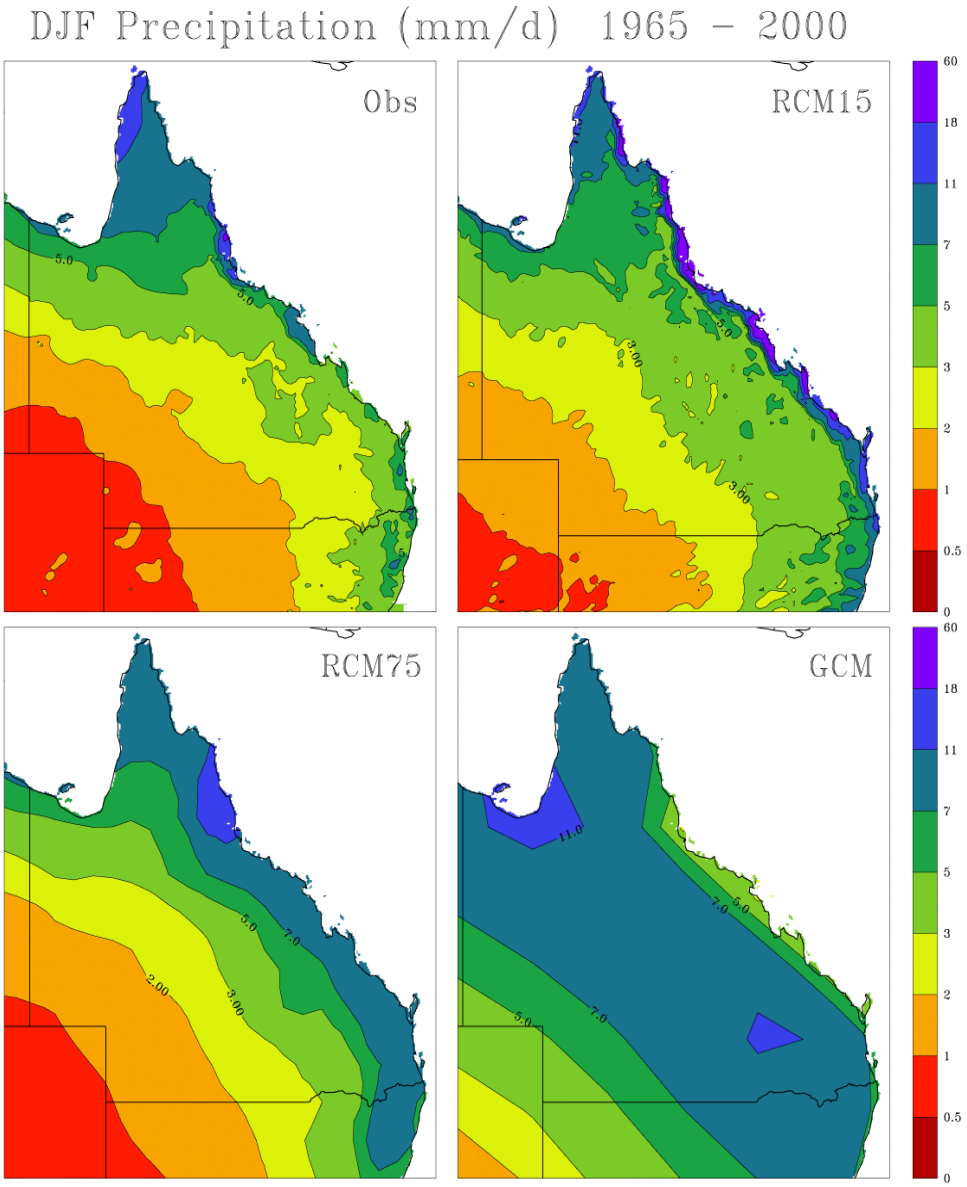

Figure 6.12c. Observed and simulated summer (DJF) rainfall for Queensland (mm/day) averaged for 1965-2000. Simulated rainfall was from models with varying resolution. T40 (280 km), RCM75 (75 km) and RCM15 (15 km).

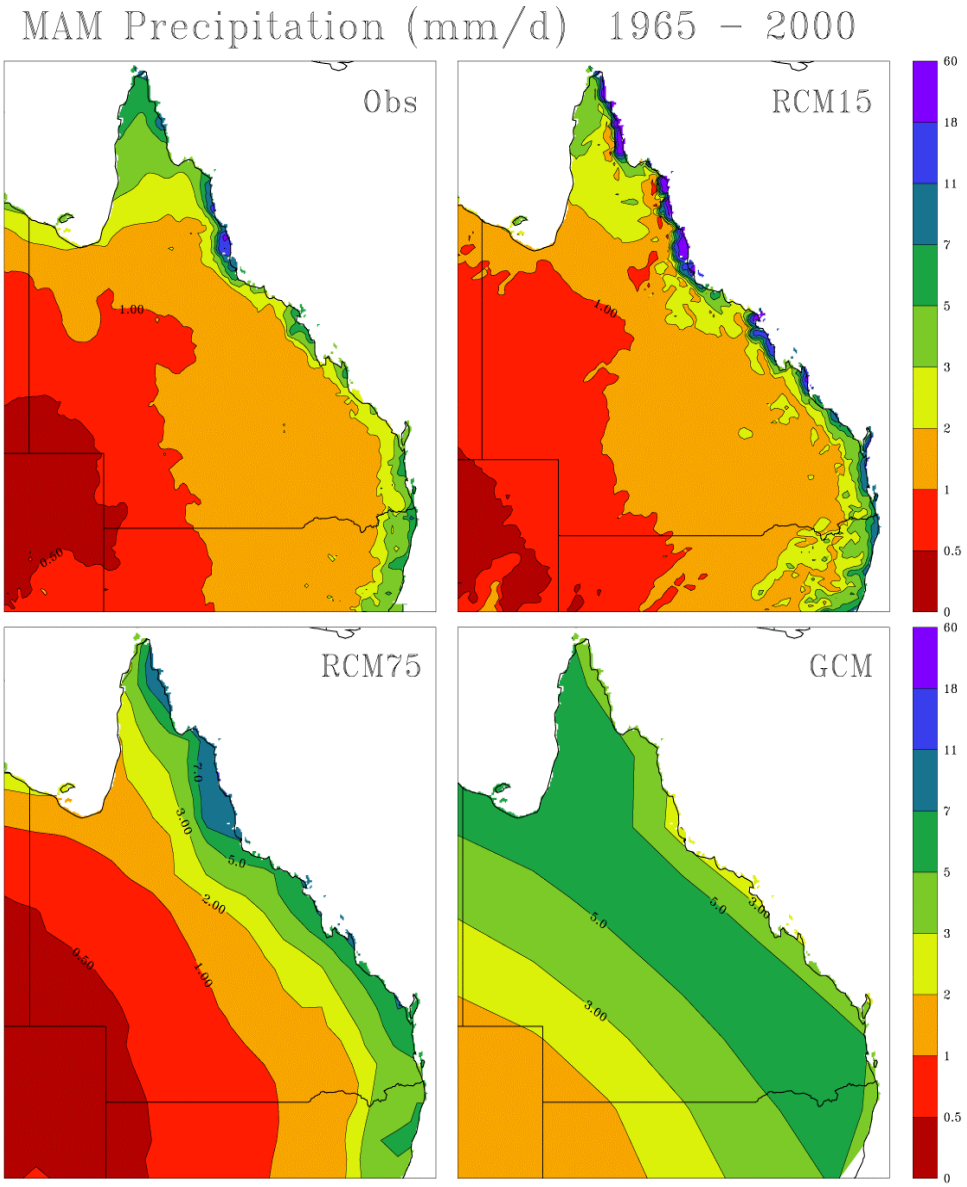

Figure 6.12d. Observed and simulated autumn (MAM) rainfall for Queensland (mm/day) averaged for 1965-2000. Simulated rainfall was from models with varying resolution. T40 (280 km), RCM75 (75 km) and RCM15 (15 km).

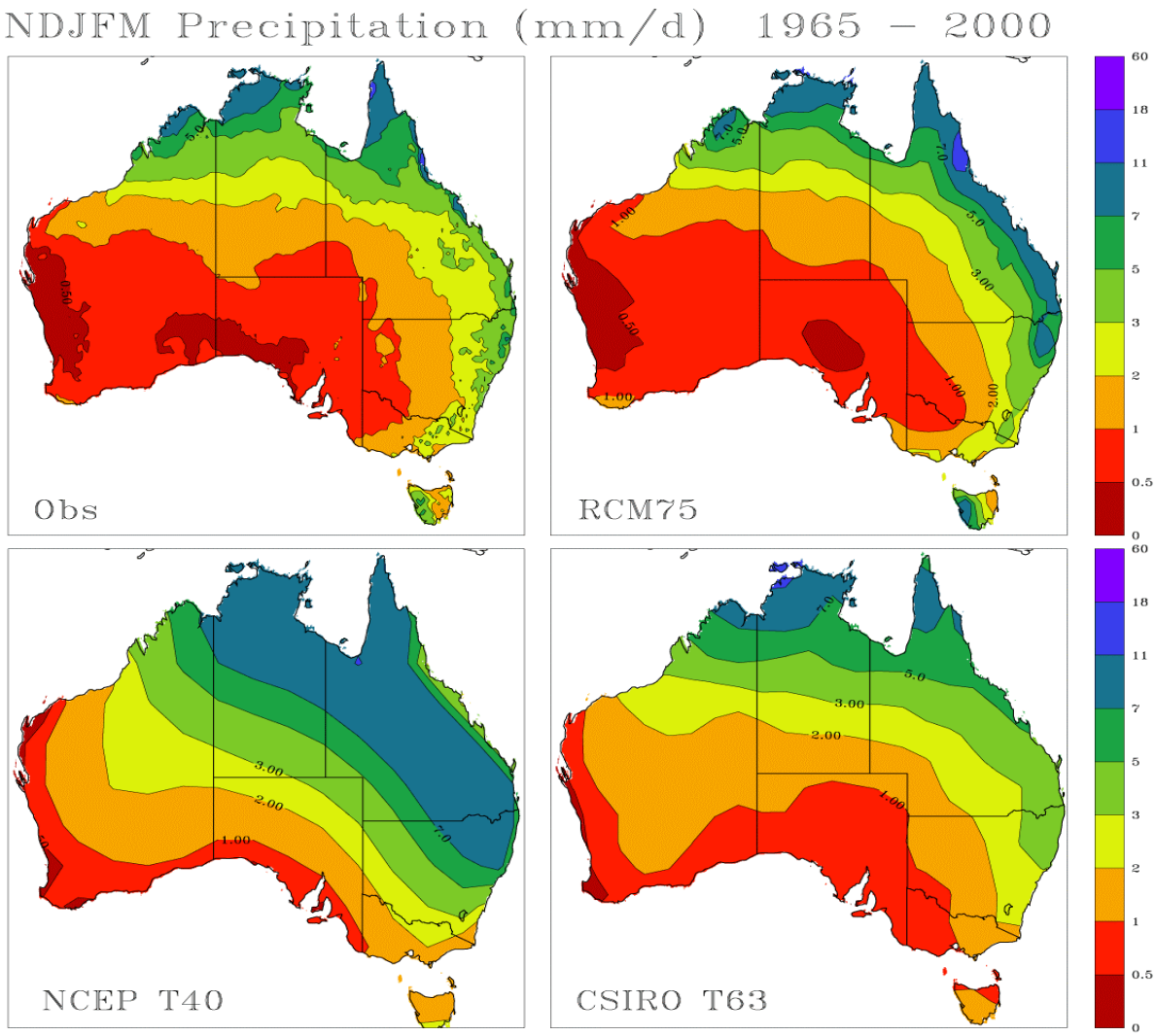

Figure 6.13. Observed and simulated rainfall for Australia (mm/day) averaged for years 1965 to 2000 for summer pasture growing season (November to March).

Figures 6.13 and 6.14 show the comparison between simulated rainfall from the various models and observed rainfall for the summer pasture growing season (November to March). For Australia (Figure 6.13) the RCM75 and T63 showed very good agreement with the continental distribution of summer rainfall (high in north-east, low in Western Australia). For Queensland the RCM15 showed improvement compared to RCM75 with high rainfall being restricted to coastal areas in agreement with observations. However, RCM15 still generally simulated wetter conditions across Queensland than observed rainfall.

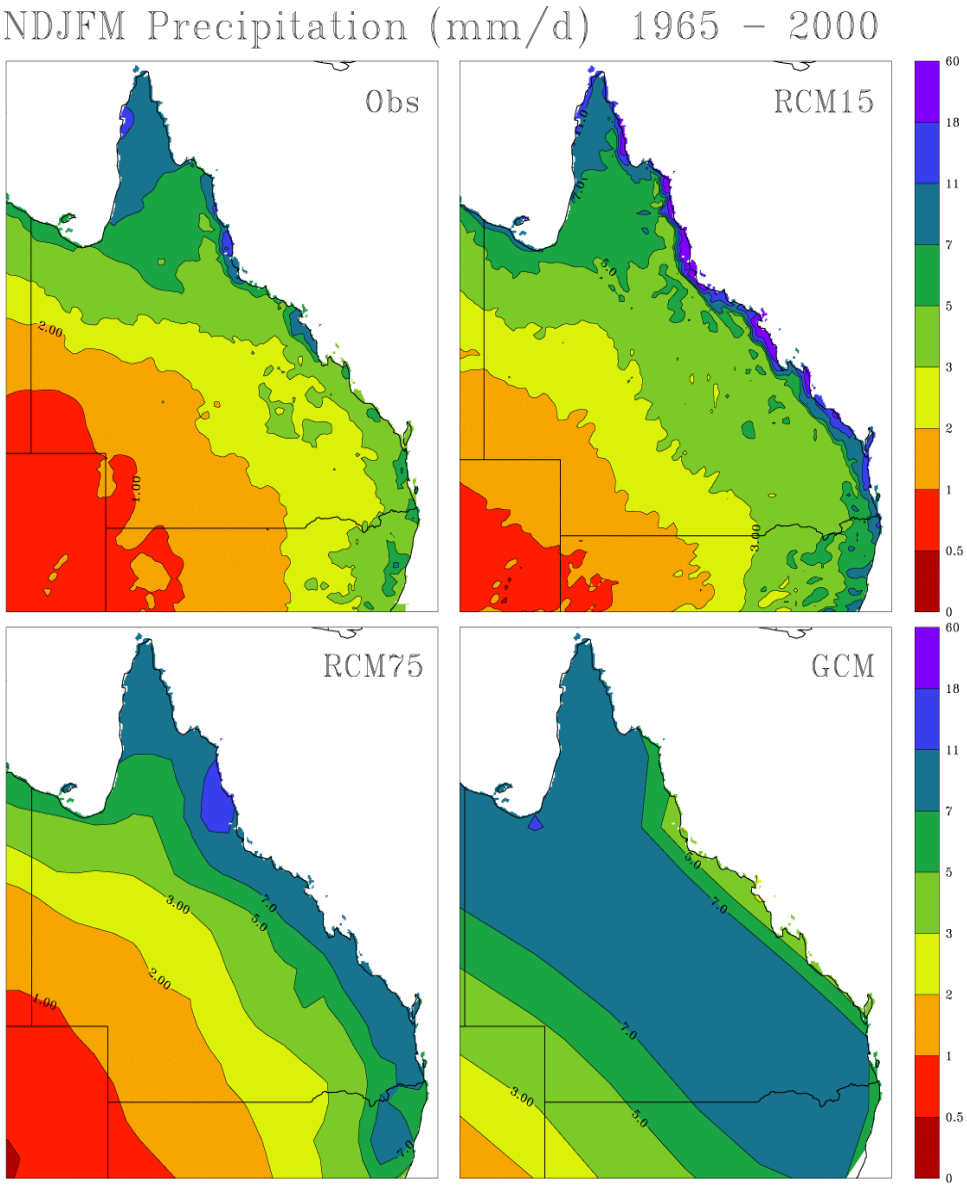

Figure 6.14. Observed and simulated rainfall for Queensland (mm/day) averaged for 1965-2000 for the summer pasture growing season (November to March).

Formal calculation of differences between observed and simulated rainfall (Figure 6.15) indicated that most of the seasons had large areas with less than +/- 1mm/day difference. An exception was spring (SON) in which the differences for a substantial part of inland Queensland were 1-2mm/day, and the coastal strip 2-10mm/day.

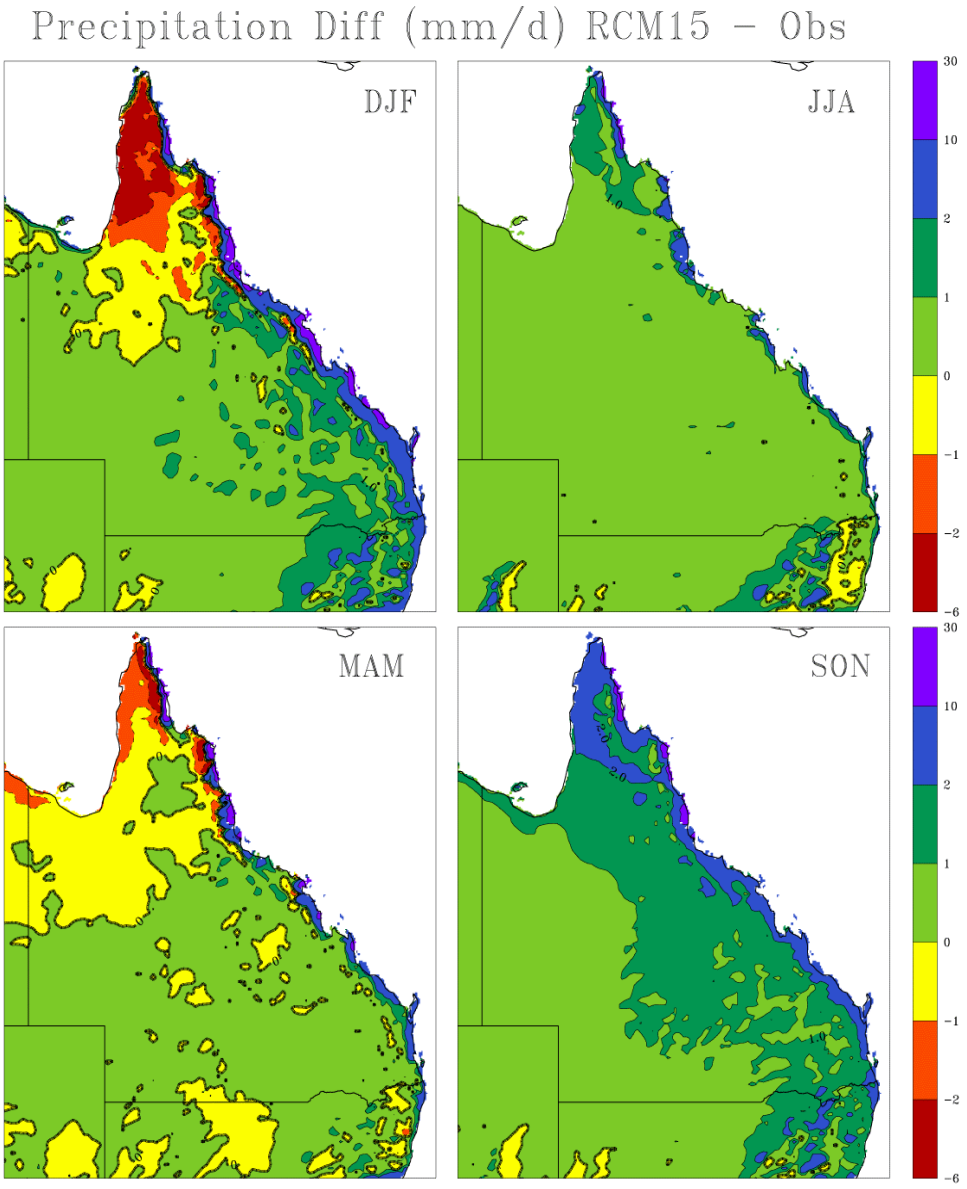

Figure 6.15. Differences between observed and simulated rainfall (15 km RCM, mm/day) across Queensland.

Comparison of models with CINRS' grided surfaces of rainfall observations in terms of mean, standard deviation and spatial correlation (Table 6.2, Figure 6.16) for different regions of Australia indicated the general superiority of the CSIRO T63 GCM compared to the NCEP GCM, and the improvement gained from the 75 and 15 km RCMs.

Table 6.2. Mean, standard deviation (SD) and spatial correlation for models compared with long-term (1965-2000) observed rainfall for DJF. The regions for area-averaged rainfall are: 1) Australia including Tasmania; 2) southern Australia, south of latitude 30; 3) northern Australia, north of latitude 30; 4) eastern Australia, east of longitude 140; 5) NSW and Victoria; 6) Queensland; and 7) the Queensland pastoral and cropping zone (see Figure 6.16). The spatial pattern correlation was calculated for the observed and simulated average (1965-2000) DJF rainfall at the resolution of the particular model. Thus the correlation values represent the explanation of spatial variation not temporal variation. Mean and SD of the observed rainfall was derived from data at 75 km resolution. Model data are the average of an ensemble of 1 to 15 model runs.

Region	Model	Mean (mm/day)	SD (mm/day)	Correlation (r)
Australia	Observed	4.2	3.2	
	RCM75	4.6	3.3	0.92
	T40	4.4	3.5	0.48
	T63	3.2	2.4	0.79
Southern Australia	Observed	1.4	1.0	
	RCM75	2.0	1.6	0.91
	T40	2.0	1.8	0.32
	T63	1.3	0.6	0.77
Northern Australia	Observed	4.8	3.1	
	RCM75	5.2	3.2	0.915
	T40	5.5	3.5	0.49
	T63	4.0	2.5	0.75
Eastern Australia	Observed	5.4	3.0	
	RCM75	6.0	2.7	0.88
	T40	5.7	3.6	0.01
	T63	3.5	1.9	0.78
NSW and Victoria	Observed	1.7	1.1	
	RCM75	2.3	1.6	0.92
	T40	5.0	3.0	0.54
	T63	1.7	0.7	0.88
Queensland	Observed	3.8	2.6	
	RCM15	4.6	3.5	0.76
	RCM75	4.6	3.0	0.79
	T40	9.7	1.5	0.52
	T63	4.0	1.9	0.95
Queensland pastoral and cropping zone	Observed	3.1	1.4	
	RCM15	4.6	3.4	0.78
	RCM75	4.4	2.5	0.73
	T40	9.7	1.4	0.73
	T63	3.5	1.1	0.88

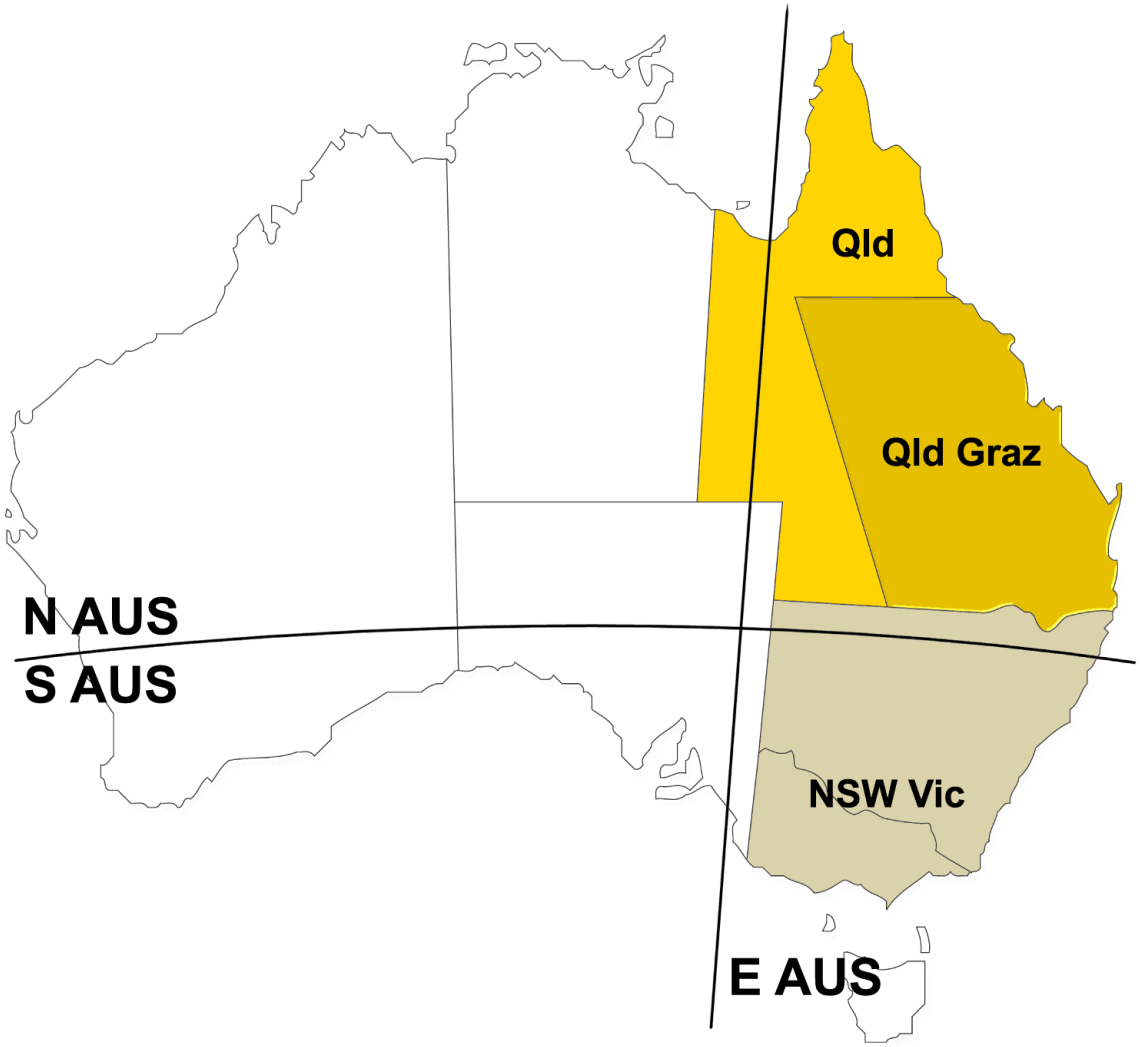

Figure 6.16. Different regions of Australia for which the models were compared with observed rainfall (See Table 6.2).

6.6 Simulation of rainfall variability over time

The capability of the models to simulate temporal inter-annual variability of rainfall was evaluated in terms of: (a) standard deviation (SD) over time; (b) spatial and temporal patterns of anomaly correlation; and (c) correlations with SOI.

The ratio of model SD to actual SD (SD ratio) provided a measure of the accuracy of the models in representing inter-annual rainfall variability (Figure 6.17a-d). There was considerable spatial variation in the SD ratio. For summer (DJF), the NCEP GCM and 75 km RCM had both areas of substantially greater and lower variation than the observed variation, whilst the CSIRO T63 GCM and 15 km RCM simulations tended to be more uniform in terms of the SD ratio. The 15 km RCM SD ratios were close to 1.0 for south-east and central Queensland but were lower in Cape York and western Queensland.

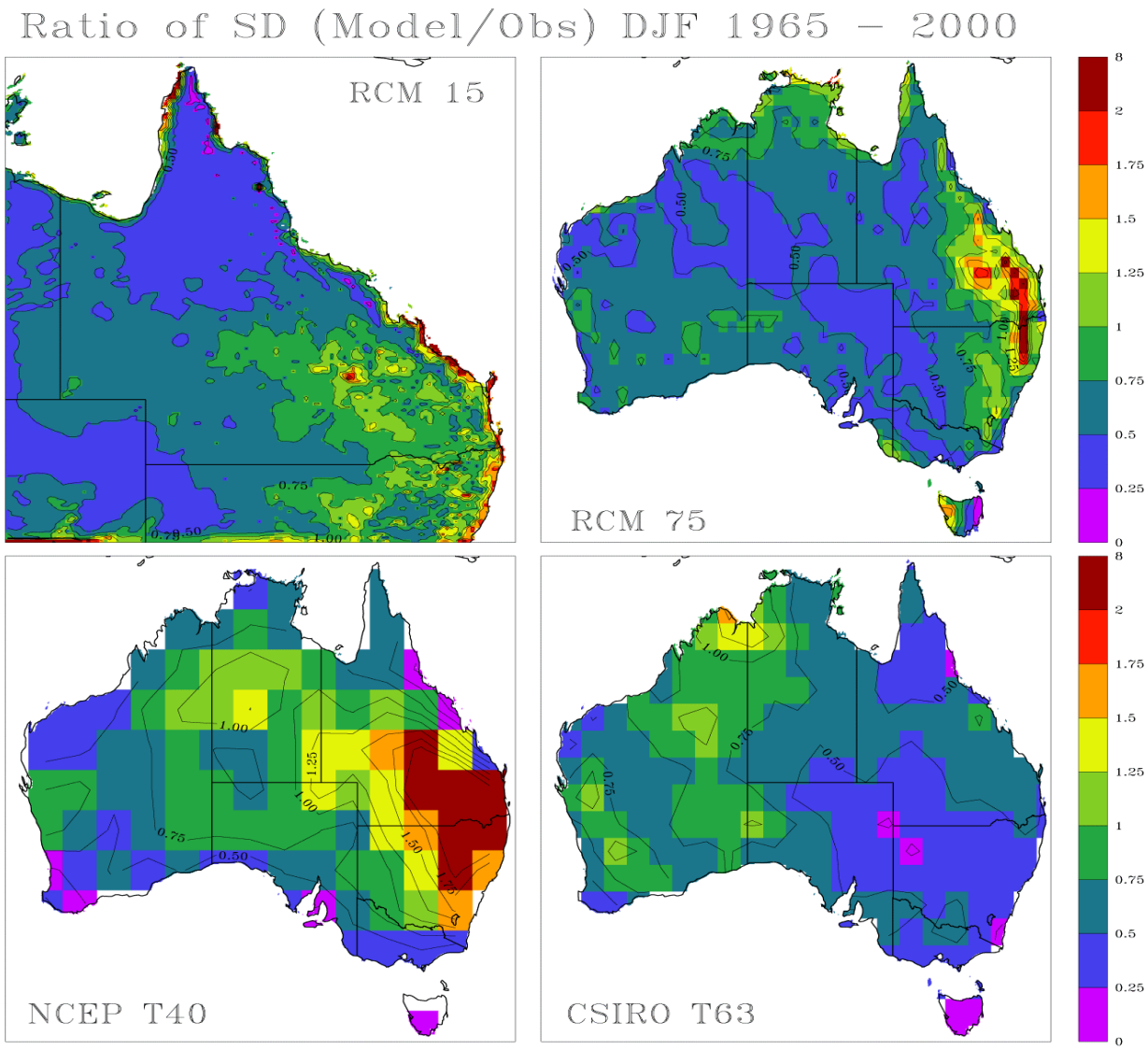

Figure 6.17a. Ratio of simulated (ensemble mean) and observed standard deviation of seasonal (DJF) rainfall for 1965-2000.

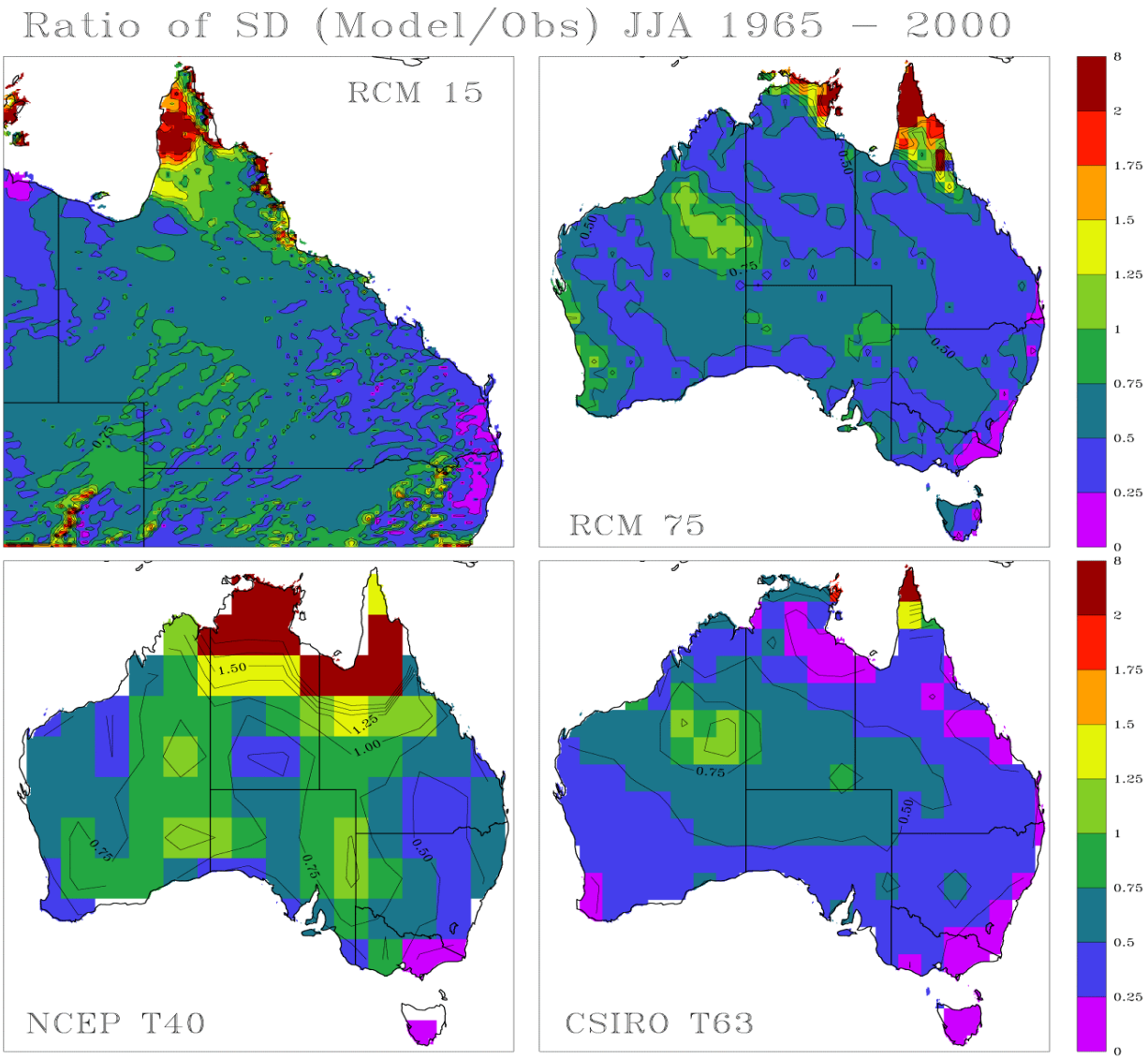

Figure 6.17b. Ratio of simulated (ensemble mean) and observed standard deviation of seasonal (JJA) rainfall for 1965-2000.

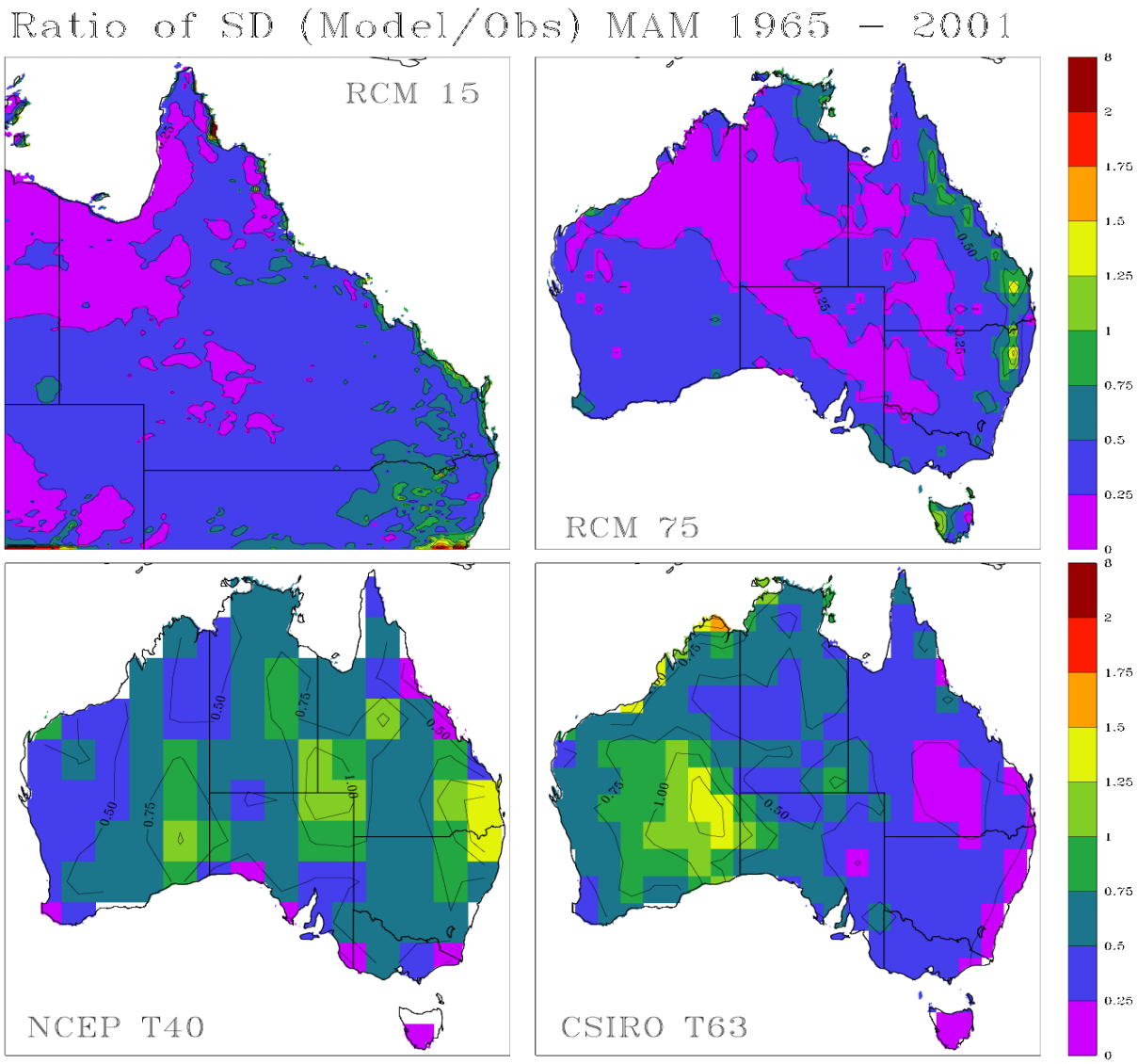

Figure 6.17c. Ratio of simulated (ensemble mean) and observed standard deviation of seasonal (MAM) rainfall for 1965-2000.

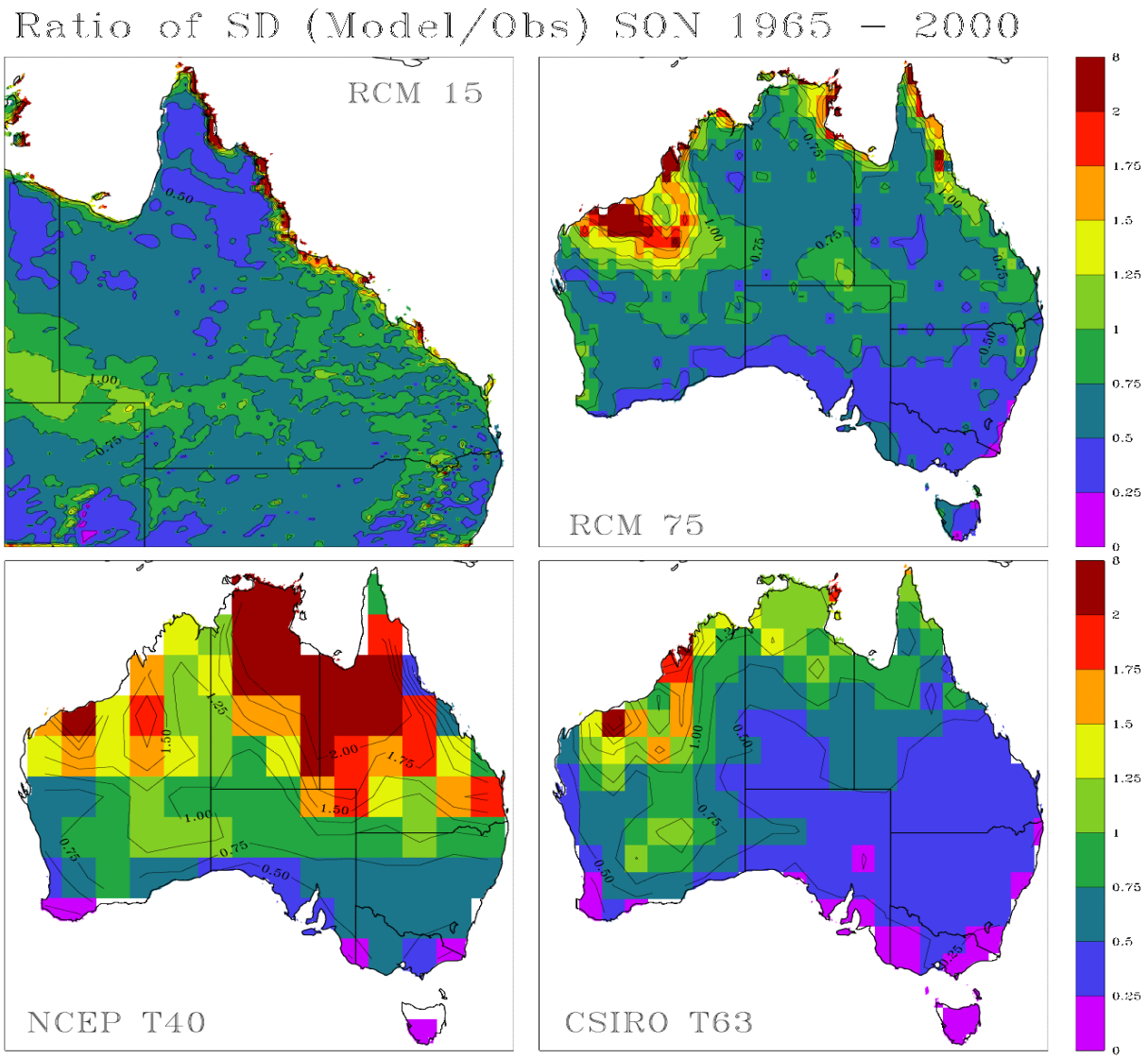

Figure 6.17d. Ratio of simulated (ensemble mean) and observed standard deviation of seasonal (SON) rainfall for 1965-2000.

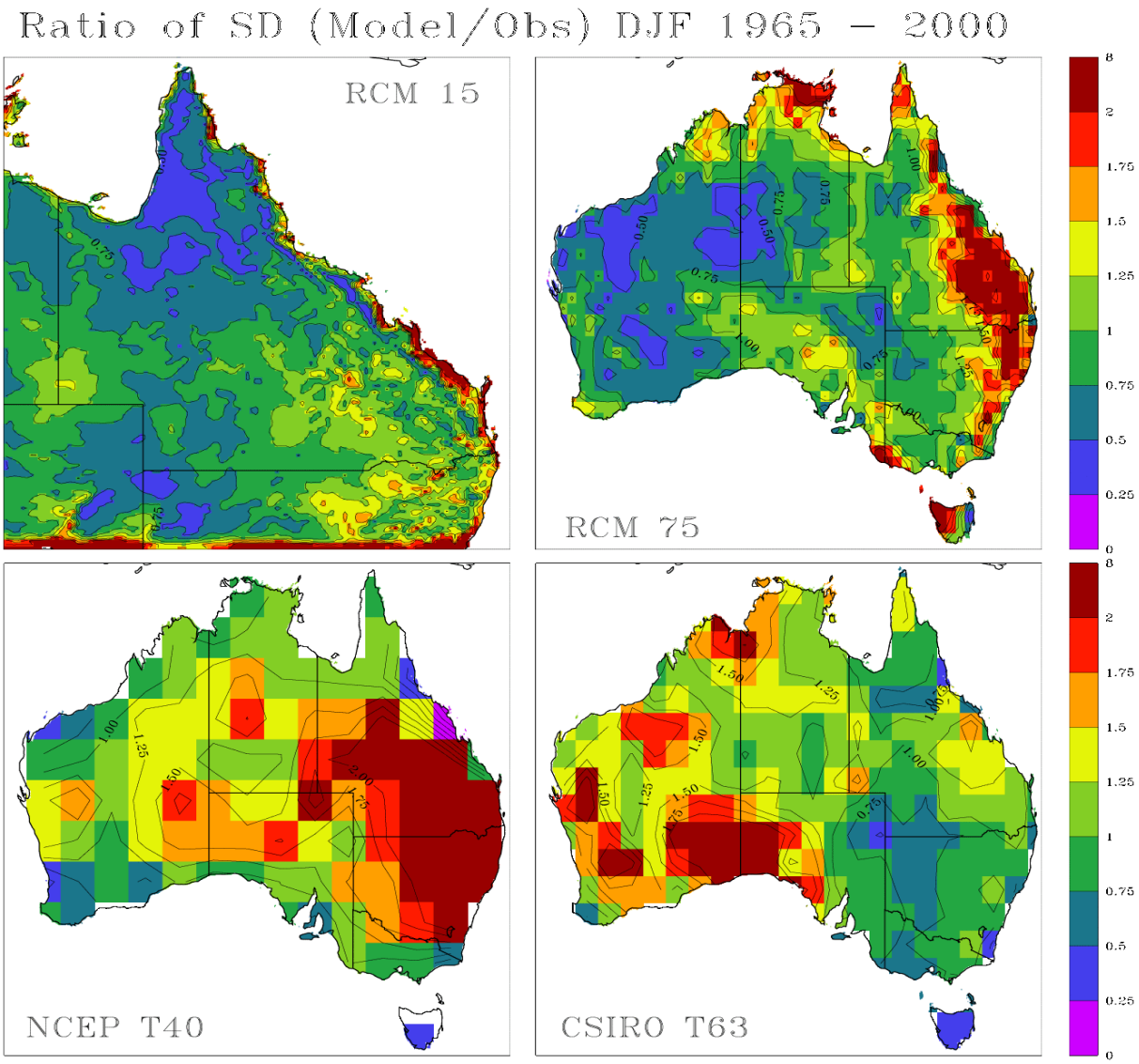

Figure 6.17e. Ratio of simulated (single model run) and observed standard deviation of seasonal (DJF) rainfall for 1965-2000.

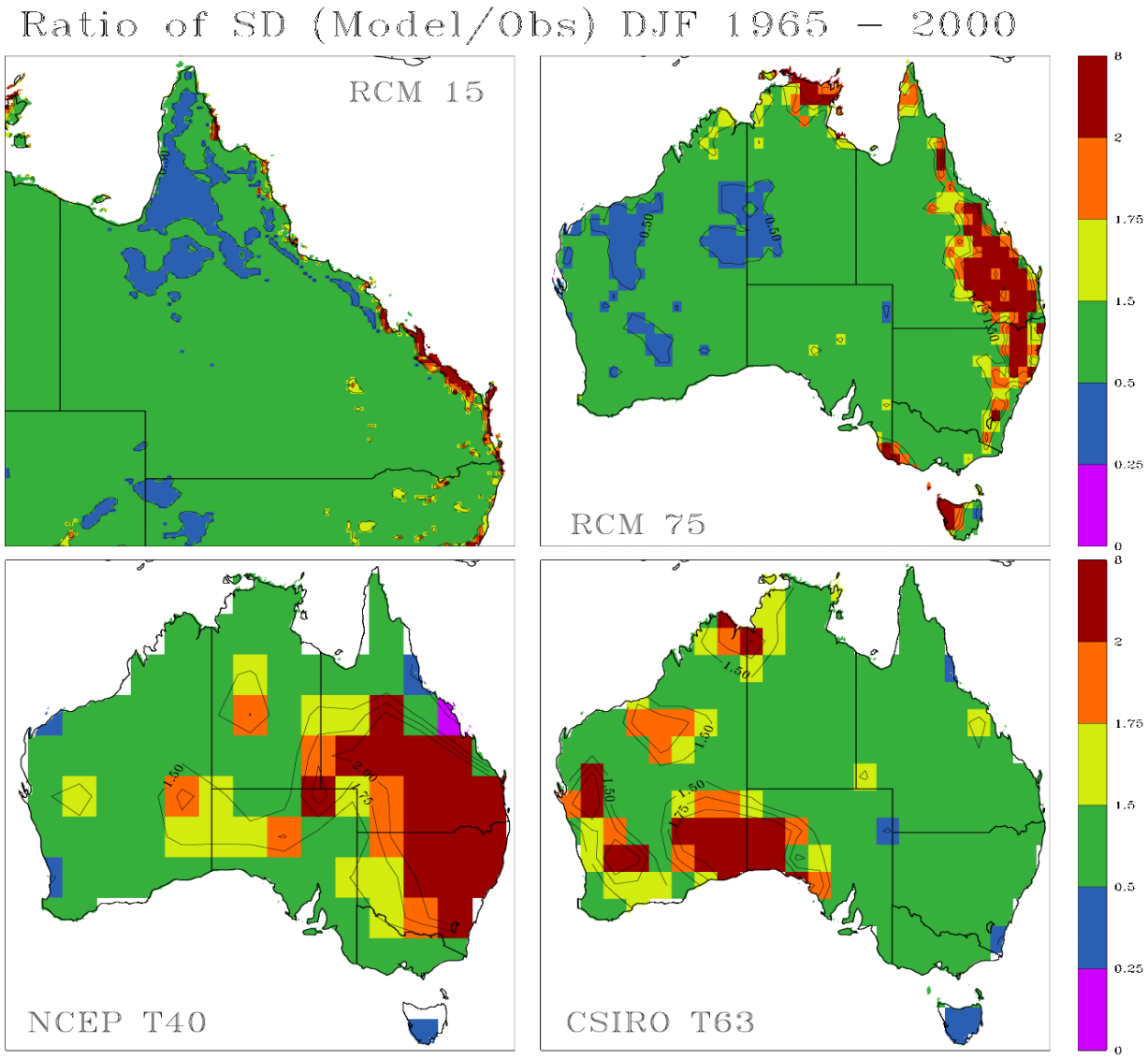

Figure 6.17f. Ratio of simulated (ensemble mean) and observed standard deviation of seasonal (DJF) rainfall for 1965-2000. This figure is the same as for Figure 6.17a but has a modified contouring interval to highlight those areas with a SD ratio between .5 and 1.5.

For winter (JJA), the CSIRO T63 GCM and the 75 km and 15 km RCMs had lower variation than observed whilst the NCEP GCM had large areas of agreement in central Australia. For autumn (MAM), the CSIRO T63 GCM and the 75 km and 15 km RCMs had substantial areas with lower variability than was observed (SD ratio 0-0.5). However, in spring (SON), agreement was closer for the 75 km and 15 km RCMs. In contrast, the NCEP GCM had much greater variability than observed spring rainfall in large areas of northern Australia (SD ratio >1.50).

In general, the climate models would be expected to have a lower-than observed standard deviation because (a) the models were forced using observed SSTs, whereas in the real climate system there are a number of other forcing factors which could result in increased inter-annual rainfall variability. In addition, the observed rainfall data used in this study is grided using interpolation of station; and (b) model runs are the average of ensembles which could dampen variability.

In our comparison (Figure 6.17a-d) the ensemble average data were used to compute the inter-annual standard deviation for the models. Figure 6.17e illustrates the standard deviation ratio for DJF seasonal rainfall where only a single model run (selected randomly) was used to compute the SD ratio. It is apparent that overall the SD ratio is closer to one when only a single model run is compared to the observed SD values. This is further emphasised in Figure 6.17f where all SD ratios between 0.5 and 1.5 are shown in one colour. Thus we believe there is close agreement between observed and simulated data given the limitations in model forcing and data collection and griding procedures. In general there is good skill in simulating inter-annual rainfall variability when using SD as a skill measure, especially for T63 CSIRO GCM and RCMs operating at 75 and 15 km.

6.7 Pattern correlation of observed and simulated rainfall over time

Correlations were calculated between observed rainfall and the mean of ensemble for each of the four models for the 36 years. Observed rainfall and correlation was calculated for each cell at the appropriate model resolution (Figure 6.18a, b). For annual rainfall, areas of reasonable correlation ($r > 0.4$, $n = 36$) were found in central Queensland and WA. For Queensland, the 15 km RCM showed large coastal and inland regions with significant ($P = 0.05$) correlations ($r > 0.2$). The important Queensland pastoral-cropping zone (Figure 6.16) had substantial areas with reasonable correlations ($r > 0.4$). All four models were similar in terms of areas with significant correlation, with the 15 km RCM performing best.

Correlations with observed seasonal rainfall varied considerably between models for each of the four seasons (Figure 6.19). For Australia, areas of significant correlation were highest in spring (SON). Winter and autumn also had large areas of reasonable correlation but summer had substantial areas of negative correlation. In autumn and winter the areas of significant correlation were in NSW and southern Queensland, enlarging to include SA, NT and some of Western Australia in spring. Only Queensland had substantial areas of significant correlations in summer across the four models (Figure 6.19).

For each season, the four models were reasonably consistent in terms of the Queensland regions where significant correlations occurred but regions varied from season to season (Figure 6.20a-d). In autumn and winter the regions of highest correlation were mainly in south-west Queensland, whilst in spring correlations were strongest in north-eastern Queensland. Correlations in summer were strongest in the south-eastern coastal region.

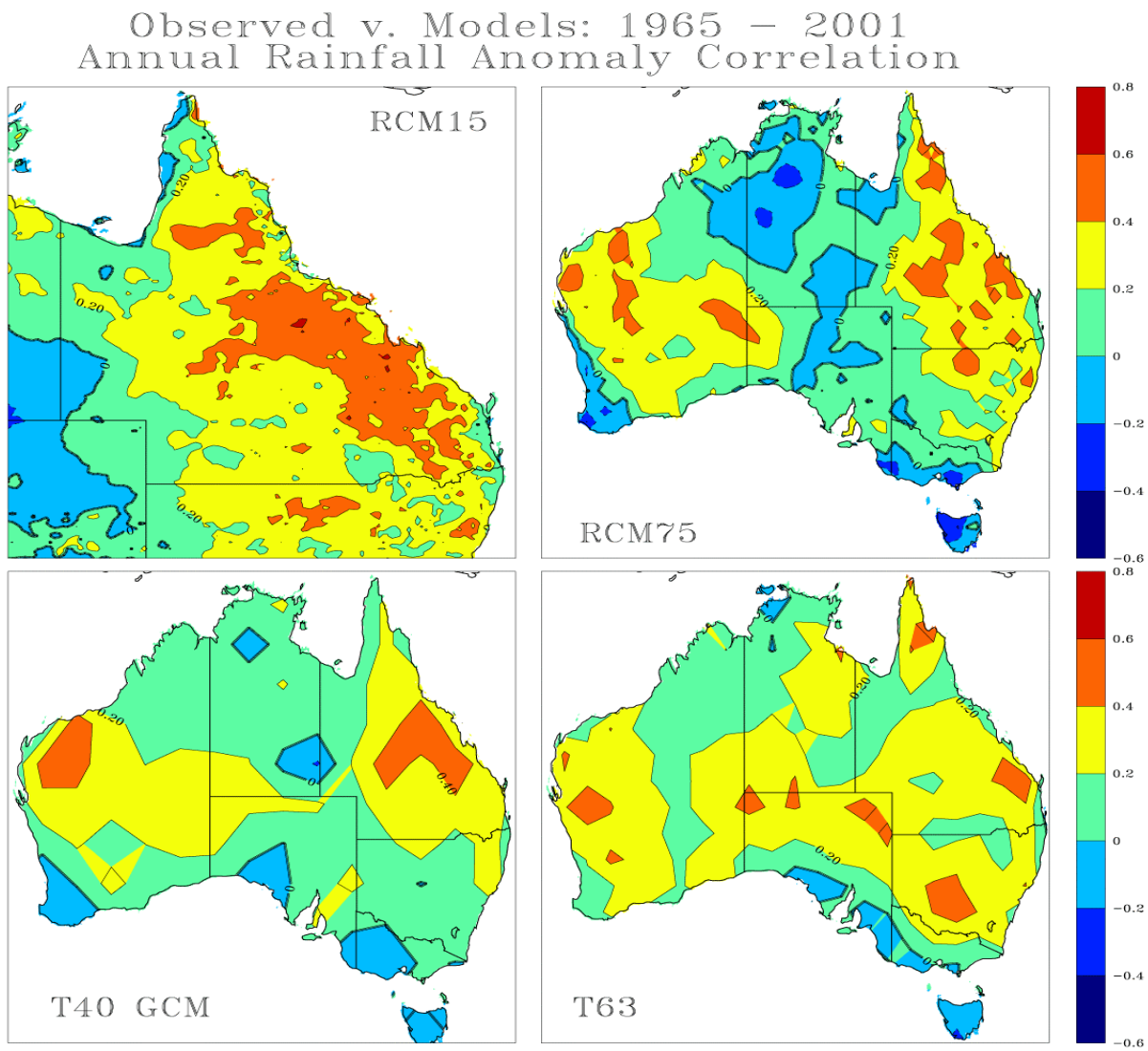

Figure 6.18a. Correlation (r) between observed and simulated annual Australian rainfall for 1965-2000 (36 years). Observed rainfall was calculated from NR&M grided rainfall surfaces and averaged for each cell of GCM and RCM output allowing direct comparison. Correlation values were then interpolated to give spatial patterns shown in the figure.

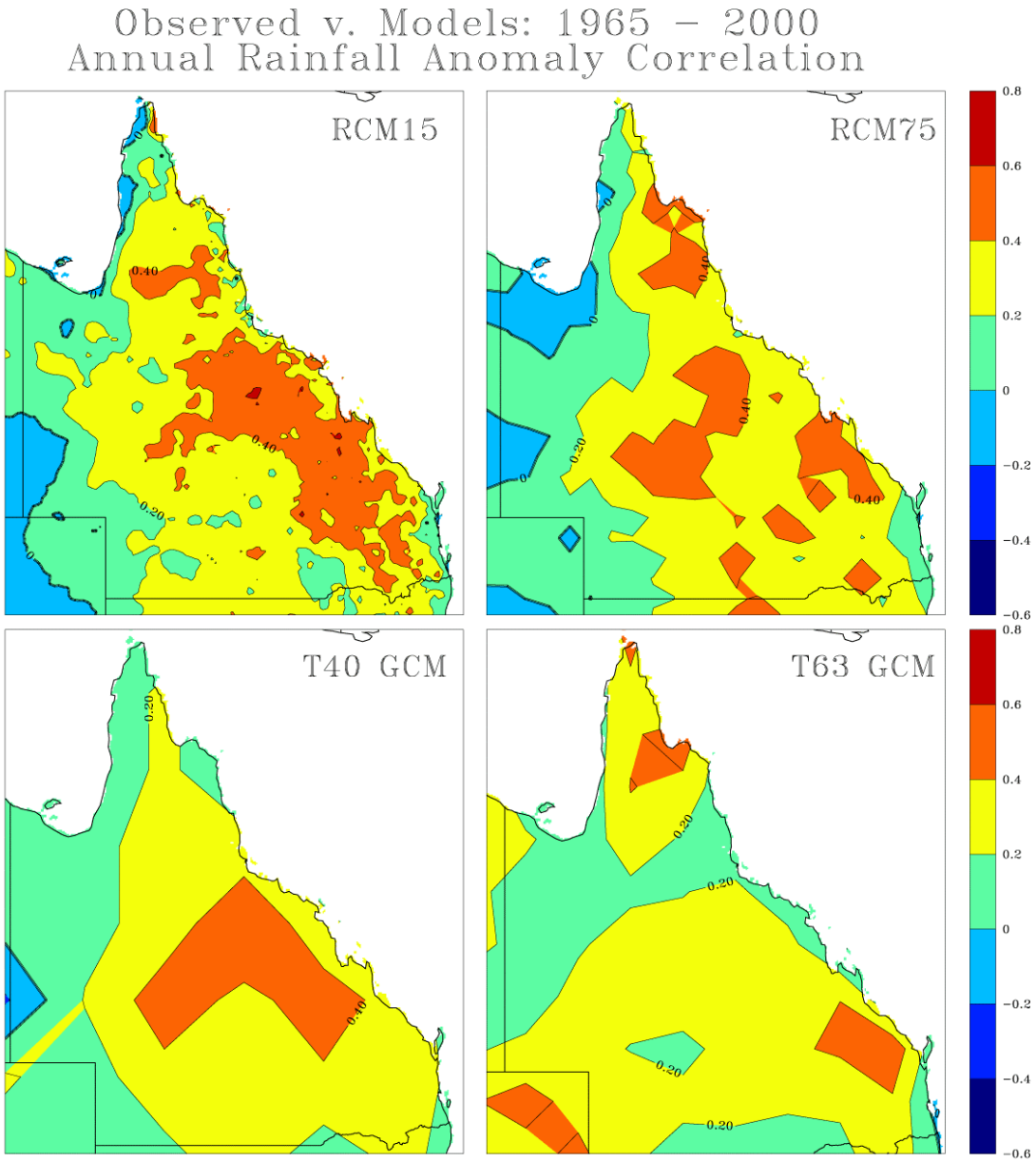

Figure 6.18b. Correlation (r) between observed and simulated annual Queensland rainfall for 1965-2000 (36 years). Observed rainfall was calculated from NR&M grided rainfall surfaces and averaged for each cell of GCM and RCM output allowing direct comparison. Correlation values were then interpolated to give spatial patterns shown in the figure.

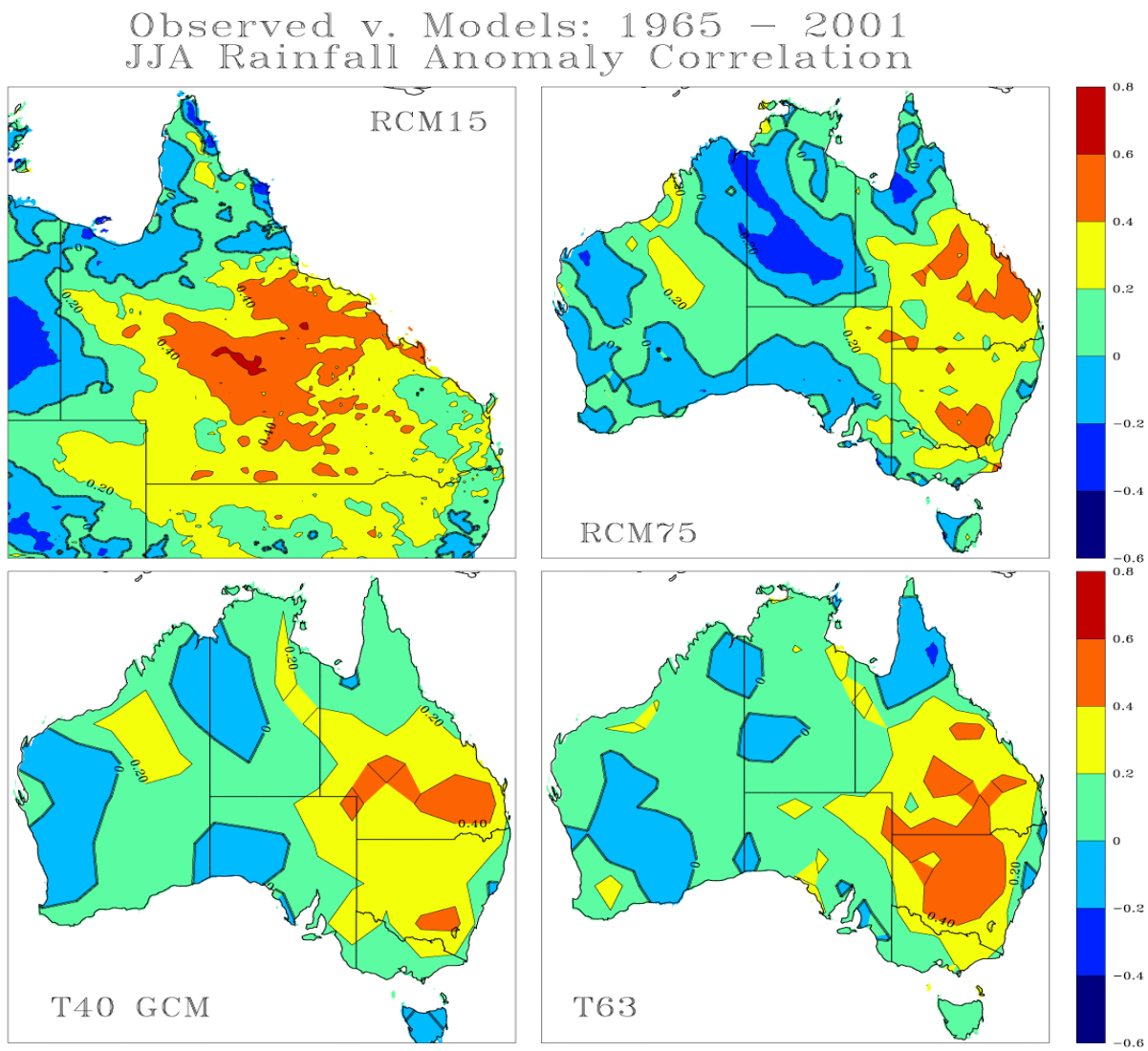

Figure 6.19a. Correlation (r) between observed and simulated winter (JJA) rainfall for 1965-2000 (36 years).

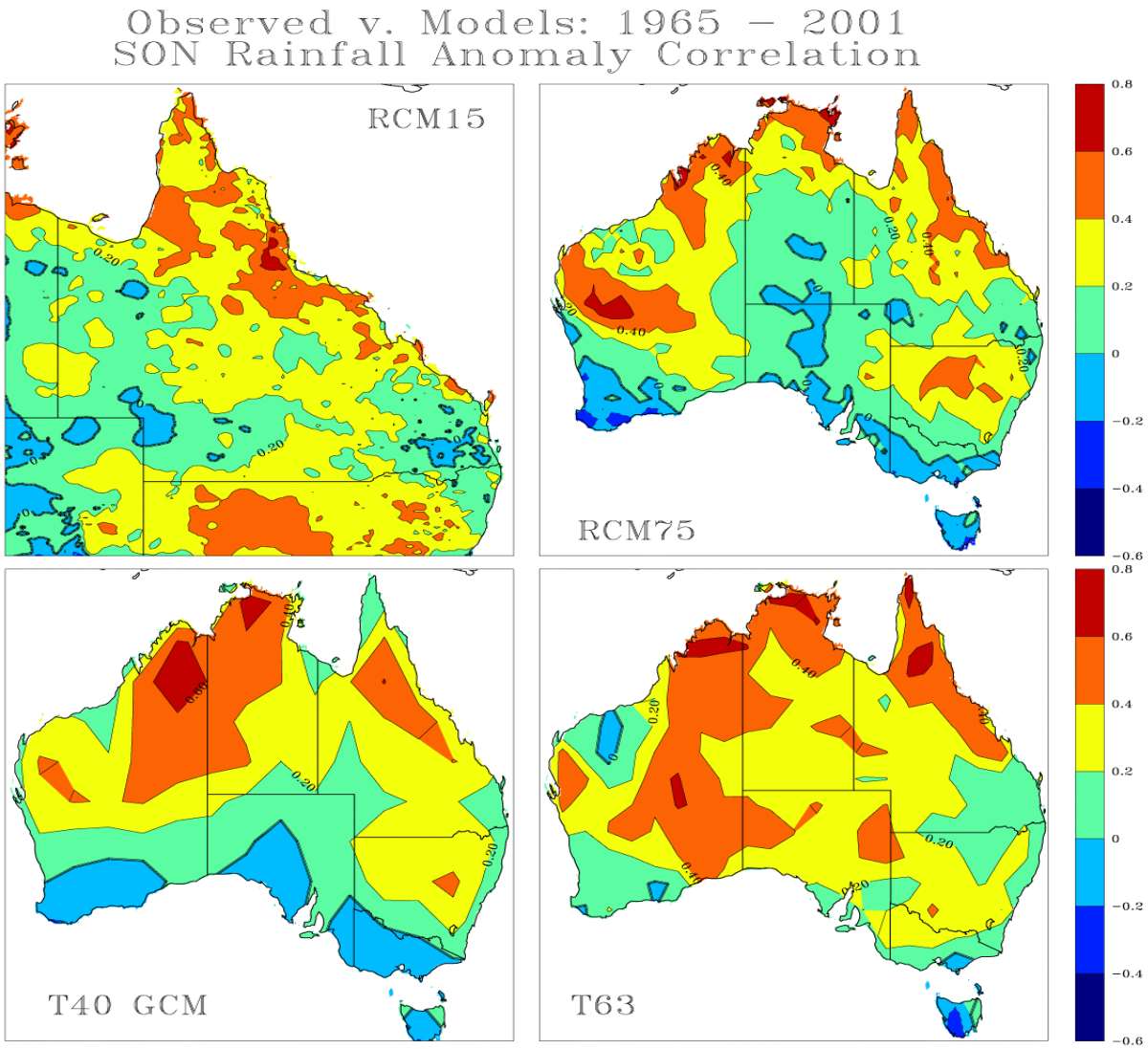

Figure 6.19b. Correlation (r) between observed and simulated spring (SON) rainfall for 1965-2000 (36 years).

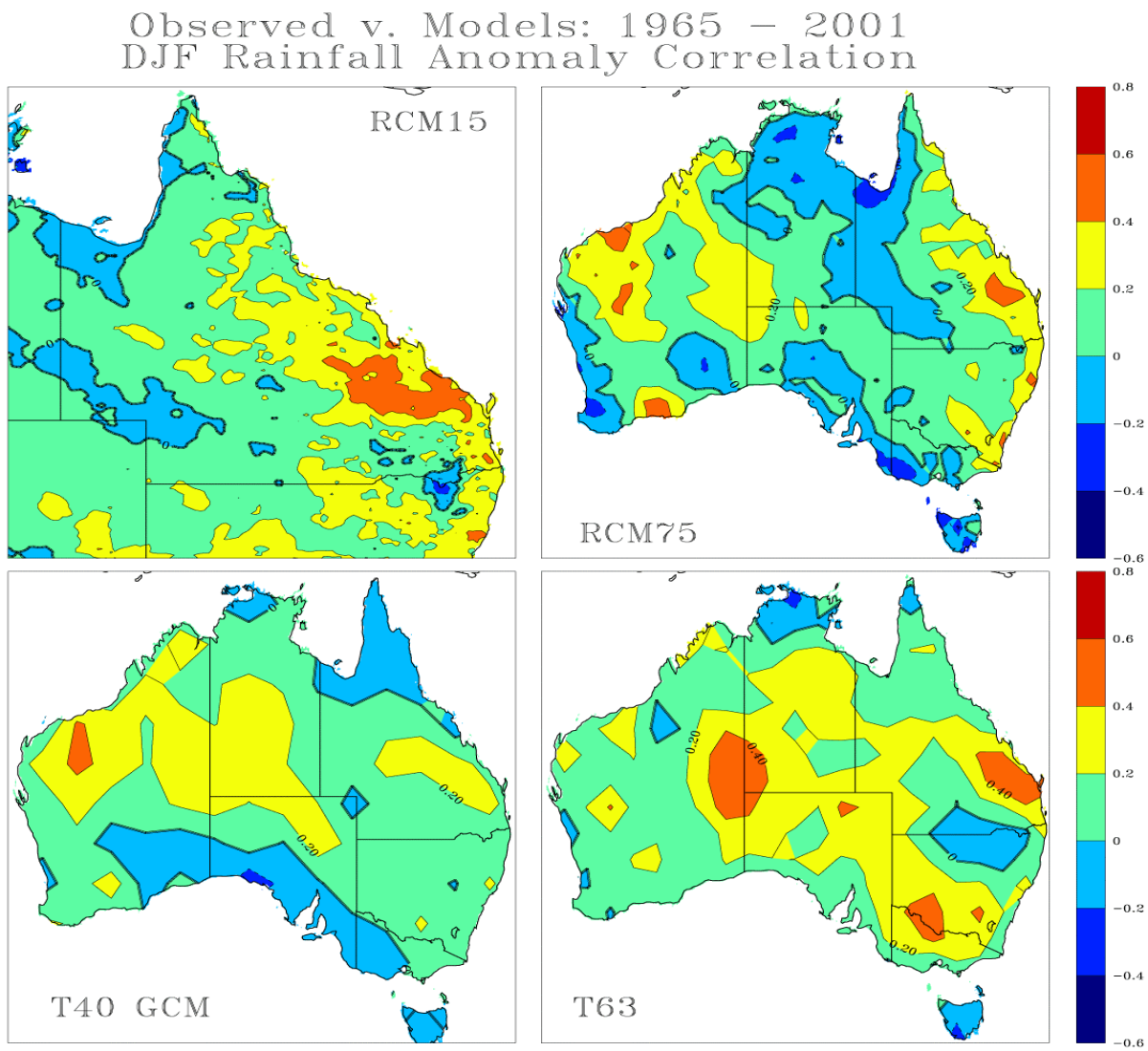

Figure 6.19c. Correlation (r) between observed and simulated summer (DJF) rainfall for 1965-2000 (36 years).

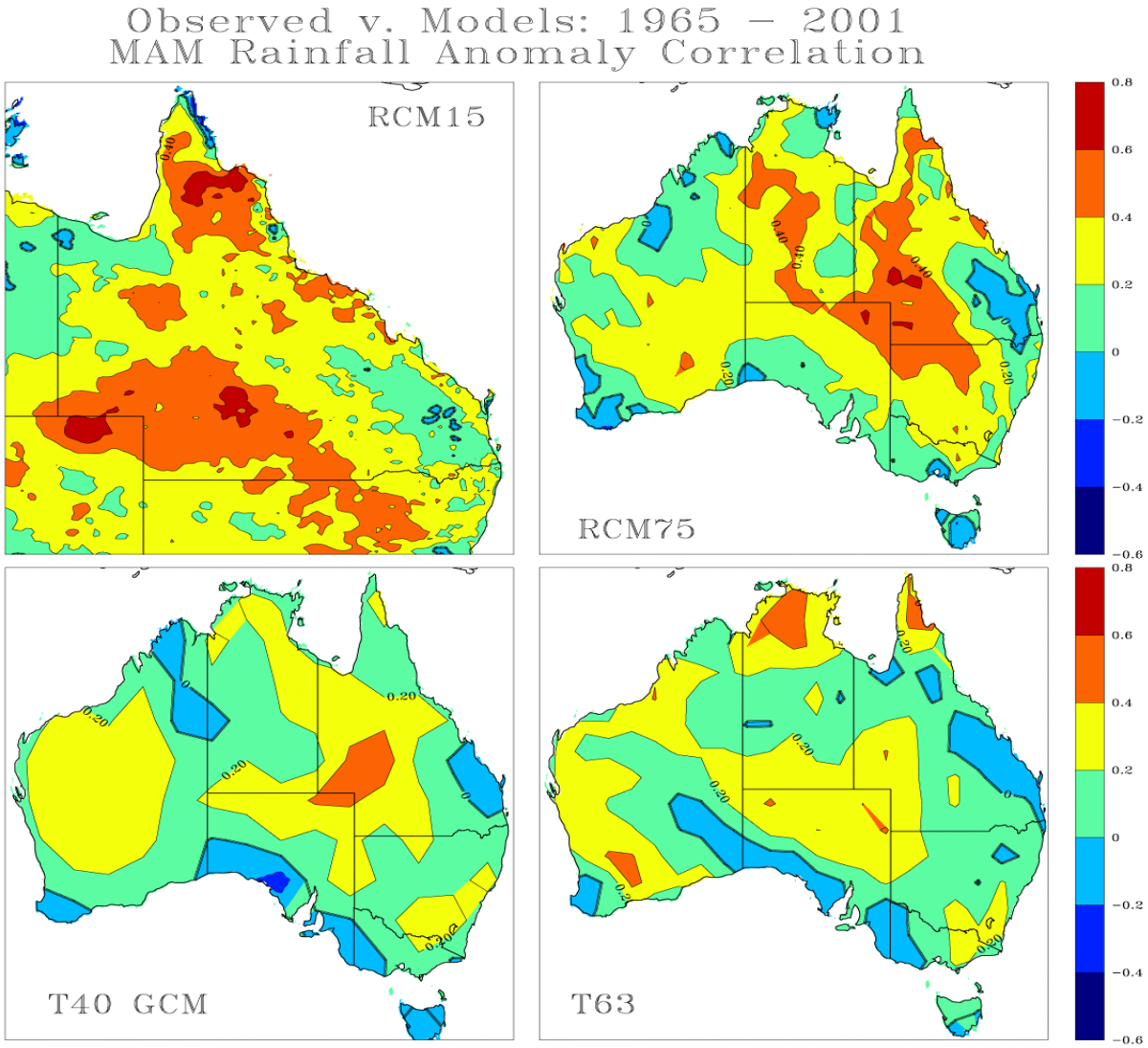

Figure 6.19d. Correlation (r) between observed and simulated autumn (MAM) rainfall for 1965-2000 (36 years).

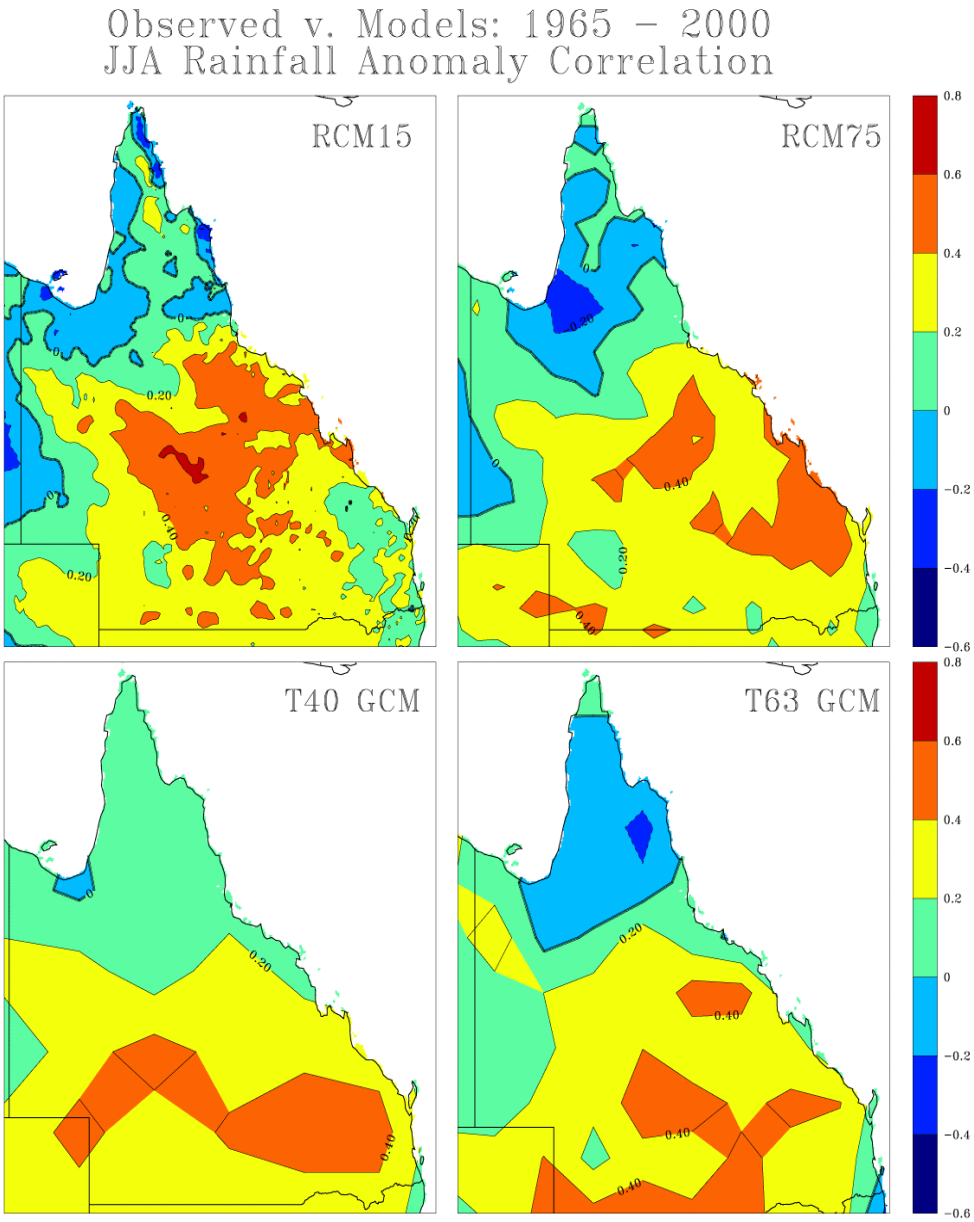

Figure 6.20a. Correlation (r) between observed and simulated Queensland winter (JJA) rainfall for 1965-2000 (36 years).

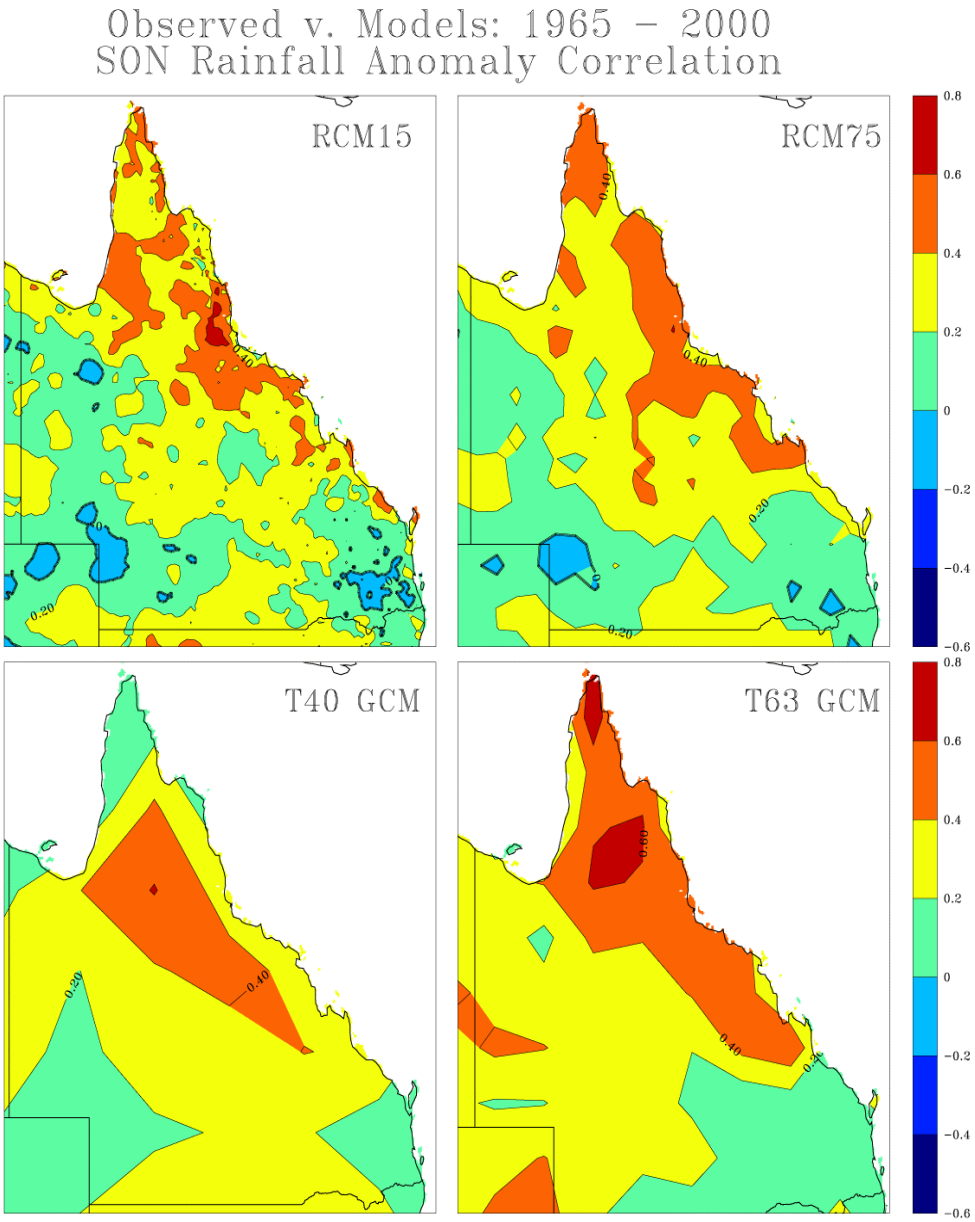

Figure 6.20b. Correlation (r) between observed and simulated Queensland spring (SON) rainfall for 1965-2000 (36 years).

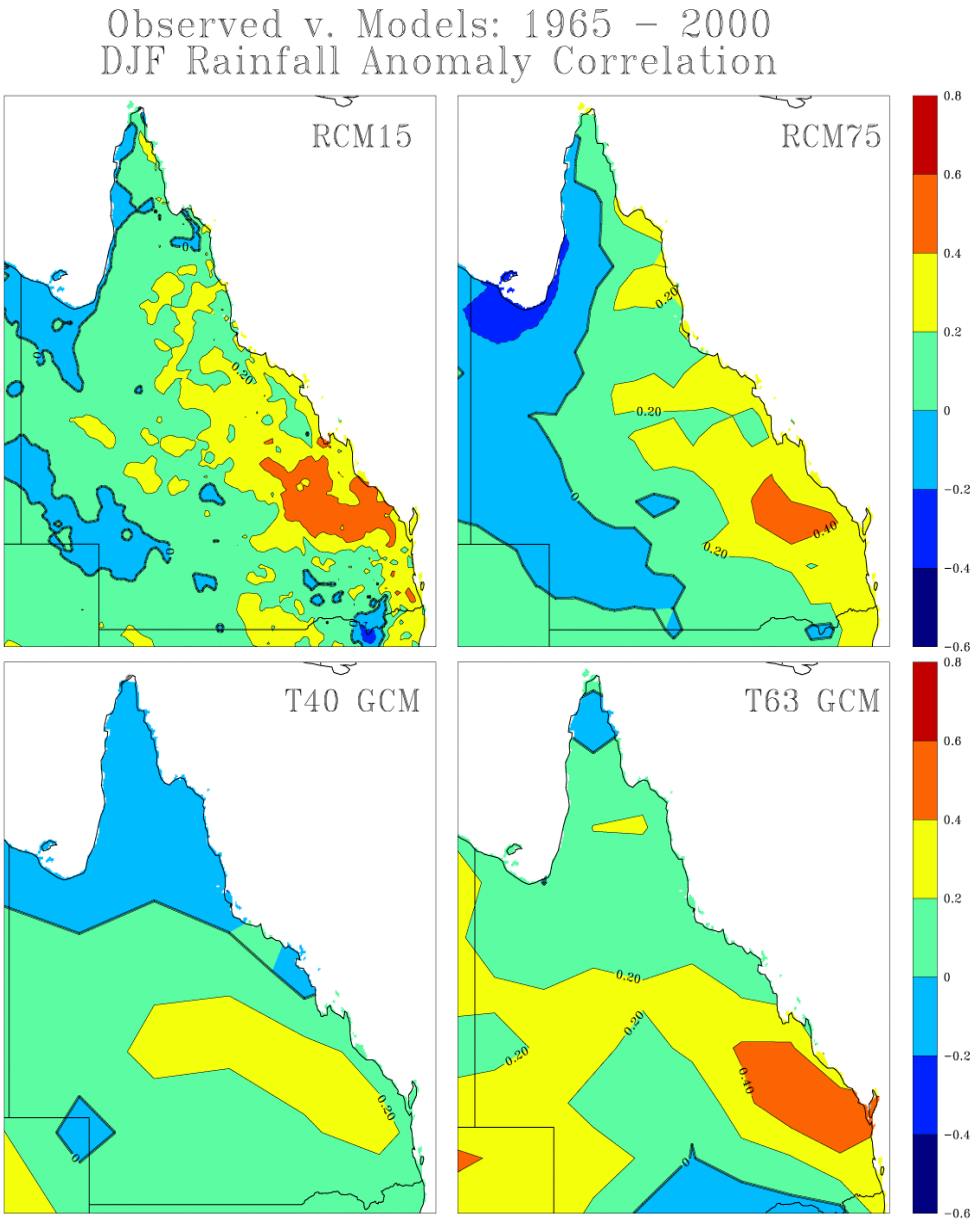

Figure 6.20c. Correlation (r) between observed and simulated Queensland summer (DJF) rainfall for 1965-2000 (36 years).

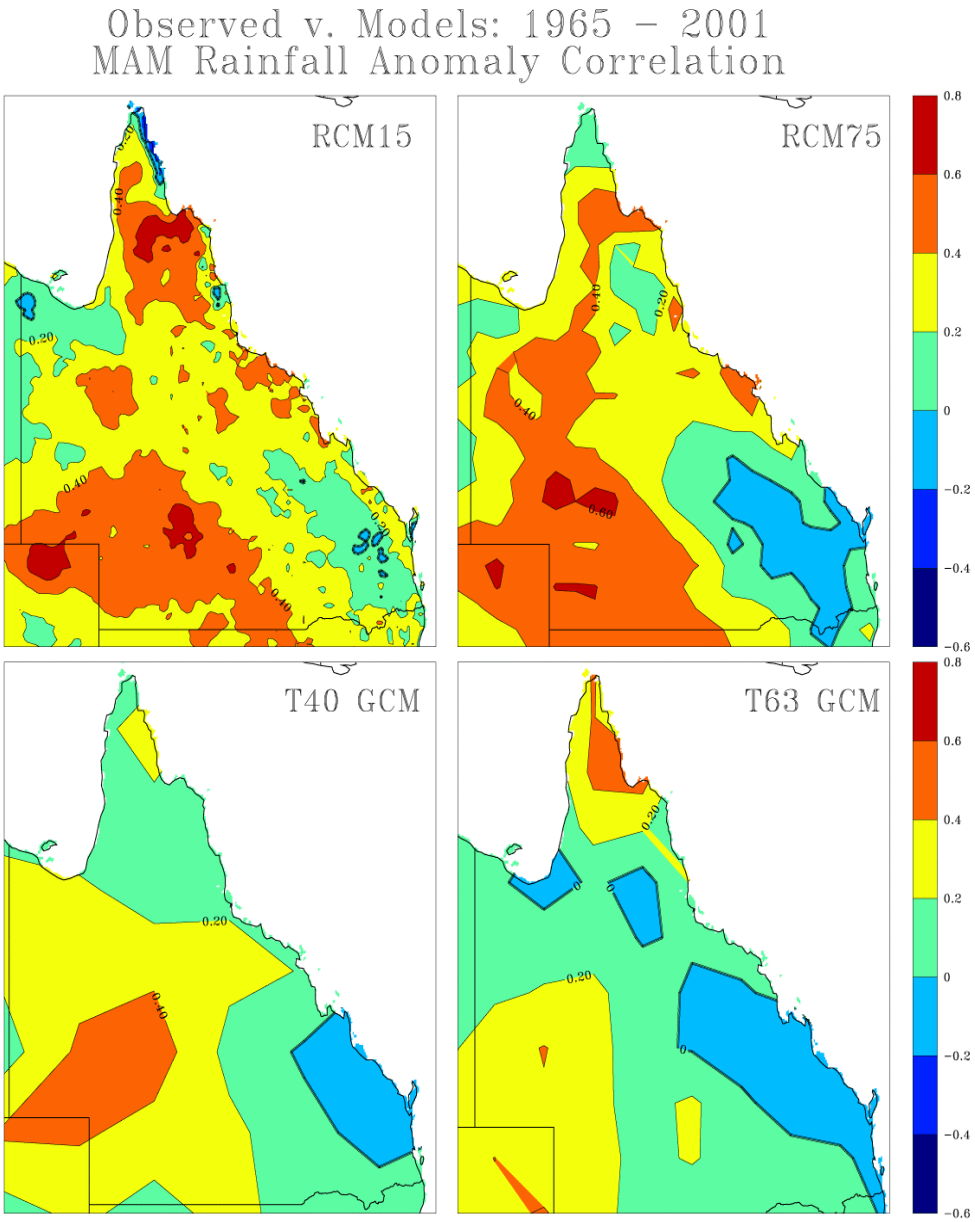

Figure 6.20d. Correlation (r) between observed and simulated Queensland winter (JJA) rainfall for 1965-2000 (36 years).

6.8 Time-series of rainfall

Simulated rainfall amounts were also compared against observed rainfall for an area averaged over the whole state of Queensland (Figure 21) and for the smaller but important Queensland pastoral-cropping zone (Figure 22) for both summer (DJF) and the summer pasture growing season (November to March).

As indicated above the GCM/RCM simulations were generally wetter than observed rainfall, especially the NCEP GCM for summer. Inter-annual variation in the simulations correctly reflected the effect of ENSO, namely low rainfall in the El Niño years of 1972/73, 1977/78, 1982/83, 1987/88, 1991/92, 1992/93 and 1993/94, and high rainfall in La Niña years of 1970/71, 1971/72 and 1973/74. However, agreement with observations did not occur in the El Niño year of 1997/98 nor in the La Niña years of the mid 1970s, 1988/89 and 1998/99. Similarly major differences occurred in 'neutral SOI' years (i.e. years that were neither El Niño nor La Niña). In particular, the low rainfall of 1968/69 and the mid 1980s was not simulated, nor the high rainfall of 1990/91. Given that the models were forced by observed SSTs the lack of agreement is disappointing. Individual members of an ensemble have yet to be examined to more fully assess the comparison with observed rainfall.

Statistical models using simple indices of SST show that a high proportion of inter-annual rainfall variation can be explained (r = 0.5 to 0.6). Reduction of model systematic errors by statistical correction has demonstrated that the skill can be doubled over the Australian region (see Figure 9 in Feddersen *et al.* 1999). Currently we are in process of applying this methodology to the model output.

Overall the strong relationship between ENSO and rainfall apparent in the simulations suggests that there is an opportunity to improve our understanding how the links between rainfall processes and ENSO are modulated.

6.9 Comparison of SOI Correlations with Australian rainfall

Correlations between the SOI and rainfall for observed and climate model simulations were evaluated for Australia for summer (DJF) and winter (JJA), and for Queensland for all four seasons of using output from the 75 km RCM (Figure 6.23). For 1965-2000 correlations between observed summer rainfall and the SOI have been reasonably strong for western NSW and northern Australia (r = 0.25 to 0.50). For the 75 km RCM, correlations between simulated SOI and simulated rainfall were much stronger in summer (r = 0.25 to >0.75). There was also some agreement with the continental spatial pattern of strong correlations north-east Australia, NSW, Victoria and Tasmania, while areas of disagreement with the observed pattern of correlation were in coastal NSW and southern WA.

(a)

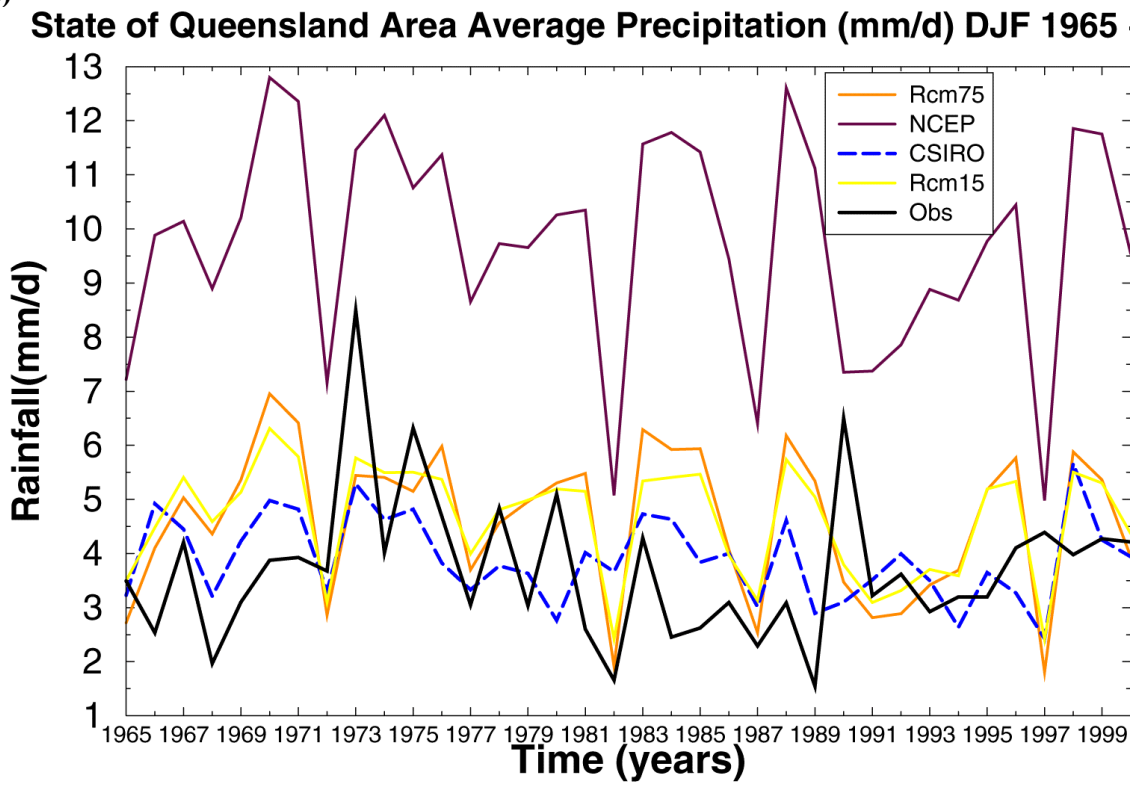

(b)

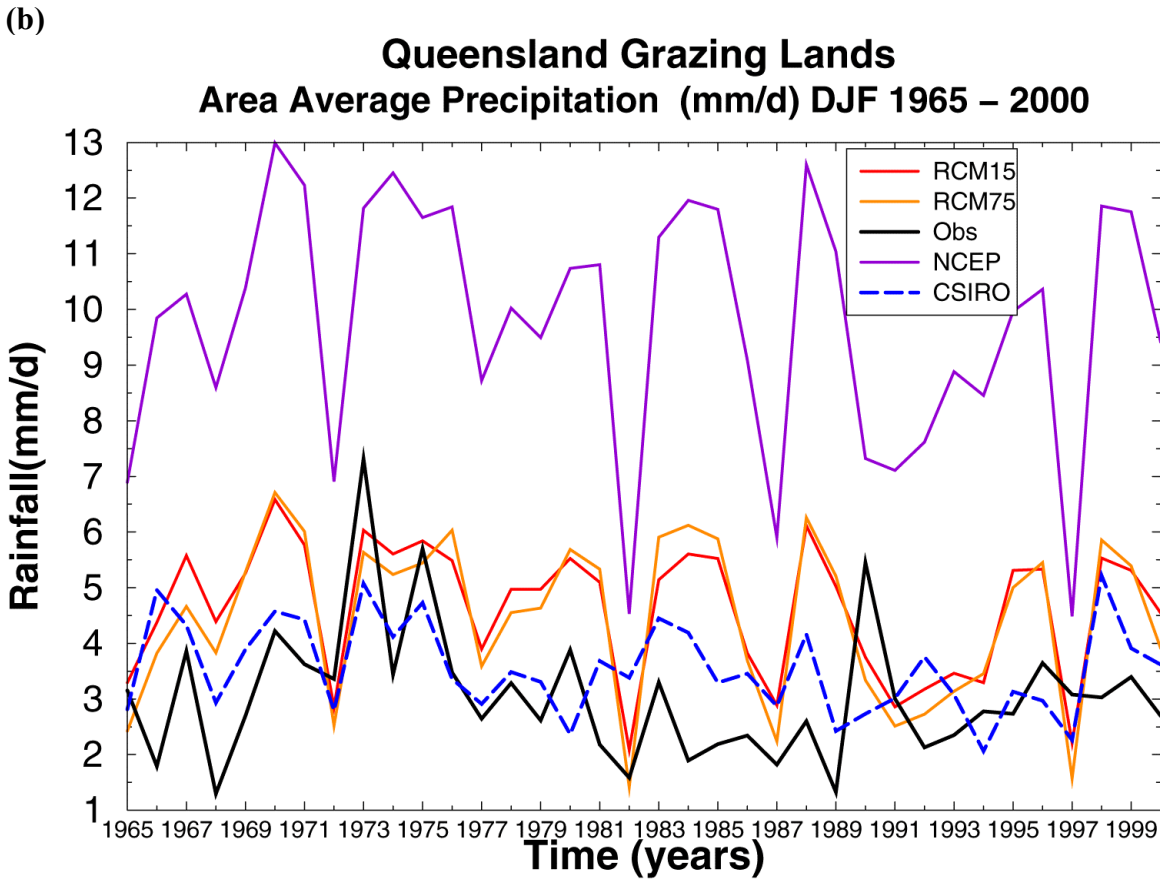

Figure 6.21. Time-series (1965-2000) of summer (DJF) rainfall averaged across (a) the state of Queensland and (b) Queensland's pastoral and cropping zone. The year on the x-axis is for December, i.e. 1982 is summer of 1982/83.

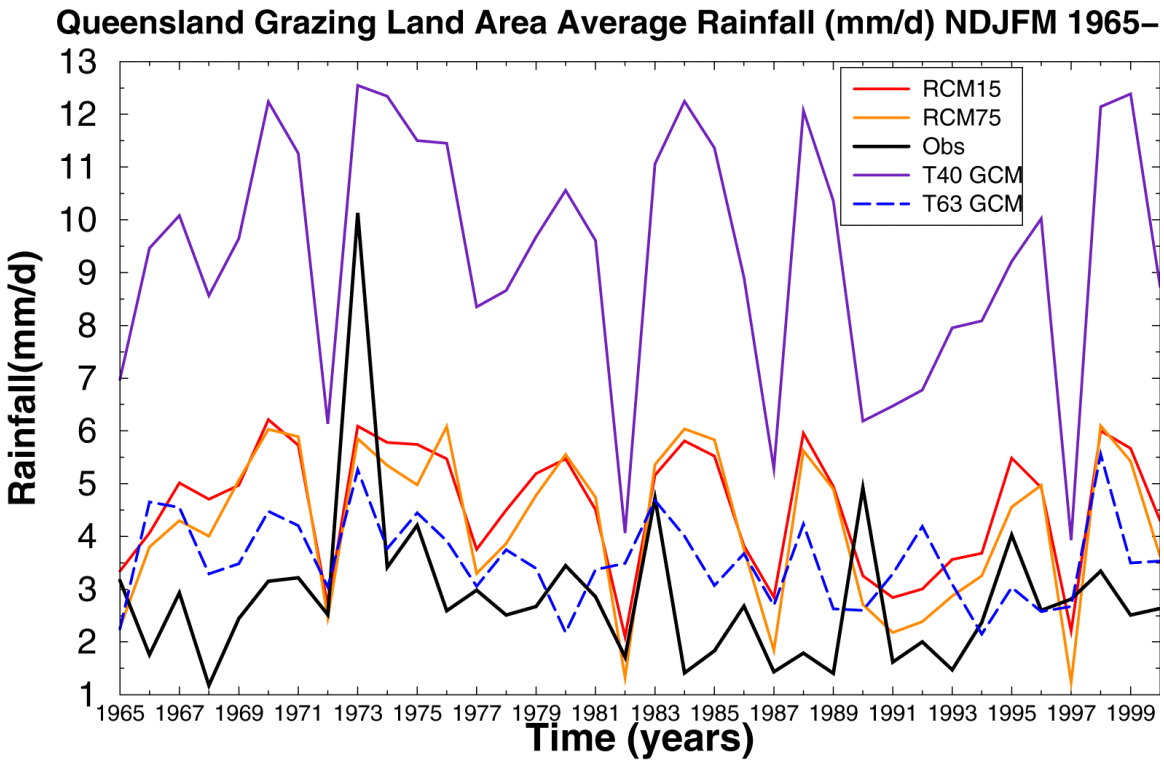

Figure 6.22. Time-series (1965-2000) of rainfall over summer pasture growing season (November to March) for Queensland's pastoral and cropping zone. The year on the x-axis is for December, i.e. 1982 is summer of 1982/83.

For winter, seasonal correlations (r = 0.25 to 0.75) occurred between observed rainfall and the SOI for eastern Australia, SA and central Australia. In contrast, similar stronger correlations between rainfall and the SOI from the 75 km RCM were restricted to north-eastern Australia with strong negative correlations in WA, SA and Victoria. Thus although the large scale atmospheric feature SOI was well represented by the 75 km model there was considerable variation in terms of SOI-rainfall correlations with both stronger and opposite relations depending on location.

6.9.1 SOI correlations with Queensland rainfall

Spatial patterns of Queensland SOI-rainfall correlations were evaluated for all four seasons using output from the GCMs, 75 km RCM and 15 km RCM. In all cases (Figures 6.24 and 6.25) the SOI-rainfall correlation were stronger for the simulated data than were observed, with very high correlations for summer. Even in autumn (MAM), the various models showed strong positive correlations whilst the observed data showed areas of negative correlation and few areas of positive correlation.

Thus despite the models' excellent representation of the SOI, the generally stronger correlations with simulated rainfall suggest that the modelled rainfall in Queensland is too sensitive to the processes driven by ENSO (Figures 6.24 and 6.25). Increasing resolution using the 75 km and 15 km RCMs did not overcome this problem. A possible reason for this stronger relationship in the models is that they were forced by observed monthly mean SSTs, whereas the real world SST forcings are more variable (diurnal and daily weather patterns). In addition, the models do not account for a number of other important

factors such as changing composition of the atmosphere (greenhouse gases including ozone, pollution and mineral aerosols), solar variability and land cover characteristics.

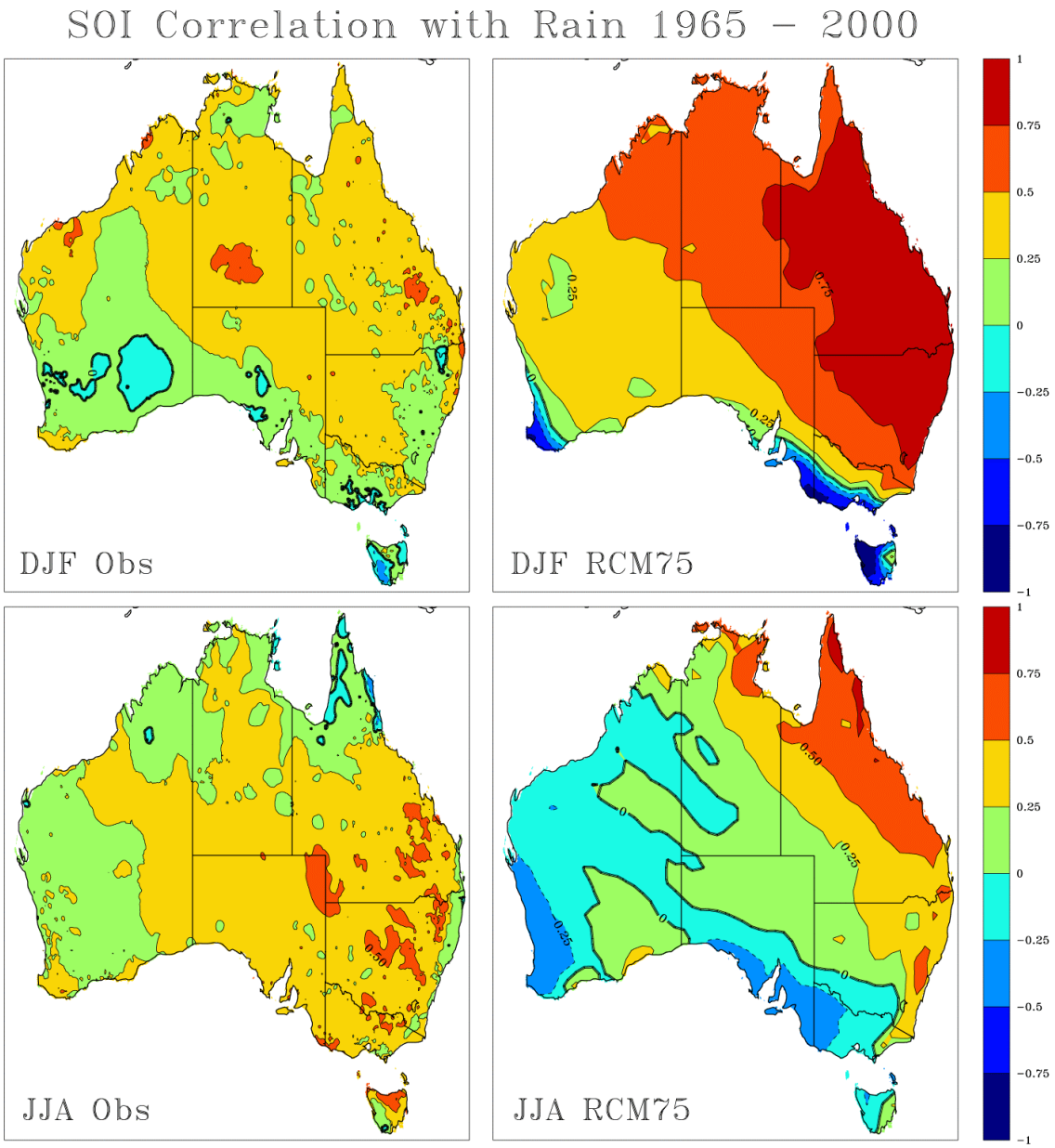

Figure 6.23. Correlations (r) between SOI and seasonal rainfall (DJF and JJA) for observed and simulated data. Correlations were calculated by averaging rainfall for each cell/season combination and correlating with SOI averaged for the same 3-month period.

We investigated SOI/rainfall correlations for individuals ensembles with two different GCMs. Figures 6.24 and 6.25 show the correlations for observed SOI and observed rainfall compared to correlations for simulated SOI and simulated rainfall both for average of ten ensembles and for individual ensemble members. For the NCEP T40 GCM the average of ensembles showed stronger (positive and negative) correlations than observed but individual ensembles (Figure 6.24c-l) were more varied. Most members had

regions of stronger correlation than observed. SOI/rainfall correlations for average of ensembles from CSIRO T63 GCM (Figure 6.25) were not as strong as NCEP T40 GCM but nevertheless there were regions in eastern Australia with stronger correlations. Individual ensemble correlations (Figure 6.25c-l) were more varied than NCEP T40 GCM ensembles with some ensemble members having regions of with correlations of opposite sign to that observed.

Across Queensland's grazing lands, area-averaged observed SOI/rainfall (for 1965 to 1999) was 0.35 and for GCMs was 0.86 (NCEP T40) and 0.46 (CSIRO T63). For individual ensemble members SOI/rainfall correlations ranged from 0.54 to 0.73 for NCEP T40 GCM, and 0.10 to 0.49 for CSIRO T63 GCM. For eastern Australia (Figure 6.16) the area-averaged SOI/rainfall from CSIRO T63 GCM was 0.33 close to observed value 0.31. Thus the CSIRO T63 GCM had a more realistic representation of the teleconnection between SOI and continental rainfall. The fact that there was large variation between individual ensemble members in regional SOI/rainfall correlations shows chaotic nature of the climate system as represented by individual realisation of ensemble members, and suggests that there is an inherent limit in forecasting rainfall using SOI. In reality the observed time-series of rainfall may be equivalent to just ensemble member and GCM studies such as this may indicate an important upper limit to predictability.

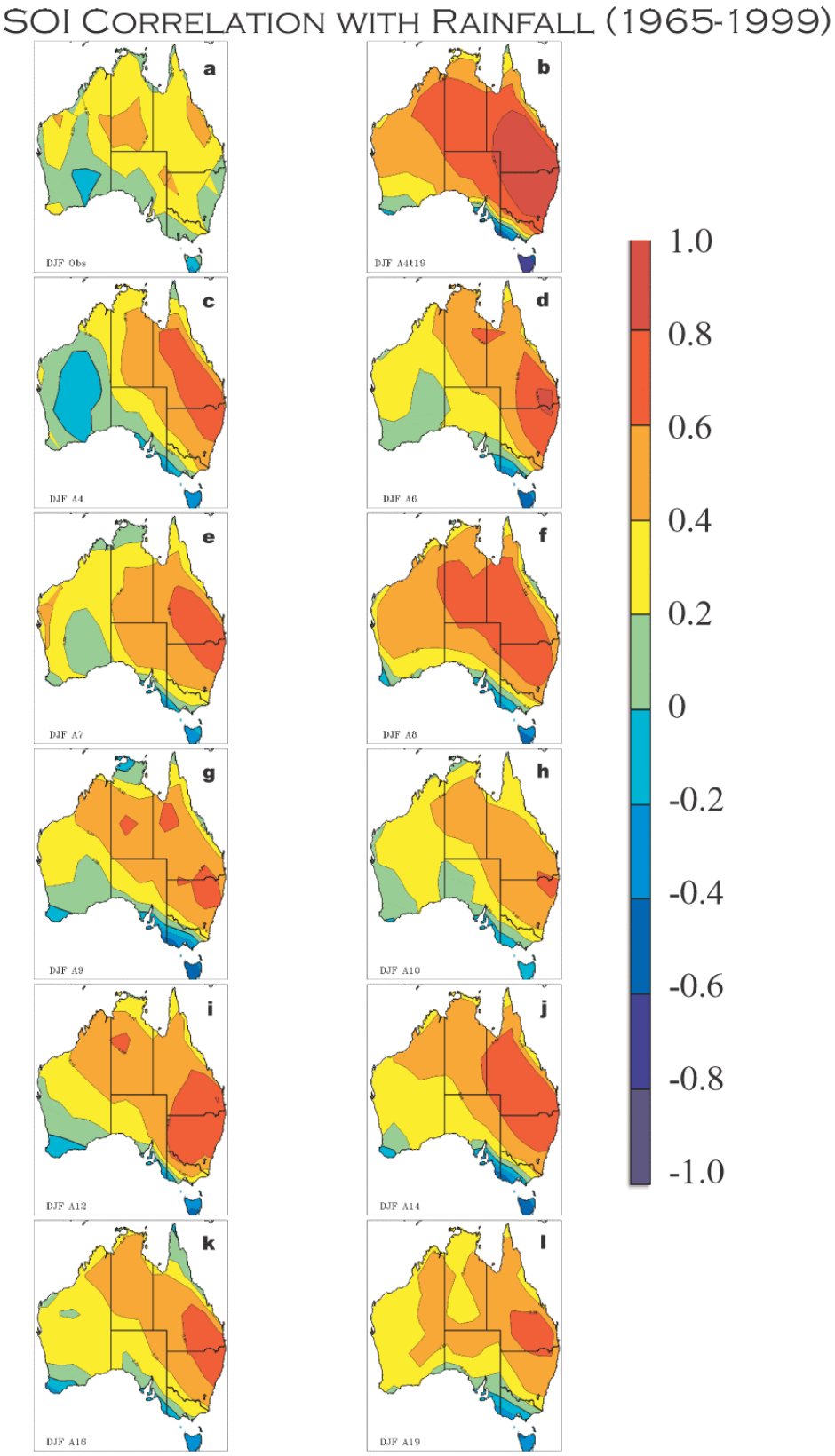

Figure 6.24. Correlations (r) between SOI and summer (DJF) rainfall for observed and simulated data (NCEP T40 GCM). Correlations were calculated by averaging rainfall for each cell/season combination and correlating with SOI averaged for the same 3-month period. For the DJF season, the following relationships are shown: (a) correlations for observed SOI and observed rainfall; (b) simulated SOI and simulated rainfall for ensemble average; and (c) to (l) simulated SOI and simulated rainfall for individual ensemble members.

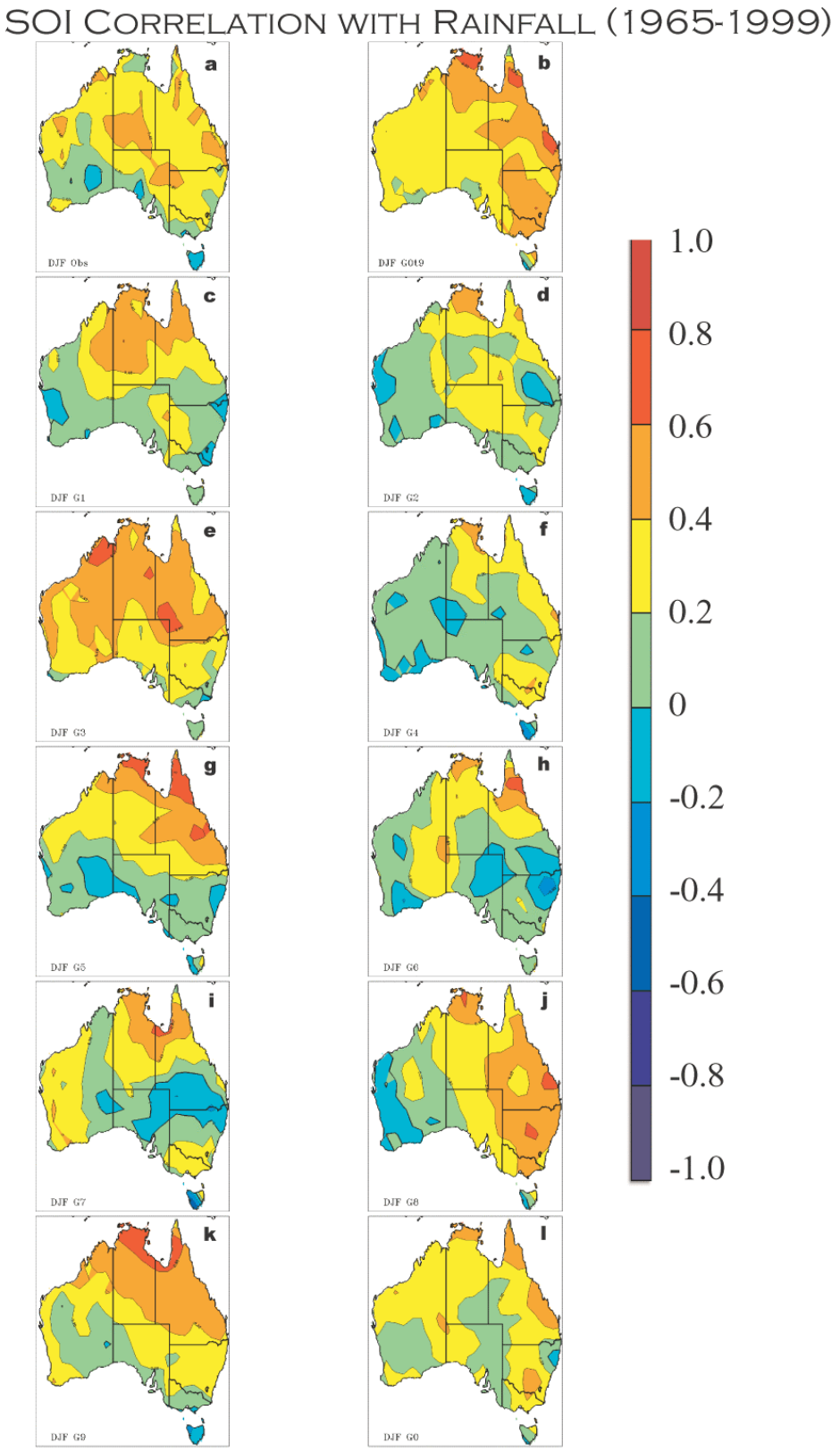

Figure 6.25. Correlations (r) between SOI and summer (DJF) rainfall for observed and simulated data (CSIRO T63 GCM). Correlations were calculated by averaging rainfall for each cell/season combination and correlating with SOI averaged for the same 3-month period. For the DJF season, the following relationships are shown: (a) correlations for observed SOI and observed rainfall; (b) simulated SOI and simulated rainfall for ensemble average; and (c) to (l) simulated SOI and simulated rainfall for individual ensemble member.

6.10 Area-aggregated anomaly correlation of observed and simulated rainfall

The anomaly correlations between simulated and observed rainfall (1965-2000) for each season-model combination are shown for area-averaged rainfall in Table 6.3. For Australia, correlations were low even for the 75 km RCM. At this continental scale, the CSIRO T63 GCM performed better than both the NCEP GCM and the 75 km RCM at annual time periods and for spring (SON), the season with highest correlations. Correlations were higher when Queensland was considered as a whole (r = 0.26 to 0.33 for annual rainfall) and higher still for the smaller Queensland pastoral-cropping zone (r = 0.38 to 0.41 for annual rainfall).

Table 6.3. Correlations (r) between area-averaged observed and simulated (GCM and RCM) annual and seasonal (MAM, JJA, SON, DJF) rainfall for the period 1965-2000 at three geographic regions: a) Queensland grazing lands; b) Queensland; and c) Australia.

Region	Model	Season				Annual
		MAM	JJA	SON	DJF	
Queensland grazing lands	CSIRO T63	0.096	0.313	0.279	0.227	0.278
	NCEP T40	0.201	0.363	0.290	0.197	0.408
	RCM 75km	0.241	0.307	0.259	0.167	0.329
	RCM 15km	0.258	0.337	0.230	0.198	0.348
Queensland	CSIRO T63	0.127	0.223	0.324	0.178	0.258
	NCEP T40	0.214	0.287	0.315	0.12	0.334
	RCM 75km	0.291	0.206	0.259	0.154	0.263
	RCM 15km	0.279	0.236	0.237	0.145	0.286
Australia	CSIRO T63	0.192	0.134	0.345	0.148	0.240
	NCEP T40	0.143	0.120	0.213	0.095	0.150
	RCM 75 km	0.183	0.106	0.157	0.160	0.102
	CCM3 T42[1]		0.210		0.097	
	COLA R42[1]		0.140		0.076	
	ECHAM 4.5[1]		0.228		0.120	

[1] Results from IRI study for the 1979-1995 period (Camarago *et al.* 2001).

The strong correlation for the Queensland pastoral-cropping zone is to be expected as this area, which excludes Cape York, the Gulf of Carpentaria and far-western Queensland, includes some of the strongest ENSO-rainfall relationships (Clewett *et al.* 1993). Although the NCEP GCM was 'too wet' in terms of average annual rainfall (Table 6.2), it did have the strongest correlations for the Queensland pastoral-cropping zone in most seasons (MAM was the exception). Both the 75 km and 15 km RCMs, although closer in agreement to observed average rainfall amounts (Table 6.2) and spatial climatology, had lower anomaly correlations with year-to-year rainfall.

The potential skill in simulating year-to-year variation was also evaluated by considering the maximum correlation co-efficient that was obtained for each region-model combination across 12 possible 'seasons', i.e. every 3-month period (Table 6.4). For the NCEP GCM and the 75 km RCM, highest correlation values (r = 0.3 to 0.4) occurred in eastern and northern Australia, particularly in Queensland. These values are less than those usually derived from correlation with lag SOI ($r \approx 0.4$) although a direct comparison is yet to be made.

Table 6.4. Maximum correlations (r) between area-averaged observed and simulated (GCM and RCM) rainfall for the period 1965-2000. The maximum value for each simulation was selected from the 12 possible 3-month periods.

Model	Australia	Eastern Australia	Southern Australia	Northern Australia	NSW and Victoria	Qld	Qld grazing lands
RCM 15km						0.33	0.39
RCM 75km	0.26	0.32	0.13	0.30	0.26	0.30	0.37
NCEP T40	0.24	0.25	0.08	0.34	0.27	0.35	0.46
CSIRO T63	0.35	0.33	0.16	0.43	0.32	0.32	0.35

6.11 GCM evaluation of SOI - Inter-decadal Pacific Oscillation interaction

Although the correlations between simulated and observed rainfall were low, the results indicated a strong correlation between simulated SOI and simulated rainfall. Thus GCMs are suitable to examine the apparent but controversial interaction between the IPO and SOI on rainfall as described in Chapters 1 and 3.

The GCM T63 was run from 1880 to 2000 (121 years) forced by observed SSTs with five ensembles. Rainfall for each year was expressed as a percentile relative to climatology. Two approaches to calculating climatology were used: 1) combining all ensembles, i.e. 121 years by 5 ensembles; and 2) a climatology derived for each ensemble. Years were then categorised into the following six year-types as described in Chapter 3:

1) SOI < -4 and IPO < 0 (i.e. SOI negative and IPO negative);
2) SOI > +4 and IPO < 0 (i.e. SOI positive and IPO negative);
3) SOI < -4 and IPO > 0 (i.e. SOI negative and IPO positive);
4) SOI > +4 and IPO > 0 (i.e. SOI positive and IPO positive);
5) SOI > -4 & < +4 and IPO < 0 (i.e. SOI neutral and IPO negative); and
6) SOI > -4 & < +4 and IPO > 0 (i.e. SOI neutral and IPO positive).

The average percentile for each group was then calculated. This method of analysis resulted in similar spatial patterns as that described in Chapter 3 where the historical rainfall for each year-type group was expressed as % years > median (Figure 3.9a).

6.11.1 Summer rainfall

For summer rainfall (November-March), the main effects of the above categorisation on **observed** rainfall (Figure 6.26) were that, for groups with same SOI value, there was greater rainfall in eastern Australia when the IPO was negative compared to when IPO was positive. In Queensland, SOI positive-IPO negative years had the highest rainfall whilst the SOI negative-IPO positive group had the lowest rainfall. In WA the latter group had high rainfall in contrast to the lower rainfall in eastern Australia (Figure 6.26).

The different methods of analysing GCM in terms of calculating percentiles output gave similar patterns for each year-type group, although there were regional differences

(Figures 6.27 and 6.28). The IPO negative groups had generally more rainfall than the IPO positive groups. The differences in terms of simulated rainfall between (positive and

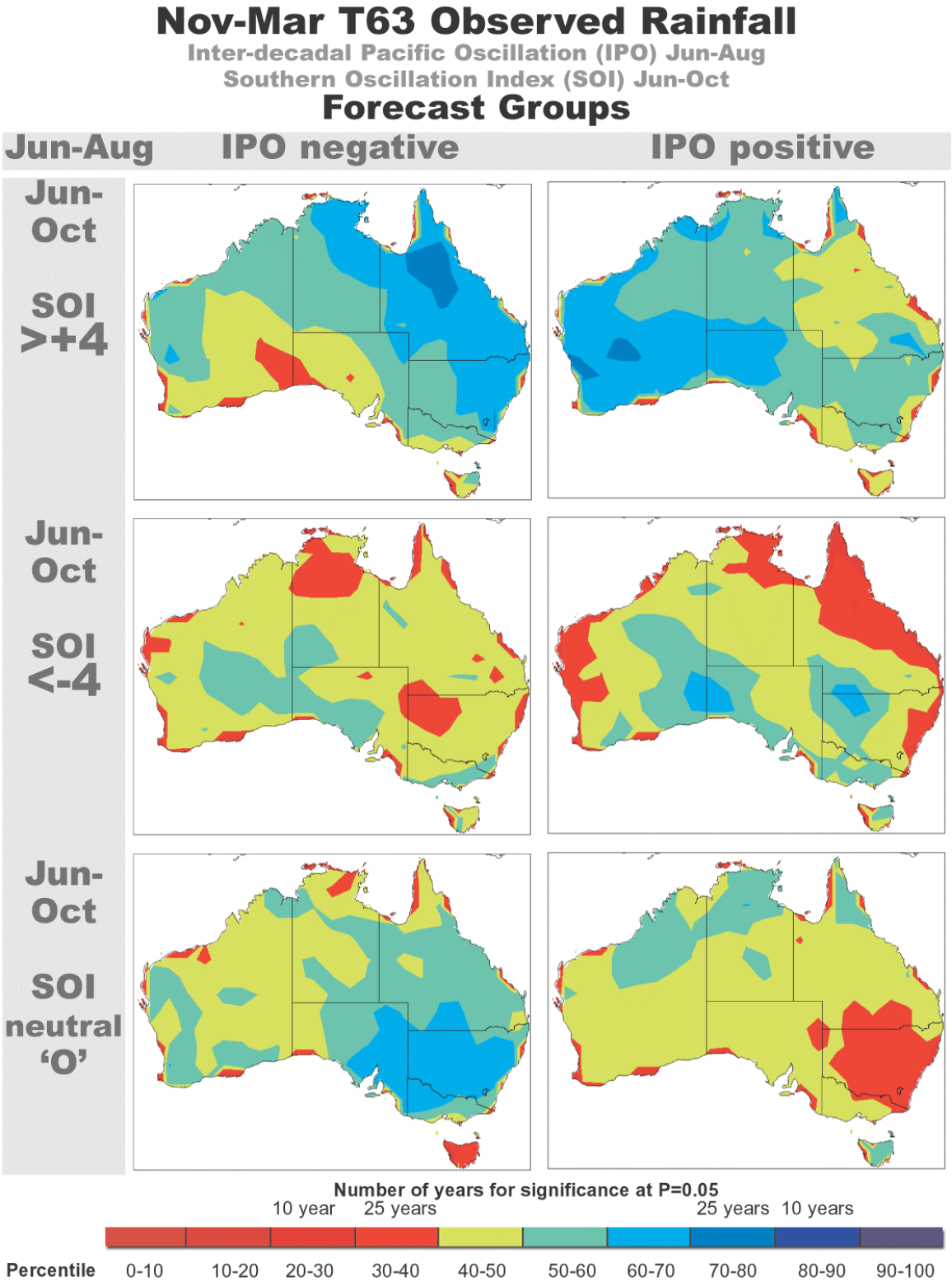

Figure 6.26. Mean percentile rainfall (November to March) calculated from historical records (1880-2000). Years were divided into six categories for year-types as described in Chapter 3: 1) SOI < -4 and IPO < 0 (i.e. SOI negative and IPO negative); 2) SOI > +4 and IPO < 0 (i.e. SOI positive and IPO negative); 3) SOI < -4 and IPO > 0 (i.e. SOI negative and IPO positive); 4) SOI > +4 and IPO > 0 (i.e. SOI positive and IPO positive); 5) SOI > -4 & < +4 and IPO < 0 (i.e. SOI neutral and IPO negative); and 6) SOI > -4 & < +4 and IPO > 0 (i.e. SOI neutral and IPO positive).

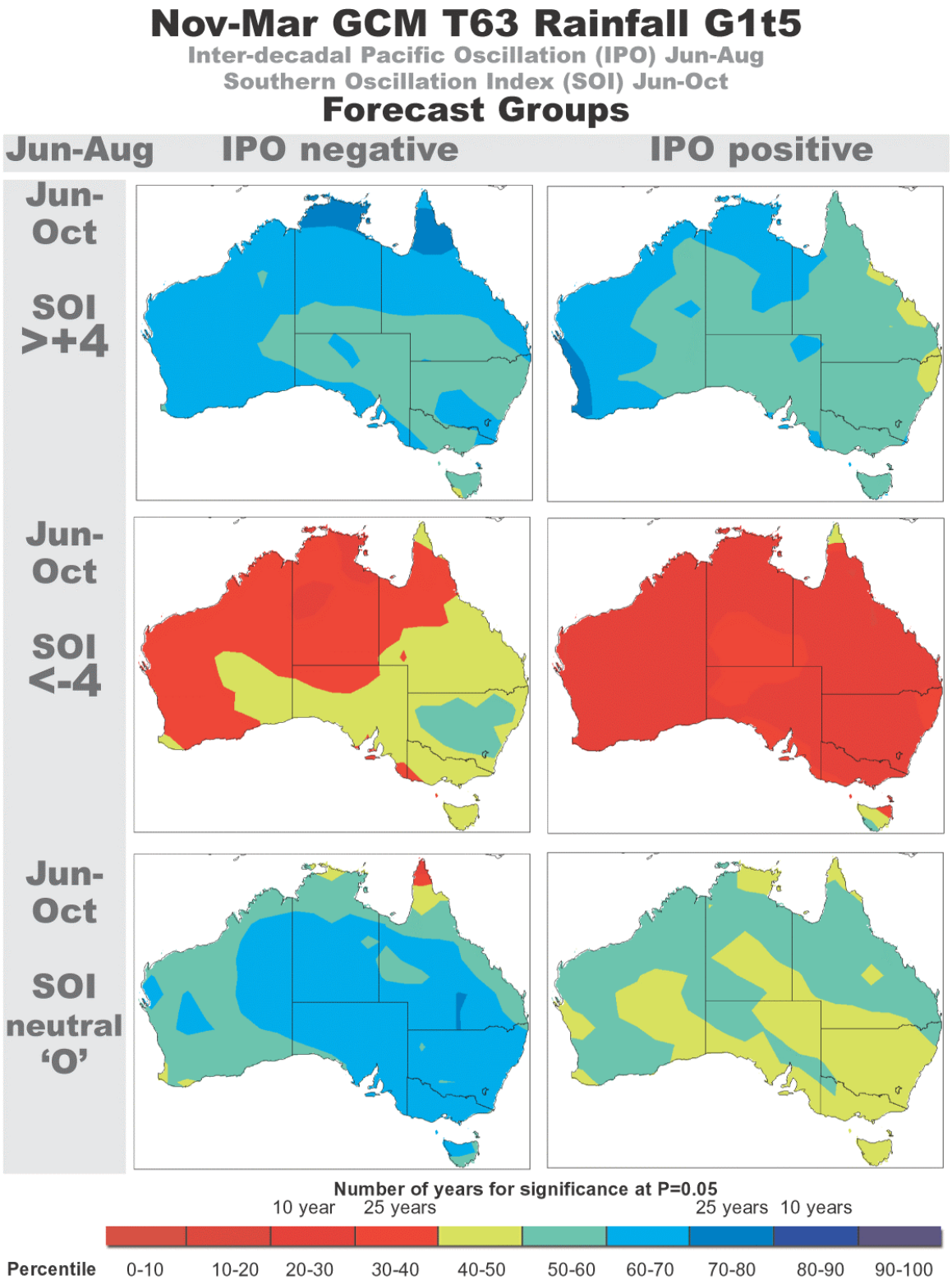

Figure 6.27. Mean percentile rainfall (November to March) calculated from simulated records (1880-2000). Percentiles were averaged from five ensembles with a separate climatology calculated for each ensemble. Years were divided into six categories for year-types described in Chapter 3: 1) SOI < -4 and IPO < 0 (i.e. SOI negative and IPO negative); 2) SOI > +4 and IPO < 0 (i.e. SOI positive and IPO negative); 3) SOI < -4 and IPO > 0 (i.e. SOI negative and IPO positive); 4) SOI > +4 and IPO > 0 (i.e. SOI positive and IPO positive); 5) SOI > -4 & < +4 and IPO < 0 (i.e. SOI neutral and IPO negative); and 6) SOI > -4 & < +4 and IPO > 0 (i.e. SOI neutral and IPO positive).

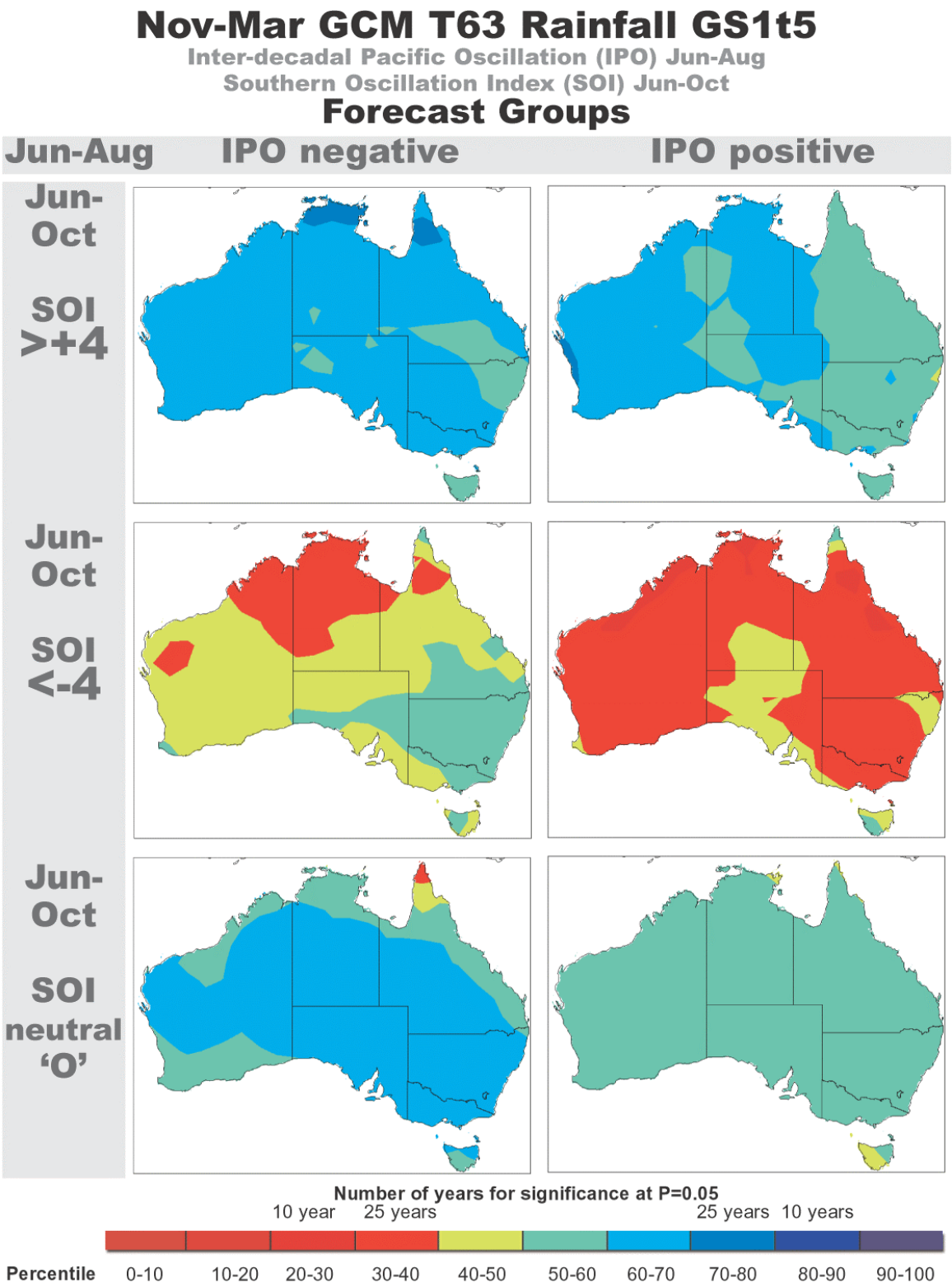

Figure 6.28. Mean percentile rainfall (November to March) calculated from simulated records (1880-2000). Percentiles were averaged from five ensembles with one climatology calculated from all ensembles, i.e. a single climatology. Years were divided into six categories for year-types described in Chapter 3: 1) SOI < -4 and IPO < 0 (i.e. SOI negative and IPO negative); 2) SOI > +4 and IPO < 0 (i.e. SOI positive and IPO negative); 3) SOI < -4 and IPO > 0 (i.e. SOI negative and IPO positive); 4) SOI > +4 and IPO > 0 (i.e. SOI positive and IPO positive); 5) SOI > -4 & < +4 and IPO < 0 (i.e. SOI neutral and IPO negative); and 6) SOI > -4 & < +4 and IPO > 0 (i.e. SOI neutral and IPO positive).

negative) SOI groups were generally greater than observed (Figure 6.26) for most of the continent, probably reflecting the stronger link between SOI and rainfall in the GCM. Thus the GCM simulations, forced by observed SSTs, confirmed the observed interaction between the IPO and SOI, especially in Queensland. In WA the models simulated a greater impact of variation in SOI on rainfall than observed. Nevertheless the models did simulate the contrasting effects between eastern and western Australia in SOI-IPO positive years. Examination of individual ensembles (data not shown) showed more varied spatial patterns of SOI effects although the general effect of the IPO in SOI positive and negative groups was simulated.

The effect of the IPO in SOI neutral years has been one important explanation of drought/degradation episodes, e.g. low summer rainfall in NSW during SOI neutral-IPO positive years (Figure 6.26). The GCM simulations had relatively lower rainfall in these year-types but not to the same extent as observed. The SOI neutral-IPO positive year-types often occurred in long sequences interposed with SOI negative-IPO positive years, including major regional droughts. As described above, there are other mechanisms resulting in lower rainfall not yet fully represented in GCMs such as the biospheric feedback of widespread drought. Similarly important SST regions may not be adequately represented in the historical SST record.

6.11.2 Winter/spring rainfall

For historical winter/spring rainfall (June to October) the differences between SOI-IPO groups were similar to summer for SOI positive groups, i.e. more rainfall across most of the continent when SOI positive and IPO negative (Figure 6.29). For SOI negative groups there was more rainfall in western Australia when IPO was positive (Figure 6.29). For SOI positive years, the IPO influence in GCM simulation was opposite to that observed in the historical rainfall, i.e. simulated rainfall in central and eastern Australia was higher in IPO positive years (Figures 6.30 and 6.31). For SOI negative years the simulated rainfall was not as low in eastern Australia as in the observations, and did not represent the effect of the IPO in WA rangelands. For SOI neutral years, the effect of the IPO on rainfall in eastern NSW was not simulated.

In conclusion the simulations for summer rainfall were in general agreement in terms of the large differences in observed rainfall between SOI-IPO year types. This result indicates the observed interaction (Figure 6.26) in mechanistically consistent with simulated rainfall from a GCM forced with observed SSTs. However, the less distinct effects of the IPO on observed winter rainfall or in neutral SOI years for summer rainfall were not reproduced in simulated rainfall and will require further exploration.

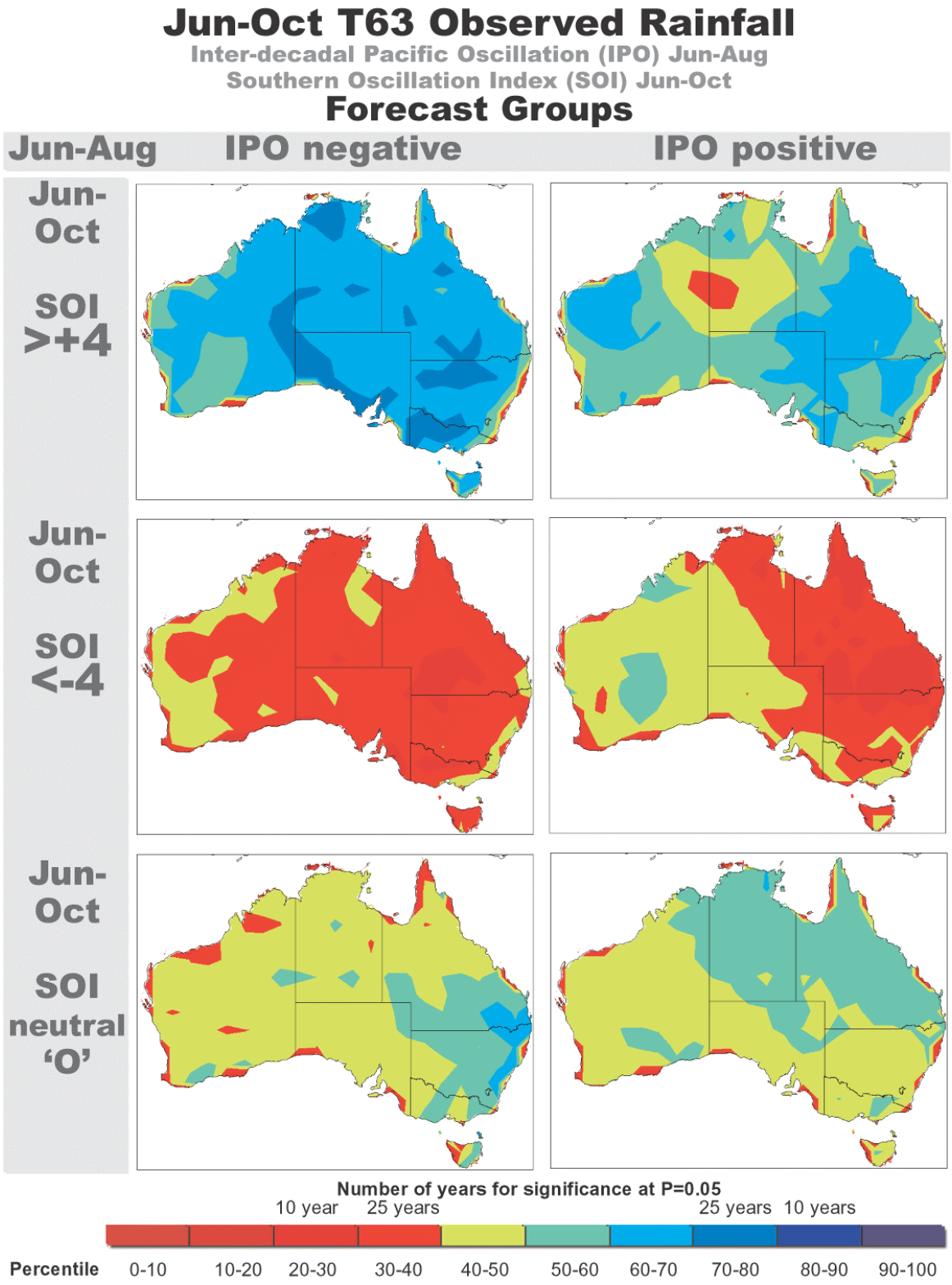

Figure 6.29. Mean percentile rainfall (June to October) calculated from historical records (1880-2000). Years were divided into six categories for year-types described in Chapter 3: 1) SOI < -4 and IPO < 0 (i.e. SOI negative and IPO negative); 2) SOI > +4 and IPO < 0 (i.e. SOI positive and IPO negative); 3) SOI < -4 and IPO > 0 (i.e. SOI negative and IPO positive); 4) SOI > +4 and IPO > 0 (i.e. SOI positive and IPO positive); 5) SOI > -4 & < +4 and IPO < 0 (i.e. SOI neutral and IPO negative); and 6) SOI > -4 & < +4 and IPO > 0 (i.e. SOI neutral and IPO positive).

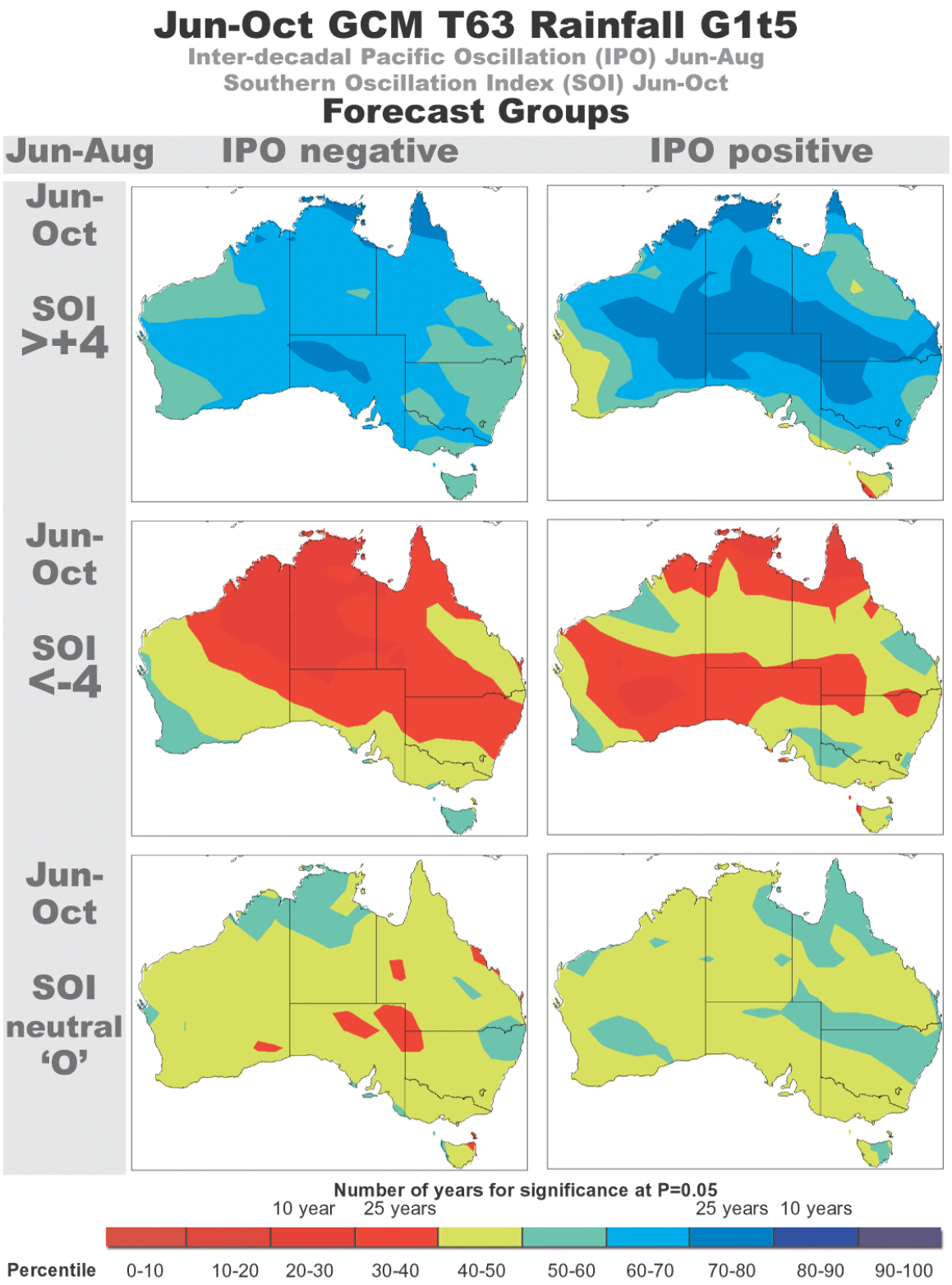

Figure 6.30. Mean percentile rainfall (June to October) calculated from simulated records (1880-2000). Percentiles were averaged from five ensembles with a separate climatology calculated for each ensemble. Years were divided into six categories for year-types described in Chapter 3: 1) SOI < -4 and IPO < 0 (i.e. SOI negative and IPO negative); 2) SOI > +4 and IPO < 0 (i.e. SOI positive and IPO negative); 3) SOI < -4 and IPO > 0 (i.e. SOI negative and IPO positive); 4) SOI > +4 and IPO > 0 (i.e. SOI positive and IPO positive); 5) SOI > -4 & < +4 and IPO < 0 (i.e. SOI neutral and IPO negative); and 6) SOI > -4 & < +4 and IPO > 0 (i.e. SOI neutral and IPO positive).

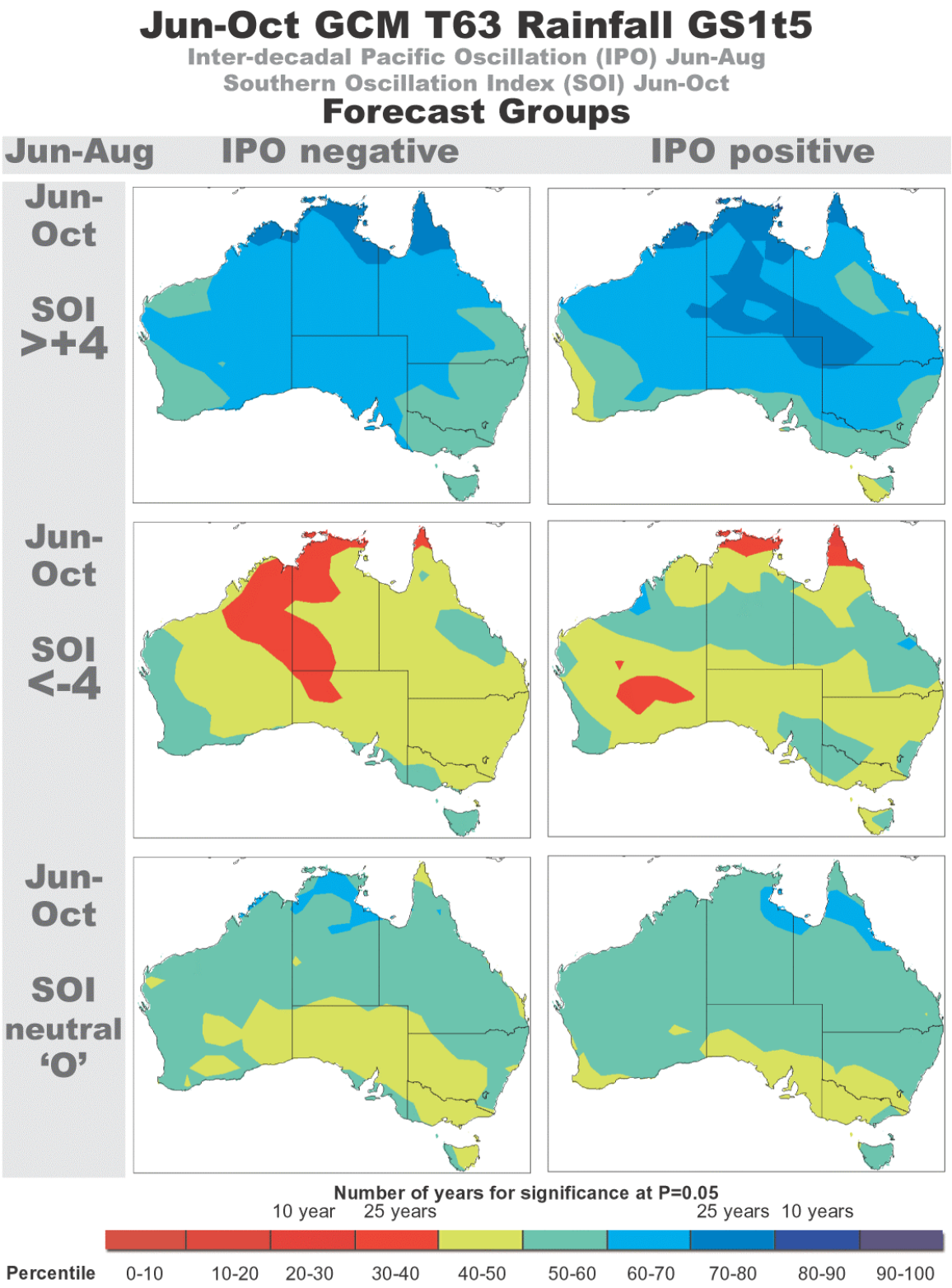

Figure 6.31. Mean percentile rainfall (June to October) calculated from simulated records (1880-2000). Percentiles were averaged from five ensembles with one climatology calculated from all ensembles, i.e. a single climatology. Years were divided into six categories for year-types described in Chapter 3: 1) SOI < -4 and IPO < 0 (i.e. SOI negative and IPO negative); 2) SOI > +4 and IPO < 0 (i.e. SOI positive and IPO negative); 3) SOI < -4 and IPO > 0 (i.e. SOI negative and IPO positive); 4) SOI > +4 and IPO > 0 (i.e. SOI positive and IPO positive); 5) SOI > -4 & < +4 and IPO < 0 (i.e. SOI neutral and IPO negative); and 6) SOI > -4 & < +4 and IPO > 0 (i.e. SOI neutral and IPO positive).

6.12 Summary of findings and discussion

The analysis of simulation results for the GCMs and RCMs forced by observed SSTs showed that:

- large scale features of the atmosphere, i.e. SOI were very well represented and that the RCMs did simulate fine resolution features such as tropical cyclones, rainfall depression and rain shadow areas;
- spatial variation in long term average rainfall was well simulated with the newer CSIRO T63 GCM and with RCMs nested within the older NCEP GCM;
- weak correlations ($r < 0.4$) occurred when year-to-year variation in seasonal and annual rainfall was considered, even for rainfall averaged over large areas;
- simulated rainfall was highly correlated with simulated SOI, especially in Queensland, but these correlations exceeded observed SOI-rainfall correlations; and
- simulations of summer rainfall between SOI-IPO year types were in general agreement with observed rainfall, however, the less distinct effects of the IPO on observed winter rainfall or in neutral SOI years for summer rainfall were not reproduced.

The analysis raised several issues regarding the use of ensembles and the potential for simulating rainfall. It could be argued that the observed rainfall time-series represents only one ensemble out of the range of possibilities. The range of possibilities could in fact be well represented by the ensemble variation found in the simulation studies. Averaging across ensembles may reduce noise compared to signal variation and hence the stronger correlation between simulated SOI and simulated rainfall, especially in Queensland. A suitable test would be to examine the correlations for each individual ensemble member and compare these correlations with correlations between observed rainfall and observed SOI and/or other SST indices (e.g. Day *et al.* 2001). The lower variation (SD ratio) generally found in simulated rainfall may be the result of not using all information available.

The climate model output can be further improved by statistical correction to eliminate model systematic errors using singular value decomposition analysis (SVDA) or leading canonical correlation analysis (CCA) (Feddersen *et al.* 1999, Moron *et al.* 2000). These studies have indicated that a two-fold increase in correlation with observed data can be achieved with this approach.

6.12.1 Biospheric feedback

A major process, biospheric feedback, is yet to be included in the models. Studies for similar environments to much of Australia (e.g. northern Africa) have shown that the inclusion of biospheric feedback changed rainfall variability simulated by GCMs (Zhang *et al.* 1999). For example, in a GCM simulation of inter-decadal climatic variability in the semi-arid grazing lands of the Sahel (northern Africa), Zeng *et al.* (1999, 2001) found vegetation changes enhanced inter-decadal variation 'substantially' but reduced year-to-year variability. They stated:

> The interactive vegetation modifies the precipitation through a chain of positive feedback loops. For instance, decreased rainfall leads to less water availability and reduces vegetation, which in turn leads to higher surface albedo and reduced evapotranspiration. This weakens the large-scale atmospheric circulation by reducing the energy and water flux into the atmosphere column, thus further decreasing the local rainfall.

During the period 1965-2000 major drought and flood events occurred in Australia. From 1961 to 1965 there was an extensive drought in central Australia extending to Queensland and NSW in 1966. The year 1969/70 (April to March) had extensive drought from Western Australia to western Queensland (including the top end of the N.T). During these long periods of drought there was greatly reduced surface cover due to grazing, low pasture growth and death/defoliation of shrubs and trees (Condon *et al.* 1969). Similarly, in Queensland the 4-year sequence of drought, 1991/92 to 1994/95, led to low surface cover and tree death/defoliation (Fensham 1998). The loss of surface cover is likely to change surface albedo (e.g. black soil plains), increase dust content of air, change the partitioning of evapotranspiration by increasing soil evaporation relative to vegetation transpiration, and increase runoff compared to infiltration.

Extensive flood periods such as 1973 to 1976 also changed vegetation cover by: (a) promoting long lived transpiring perennial plants (Friedel 1984) rather than short lived ephemeral vegetation; (b) providing large areas of surface water, e.g. flooded channel country in western Queensland (Allan 1985); and (c) stimulated growth of vegetation which went on to become fuel for extensive bush fires once the vegetation had been cured (Noble and Vines 1993). Anthropogenic effects associated with rangeland management and cropping area expansion (tree clearing, overgrazing) have also contributed to cover changes (Burrows *et al.* 1990).

Thus there is ample evidence that large and extensive fluctuations in surface cover and other important meteorological attributes can occur as a result of temporal climate variability. Studies on the importance of this process in GCMs are currently underway (P Lawrence, pers. comm.).

Different vegetation and soil parameterisation were used for each of the models. All four models use time invariant values of surface characteristics such as surface albedo, vegetation type and surface roughness. There is a need to include an interactive biosphere into climate models. Zeng *et al.* (2001) have demonstrated for the Sahel that inter-annual rainfall variability was simulated realistically only when dynamic vegetation was included in their model. If biospheric feedbacks are as important as Zeng *et al.* (2001) indicate, then improvement in model performance is to be expected for the Australia.

The improvement gained in spatial agreement by using RCMs nested within the NCEP GCM was encouraging. The NCEP GCM was 'too wet' in Queensland and not surprising the 75 km and 15 km RCMs were also 'too wet', although substantially closer to observed climatology than the NCEP GCM. The CSIRO T63 GCM was better than NCEP GCM in terms of climatology. It would be expected that nesting RCMs within the CSIRO T63 GCM would further improve their capability. Thus there are several steps yet to be explored which could further increase the skill of GCMs/RCMs in simulating rainfall variability.